RESOURCE DIMENSIONING AND MANAGEMENT FOR SOLAR POWERED CELLULAR BASE STATIONS

VINAY CHAMOLA

NATIONAL UNIVERSITY OF SINGAPORE
2016

RESOURCE DIMENSIONING AND MANAGEMENT FOR SOLAR POWERED CELLULAR BASE STATIONS

VINAY CHAMOLA

(B.E.), (M.E.), Birla Institute of Technology and Science (BITS) Pilani, Rajasthan, India

A THESIS SUBMITTED

FOR THE DEGREE OF DOCTOR OF PHILOSOPHY

DEPARTMENT OF ELECTRICAL AND COMPUTER ENGINEERING

NATIONAL UNIVERSITY OF SINGAPORE

2016

DECLARATION

I hereby declare that this thesis is my original work and it has been written by me in its entirety. I have duly acknowledged all the sources of information which have been used in the thesis.

This thesis has also not been submitted for any degree in any university previously.

Vinay Chamola
30th September 2016

ACKNOWLEDGEMENTS

I would like to express my sincere gratitude and appreciation to my advisor Prof. Biplab Sikdar for his valuable guidance and support throughout my Ph.D. He has been always kind to give time and support whenever asked for. I have enormously benefited from his profound thinking, technical insights and broad vision which have helped me improve my research skills. Without his continual direction, encouragement and guidance, this thesis would certainly have not been possible.

I thank Dr. Bhaskar Krishnamachari for hosting me as a visiting researcher at the University of Southern California, LA, USA during my Ph.D; where I greatly benefited in my research work by collaboration with his research group.

I thank my colleagues in the Communication and Network Laboratory at the Department of Electrical and Computer Engineering of NUS for their sincere help during my Ph.D.

Lastly, and most importantly, I would like to express my gratitude to Almighty God who has kindly given all intelligence and ability to write this thesis. My gratitude also goes to my dear family members who have been always eager to extend their love, care and support to me.

Table of Contents

Summary

The increasing deployment of cellular networks across the globe has brought two issues to the forefront: the energy costs of running these networks and the associated environmental impact. Cellular base stations (BSs) powered by renewable energy sources such as solar power have emerged as one of the promising solutions to these issues. This thesis addresses issues centering around deployment and operation of solar powered base stations.

The thesis starts with addressing the problem of optimally dimensioning resources (photovoltaic (PV) panels and batteries) for solar powered BSs. We propose a framework for cost-optimally dimensioning these resources such BSs. An important input for such dimensioning is the solar energy data. Cellular networks require a high degree of reliability and thus accurately characterizing the solar energy is imperative for successful resource dimensioning. To accurately characterize the solar energy, we propose a multi-state Markov model which combines daily and hourly transitions in weather conditions which are then used for resource dimensioning. Also, from the resource dimensioning we present useful insights that may serve as guidelines for cellular operators planning to deploy solar powered BSs.

One of the fundamental steps in the dimensioning of resources is to evaluate the energy outage probability and battery lifetime associated with a particular configuration of PV panel and battery size. Thus, we propose

an analytic model to evaluate the outage probability and battery lifetime of a solar powered BS for a particular resource configuration. The proposed model accounts for hourly as well as daily variations in the harvested solar energy as well as the load dependent BS power consumption and the battery levels. The model evaluates the steady state probability of the battery level which is then used to estimate the outage probability and the battery lifetime associated with the particular resource configuration.

Next, the thesis develops resource management strategies for off-grid solar powered BSs aimed towards avoiding energy outages, while simultaneously deriving maximum benefit from the green energy harvested in terms of reducing the traffic latency in the network. We present a methodology for minimizing the traffic latency, given the constraints on the energy availability at the solar powered BSs. Our methodology uses a combination of intelligent energy allocation over time, and green energy and delay aware downlink power control and user association.

In the last part of the thesis we consider grid connected BSs equipped with resources to harvest solar energy. The solar energy harvested can reduce the grid energy consumed, thus bringing cost savings for cellular operators. Intelligent management of such harvested energy can further maximize the cost savings. Such management of energy savings has to be carefully coupled with managing the traffic latency so as to ensure customer satisfaction. We propose a framework for jointly managing the grid energy savings and the traffic latency which is achieved by downlink transmit power control and user association reconfiguration. We also show the trade-off between the grid energy savings and the traffic latency for the proposed scheme.

List of Figures

List of Tables

List of Algorithms

List of Abbreviations

AC	Alternating current
ARMA	Autoregressive moving average
AWGn	Additive white gaussian noise
BS	Base station
CAPEX	Capital expenditure
CoMP	Coordinated multipoint
DC	Direct current
DoD	Depth of discharge
EH	Energy harvesting
ICI	Inter cell interference
ICT	Information and communications technologies
IPU	Integrated power unit
LTE	Long term evolution
MIMO	Multi input multi output
MT	Mobile terminal
NREL	National renewable energy laboratory (USA)
OFDMA	Orthogonal frequency division multiple access
OPEX	Operating expenditure
PV	Photovoltaic
QoS	Quality of service
SAM	System advisor model
SD	Standard deviation
SINR	Signal-to-interference-plus-noise ratio
TCO	Total cost of ownership
TMY	Typical meteorological year

Chapter 1

Introduction

With more than six billion subscribers [1], the cellular networking and communications industry is growing rapidly. To support this growth in the subscriber base, cellular operators have expanded their coverage and capacity by deploying additional network infrastructure. This in turn has increased the energy consumption of cellular networks and their contribution to greenhouse gas emissions. With more than three million base stations worldwide, cellular networks currently contribute to around 3% of the worldwide energy consumption and 2% of carbon emissions [2]. Also, it is predicted that the carbon emissions of information and communication technologies (ICT) will increase from 170 metric-tons in 2014 to 235 metric-tons by 2020. This increase in the power consumption and carbon footprint of cellular networks has led to various initiatives for "green" solutions from telecom providers, government agencies and researchers.

One of the key components of a cellular network is the base station (BS). A base station provides coverage to the cellular users in its vicinity. BSs are categorized according to their power consumption and coverage in descending order as: macro, micro, mini and femto. Among these, macro

base stations are the primary ones in terms of deployment and have power consumption ranging from 0.5 to 2 kW/hr. BSs consume around 60% of the overall power consumption in cellular networks [2]. Thus one of the most promising solutions for green cellular networks is BSs that are powered by solar energy. Base stations that are powered by energy harvested from solar radiation not only reduce the carbon footprint of cellular networks, they can also be implemented with lower capital cost as compared to those using grid or conventional sources of energy [3].

There is a second factor driving the interest in solar powered base stations. In the recent past, the bulk of the growth in the deployment of cellular base stations has been in parts of the world such as Africa and Asia where the penetration of cellular communication is still low. For example, the penetration of cellular networks in rural India is currently estimated to be 30-40%, implying that 200 million people are yet to be connected to cellular networks [4]. Unfortunately, many of these regions lack reliable grid connectivity and the telecom operators are thus forced to use conventional sources such as diesel to power the base stations, leading to higher operating costs and emissions. For example, studies indicate that of the 400,000 base stations in India, more than 70% face power cuts for more than 8 hours a day [5]. As a result, the telecom industry in India consumes more than 2 billion litres of diesel per year, spending around US$ 1.4 billion and producing more than 5 metric-tons of carbon dioxide emissions[5].

Current estimates suggest that there are 320,100 off-grid (i.e. without any grid connectivity) and 701,000 bad-grid (i.e. connected to a grid supply with frequent power outages, loss of phase, or fluctuating voltages) BSs in the world [4]. The off-grid and bad-grid BSs are predicted to grow by 22% and 13% by the year 2020, respectively. This would imply that around

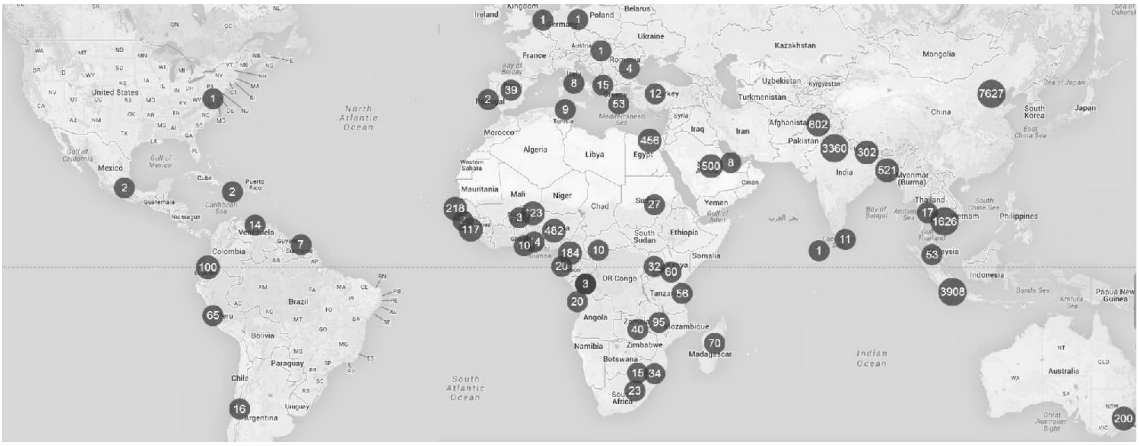

Figure 1.1: Worldwide deployment status of solar powered base stations at the end of 2014.

70,000 off-grid and 90,000 bad-grid BSs will be installed between the years 2014 and 2020. Around 80% of these would be installed in African and Asian countries. It is noteworthy that although many of the countries in these regions have poor grid connectivity, they are rich in terms of solar resources. Consequently, solar powered BSs are a viable and attractive option in these regions. As can be seen from Figure 1.1 that shows the status of solar powered BS deployment in the world at the end of 2014 [4], the vast majority of such BSs are in Asia and Africa. The number in the circles indicate the number of solar powered BSs in a particular country. This thesis addresses two key issues in the deployment and operation of a network of solar powered base stations. The first issue addressed in this thesis is to determine the cost-optimal configuration of energy harvesting resources (PV panels and batteries) for such base stations. The second issue addressed in this thesis is to develop resource management strategies for a network of solar powered base stations so as to avoid energy outages while improving the quality of service offered to the users in terms of reducing the traffic latency. We develop operational strategies for both off-grid as well as grid connected solar powered base stations.

The rest of this chapter is organized as follows. Section 1.1 describes the various factors which have motivated the popularity of solar powered base stations. Section 1.2 describes the key components of a solar powered base station. Section 1.3 discusses the various configurations for a solar powered BS. Section 1.4 presents the current status of deployment of solar powered BSs and a case study. Section 1.5 presents few challenges in the deployment and operation of solar powered BSs, existing solutions and some un-solved issues. Section 1.6 presents the thesis outline and the contributions made in this thesis for addressing the un-solved issues centring around deployment and operation of solar powered BSs. Section 1.7 presents the bibliographical note.

1.1 Motivating factors for solar powered BS's

In addition to the environmental benefits of using renewable energy sources, solar powered BSs have a number of additional advantages. This section presents the various advantages and other factors that have motivated the increasing deployment of solar powered base stations.

1. **Cost savings:** Although solar powered BSs have a high CAPEX (capital expenditure), the OPEX (operating expenditure) is much smaller, leading to cost savings on the long run. Solar powered BSs do not require the laying of cables for grid connections, which reduces the CAPEX and also speeds up the deployment. Also, the cost of solar panels has decreased significantly over the years, with their efficiency increasing every year. The bulk of the savings in the OPEX comes from the cost of energy, specially in areas without grid connectivity where network operators have to rely on diesel generators. The OPEX

for solar powered BSs primarily comprises of the cost of replacing the batteries (required every 2-8 years based on the battery usage pattern).

2. **Greener operation:** The use of a renewable energy source implies that there are no harmful emissions during the operational stage. Consequently, the deployment of solar powered BSs is encouraged by many governments and telecom operators.

3. **Simpler maintenance:** BSs powered by diesel generators have greater maintenance requirements as well as the need to regularly refill the fuel for the generators. In comparison, solar powered BSs have lower maintenance needs and such sites can easily be unmanned.

4. **Greater disaster resistance:** Traditional grid connected BSs fails in the case of extended grid failure. For example, during the 2011 earthquake in Japan followed by a tsunami, more than 6,700 cellular BSs experienced outages [6]. In contrast, solar powered BSs are immune to grid outages and can restore their services faster.

5. **Government regulations and subsidies:** Many countries currently offer subsidies for promoting the use of solar power that can lower the CAPEX of installing solar powered BSs. In addition, some governments are making it mandatory for telecom operators to have a certain fraction of their BSs powered by renewable energy (e.g. in India).

6. **New base stations with low power consumption:** Large macro base stations typically have high power consumption, which in turn requires large solar panel dimensions, thereby making solar powered solutions impractical. However, recent developments in the design

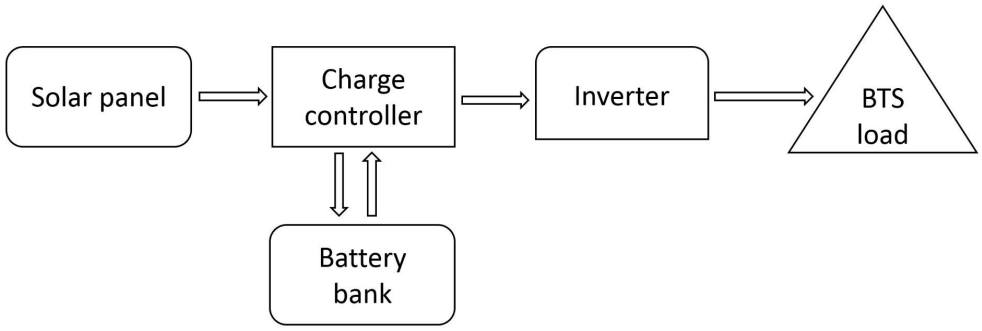

Figure 1.2: Key components of a solar powered base station.

of cellular network infrastructure have resulted in macro base stations that consume around 500-800 W and smaller base stations that consume around 50-120 W, making solar powered BSs a practical alternative to traditional BSs.

1.2 Key components of solar powered BSs

In this section we describe the various components of a solar powered base station, with emphasis on the features that differentiate it from a traditional base station. Figure 1.2 shows a schematic of solar powered BSs. A solar powered BS typically consists of PV panels, batteries, an integrated power unit, and the load (e.g transceivers, cooling equipment etc.) and these are described in detail below.

1.2.1 Base station subsystem (BSS)

Traditional base station:

A traditional base station consumes 0.5-2 kW based on the type. The power consumption of a traditional base station is shared by the radio equipment (power amplifier) which consumes around 65% of the overall power, fol-

lowed by the cooling equipment and base band processing which consumes around 17% and 10%, respectively. Rest of the power is used for the control operations. The cooling is for both the batteries as well as the radio equipment (which is generally done by air conditioners and in some rare cases using an ordinary fan) [1].

Next generation base stations:

In contrast to the traditional base stations, as a result of telecom companies and BTS manufacturers looking for reducing power consumption of the base station, many new models for base stations have been developed which are becoming increasingly popular. For example, Nokia Siemens has introduced flexi BSs which require reduced installation cost and time, are much more compact and lighter, and achieve upto 70% reduction in site power [7]. These base stations can be placed either indoor or outdoor and do not require cooling which contributes a significant part in the power consumption of a traditional BS. Similarly Ericson's soltuion *Tower Tube* has the radio BS placed at a height which gives better coverage, network, capacity and has lower feeder losses [8]. In addition, it is space efficient and does not require air-conditioning. There have been many other similar initiatives like WorldGSM that have developed compact low power consuming base stations specifically designed for rural areas [9].

1.2.2 Photovoltaic panels

Photovoltaic panels are arrays of solar PV cells to convert the solar energy to electricity, thus providing the power to run the base station and to charge the batteries. Photovoltaic panels are given a direct current (DC) rating

based on the power that they can generate when the solar power available on panels is 1 kW/m^2. For example, a PV panel with 8 kW DC rating will produce 8 kW power when the solar power directly falling on it is 1 kW/m^2. Further, a 1 kW PV panel is typically 5 m^2 in area and the lifetime of a typical PV panel is more than 25 years [3]. There are various factors which affect the power produced by a PV panel:

1. DC rating of the PV panel: The solar power generated by a PV panels is directly proportional to its DC rating.
2. Geographic location (or solar irradiation profile) of the site: A site with higher solar irradiation will naturally have more solar energy available for the solar panels, and will thus generate more power.
3. Tilt of the PV panel: The energy harvested by the PV panels also depends on the tilt angle of the PV setup. If not chosen properly, it can lead to reduced energy production. The default value of the tilt angle is generally taken as the latitude of the place.
4. DC-AC loss factor: This comprises of the aggregate of various system losses such as those due to the presence of diodes, losses due to dirt on the PV panel, etc.

The current cost of PV panels is around US$ 1000 for a PV panel with DC rating of 1 kW. Currently PV cells based on mono and poly-crystalline silicon are common in large scale applications and they have an efficiency of around 14-19%. The next generation high concentration solar cells (e.g. based on germanium, gallium arsenide and gallium indium phosphide) have been shown to reach efficiencies of around 40% [10]. This augurs a positive future for solar powered applications with increasing efficiencies and lower costs.

1.2.3 Batteries

Solar powered BSs are equipped with batteries to power them during periods without sufficient solar power, such as nights and bad weather periods. The batteries are charged during the day with the excess energy produced by the solar panels. The cost of batteries forms a significant part of the overall cost of a solar powered BS and thus their lifetime is of critical importance.

The lifetime of a battery depends on the conditions in which it operates, with the depth of discharge (DOD) during each diurnal charge-discharge cycle playing a dominant role. The DOD refers to the percentage of battery capacity that has been discharged expressed as a percentage of maximum capacity. A typical lead-acid battery with a DOD of 60% has an expected lifetime of 1000 charge-discharge cycles (called cycles to failure). In contrast, increasing the DOD to 90% decreases the expected lifetime to 500 charge-discharge cycles. Thus the permissible DOD is one of the important features to be considered in deciding the battery bank capacity of the BS. A larger number of batteries avoids deep discharges thereby increasing the lifetime of the batteries, but increases the capital cost. Since the batteries go through discharge cycles daily, and they may discharge to very low levels in bad weather, deep discharge batteries are preferred in telecom applications.

Various battery types used in cellular BSs and their salient features are listed in Table 1.1 [11]. Among the existing battery technologies, lead-acid batteries are the most popular for solar powered BSs because of their reliability and lower cost. A major disadvantage of lead-acid batteries is that their disposal is not environmental friendly. Though there is ongoing

Table 1.1: Battery Technologies.

Battery Type	Cost ($/kWh)	Efficiency (%)	Max. DOD (%)	No. of cycles (at Max. DOD)	Energy density (Wh/kg)	Self-discharge (%/month)
Lead-acid (conventional)	110-140	75-85	70	500-1000	30	1.5-5
Lead-acid (FLA-VRLA)	140-340	80-90	80	1200-1800	30	1.5-5
Nickel-Cadmium	400-900	70-80	100	1500-3000	50	5-20
Nickel Metal Hydride	800-1200	65-70	100	600-900	80	10-25
Lithium-Polymer	950-1650	90-100	80	600	100-150	2-5
Lithium-Ion	1000-1700	95-100	80	1500-3000	90-150	1-5

research on batteries that are environment friendly, they are not widely used due to cost constraints.

1.2.4 Integrated power unit

The power requirements of a BS include the load offered by the transceiver equipment, cooling, and other miscellaneous loads (e.g. lights). The power supply to these loads as well as the conversion and storage of the harvested solar energy is managed by the integrated power unit (IPU). The IPU in a solar powered BS typically consists of DC-DC and DC-AC power converters, battery charger, charge level monitors and regulators, and a power management unit. The power management unit controls the charging of the batteries and the supply of power to the loads. The DC-DC converters are used to supply power to the transceiver equipment and store the power from the solar panels in the batteries, while the DC-AC converters supply power to the AC loads such as the cooling equipment. The battery charge regulator monitors the battery state and disconnects them from the system when the overall charge goes below a specified DOD (generally 50-80%).

1.3 Configurations for solar powered BSs

Depending on the availability of grid or other power sources, a BS may be powered solely or partially by solar energy. The following configurations are common for solar powered BSs:

1. **Solar stand alone:** The BS is powered solely by solar power and the batteries.
2. **Grid-connected:** The BS is powered by energy harvested from PV panels, but in case it falls short, power from grid is used.
3. **Solar-diesel:** The BS is powered by solar energy, but in cases of prolonged bad weather periods, diesel generators are used to meet the power the BS.
4. **Hybrid:** Such a configuration can include a combination of PV arrays, grid power, diesel generators and other renewable sources such as wind energy to power the BS.

1.4 Current deployment efforts

As of 2014, estimates suggest that there are roughly 42,951 solar powered base stations across the globe and Figure 1.1 shows their distribution across various countries [4]. This section presents some of the ongoing efforts towards the development and deployment of solar powered BSs. Examples of ongoing deployment efforts include:

- **Zong Pakistan:** Zong is a China Mobile owned telecom service provider in Pakistan that has deployed more that 400 solar powered base stations. Many of these BSs are deployed in remote and mountainous

areas that do not have grid connectivity. With electrification rates of approximately 70% and frequent outages, using solar powered BSs is Zong's approach for expanding cellular networks in off-grid and rural regions of Pakistan.

- **Project Oryx:** This is an initiative by the telecom provider Orange and covers various parts of Asia, Middle East and Africa [12]. By the end of June 2011, around 1165 solar BSs were deployed in 17 countries under this project, mainly in Africa. Few examples of these deployments are the solar BSs in countries like Egypt, Kenya and Armenia.

- **Bhutan Telecom Limited (BTL):** BTL has partnered with Vihaan Networks Limited (VNL), an India based telecom equipment manufacturer, to provide cellular connectivity to remote regions of Bhutan that lack infrastructure and have difficult terrain. The deployed solar powered BSs are designed for use in rural areas, with ability to handle hundreds of users (in a range of few kms). These BSs require only between 50-150 W of power and have batteries designed for 3-7 day backup, aimed at providing autonomy during cloudy days.

- **Telkomsel:** Telkomsel is the leading telecom operator in Indonesia and by 2012 had 234 BSs powered by solar energy. An example of their solar powered BS is in Sangatta which requires an average daily power of 26 kW. The BS is powered by 60 solar panels each with a DC rating of 205 W (giving a total rating of 12.3 kW). The BS uses 24 batteries each with rating 2000 Ah thus ensuring autonomy of 4 days.

- **Case study**

  While the examples above only describe a handful of ongoing efforts

at deploying solar powered BSs, a number of other initiatives have been undertaken in emerging telecom markets. To provide a more comprehensive description of a practical deployment scenario, we now present a case study of the initial deployment of solar powered based stations in rural Ghana by the telecom provider Tigo Ghana [13].

In 2012, 60% of the land area and 20% of the population (5 million people) of Ghana had no mobile coverage. The primary reasons for the lack of network access in these areas are: (i) the lack of necessary infrastructure such as reliable grid power and (ii) too low average revenue per user (ARPU) to justify the deployment costs. As an initial step to providing network connectivity in these regions, in 2012, Tigo Ghana partnered with network solutions provider K-NET and telecom equipment manufacturer Altobridge to deploy 10 solar powered base stations. The base stations from Altobridge optimize capacity for rural environments and have substantially lower power consumption than conventional systems. In particular, the deployed BSs use compression techniques so that voice calls require rates of 4 kbps (compared to 14 kbps in conventional systems) and each cell site has an average power consumption of 90 W (compared to 130 W or more). The BSs use satellites for backhaul, have a coverage range of 10 km, and capacity for up to 1500 subscribers. The lowering of costs brought about by the design optimizations has the capability to bring in a return on investment for the operator in less than 24 months, assuming 600 subscribers with APRU of $4 per month. Table 1.2 shows some of the specifications of the solar powered base stations used in this project and the network architecture is shown in Figure 1.3 [14].

Table 1.2: Altobridge altoPod Specifications.

Feature	2G	3G
Frequency Band	GSM 850/900/1800/1900 MHz	UMTS 2100 MHz
Capacity	2 TRX (FR/AMR-HR)	16 sessions (voice or data)
RF power output	+40 dBm (10W)	+40 dBm (10W)
Receiver sensitivity	-108 dBm at 2% BER	-121 dBm at 0.1% BER for 12 kbps
Data throughput	GPRS/EDGE	HSPA (14 Mbps downlink, 5.8 Mbps uplink)
Input volatge	-48V DC	-48V DC
Average power	90 W	90 W
Operating temperature	-30 to + 55 deg C	-30 to + 55 deg C
Cooling	Passive cooling	Passive cooling

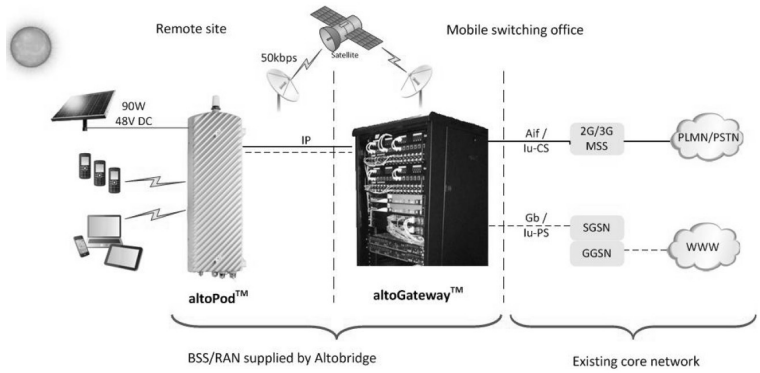

Figure 1.3: Network architecture based on Altobridge hardware.

Currently there are plans to expand to 300 additional sites, some of which have already been implemented.

1.5 Challenges, existing solutions and motivations

This section lists some of the current technical as well as non-technical challenges that stand in the way of widespread deployment of solar powers BSs. We also review some of the existing solutions addressing these issues and the various research gaps which we intend to address in this thesis.

1.5.1 Economic challenges

- **High CAPEX:** Though on the long run solar powered BSs are more economical due to lower OPEX, the initial installation cost is consid-

erably higher. However, technical advances such as more efficient and cheaper solar panels have decreased the CAPEX/TCO (total cost of ownership) ratio by around 40% between 2009 and 2013 [4]. Also, government initiatives such as subsidies given in various countries for the use of renewable energy is effectively reducing the CAPEX and motivating operators to switch to solar powered BSs.

- **Market forces:** Increasingly, the industry's attitude towards green technologies is changing due to the awareness of environmental issues. In addition, some governments (e.g. India) are enacting rules making it mandatory for telecom operators to consider green energy. The market dynamics have also changed with the emergence of an increasing number of companies specializing in developing technologies for renewable energy based, off-grid base stations (e.g. Flexenclosure, VNL, Altobridge).

- **Large BSs:** For base stations whose power consumption is more than 3 kW, solar power is currently not an attractive option due to the large PV panel dimensions required, which in turn require a large area as well as investment for installing them. For example, powering a macro BS with power consumption of 3 kW would require an area of around 180 m^2 for the PV panels. However, larger BSs can still be cost effective, e.g. in the presence of government subsidies, though the payback period is still high (7-10 years) [15].

1.5.2 Geographical limitations

- **Regions with poor solar insolation:** Solar powered BSs are not very attractive options for regions with poor solar insolation. However, in

such regions solar power may be used in conjunction with the grid to power the BSs.

- **Urban deployments:** PV panels should ideally be installed in open areas where shadows from obstructions due to buildings or trees can be avoided. Although such settings are easier to find in rural scenarios, it may be difficult and expensive to procure such sites in urban areas.

- **Long stretches of bad weather:** In areas that are prone to frequent and prolonged periods of bad weather with accompanying cloud cover, the required size of the battery banks is very large. This not only increases the CAPEX, but also increases the possibility of outages during these periods.

1.5.3 Resource provisioning and deployment

- **Resource provisioning:** The successful deployment of a solar powered BS requires meticulous planning to determine the appropriate dimensioning of the PV panels and backup batteries [3, 12]. While over-dimensioning leads to higher than necessary CAPEX, under-dimensioning can lead to frequent outages, thus dissatisfying the customers. Existing works in the literature consider dimensioning the battery size for a given PV panel size, but a framework for evaluating the cost-optimal resource dimensions is missing. To address this open problem, this thesis presents a dimensioning methodology which considers a stand-alone solar powered BS. The resource dimensioning problem seeks to determine the cost optimal PV panel and battery size while satisfying the desired threshold on the energy

outage probability (i.e. the probability that the battery runs out of energy). The cost to be minimized includes the CAPEX as well as the OPEX, which consists of the cost of replacing dead batteries.

Another challenge in the dimensioning the resources for a solar powered BSs is to accurately characterize the solar energy. Inaccuracies in the solar energy model can lead to under-dimensioning which is unacceptable for cellular applications which require a high degree of reliability. Thus, in this thesis, we also propose models which accurately characterize the solar energy.

Dimensioning resources for a solar powered BS include modelling the dynamics between various system parameters like PV panel size, batteries and the base station load. Existing literature does not have any analytic models which integrates the modelling of all these system parameters. We address this issue in this thesis by proposing an analytic model for outage estimation which is further used for resource dimensioning.

- **Choosing a configuration:** Section 1.3 presents the different configurations for solar powered BSs. The choice of a configuration for a given location depends on parameters such as the daily grid-outage period, cost of diesel fuel and generators, location specific solar and wind speed data etc. Based on these information, the overall cost (CAPEX + OPEX) for the different configurations for the desired operational period is computed and the cost-optimal configuration is chosen [5].

- **Deploying small cells:** Small cells BSs have the advantage of reduced transmitter to mobile terminal (MT) distance, reduced transmit power

requirement, higher data rates and low BS power consumption, and are thus an attractive option for increasing network capacity and spectral efficiency [18]. Further, these BSs are typically placed at the cell edges so that the quality of experience of the cell edge users is improved. Due to their low power consumption, they can be easily powered by solar energy.

The main challenges associated with deploying small cell BSs is to determine the number of BSs to deploy and their locations. Given the tradeoff between the outage probability and the number of BSs, recent studies have shown that it is preferable to have more small cell BSs with less energy harvesting (EH) resources rather than few BSs with larger EH resources [19]. Due to the complexity of the problem, the required number of small cell BSs is determined keeping in mind only the desired outage probability, with other parameters (like the macro BSs and their location) kept as fixed. The small cell locations are determined by factors such as the spatial distribution of traffic hotspots and solar insolation.

1.5.4 Operational strategies for resource management

For energy harvesting BSs, the major resources in the network are: the energy harvested by the BSs, the transmission power level at which the BSs choose to operate, and the spectrum available for transmission. Due to the stochastic nature of the traffic intensity and solar insolation, deciding operating strategies for the BSs is a challenging problem. In most cases, weather forecast data and historical traffic models may be required for determining the network's operating conditions. The most widely explored

problems in this context aim to minimize the overall energy consumption of the network through a variety of mechanisms. Existing methodologies for resource allocation and management consider both centralized (where a central server acquires the network state information and periodically updates the resource allocation of the BSs) and distributed mechanisms (where the BSs share information with each other and the MTs to determine the operating conditions). Some of the resource allocation strategies considered in literature are as follows.

- **Load balancing:** While operating the BSs, the operator has to take into account the available energy, the expected harvested energy in the near future, and the traffic load at the BSs, with the objective of preventing the BSs from running out of energy or being over-loaded. To ensure continued coverage, BSs may cooperate by dynamically changing the area covered and traffic handled by each BS, in accordance to the energy available at each BS. There are two main techniques for load-balancing among BSs:

  Base station beacon power control: In this approach the BSs either increase or decrease the power of their beacon signals in order to control the area served by them. This in turn changes the traffic load at the BSs and thus their rate of energy consumption. The problem of optimally controlling the range of the base stations in order to minimize the overall energy consumption, under constraints on the minimum received power at the MTs is NP-hard. Heuristic solutions to the power control problem usually employ greedy algorithms. For example, the algorithm in [20] first obtains the set of BSs with the highest energy depletion rate. For each BS in this set, the beacon power level of each BS is iteratively reduced till the constraint on the minimum

received power at the MTs is violated. This process of choosing the BSs and reducing their power continues till no further decrease is possible.

Although such a scheme benefits the BSs running out of energy by offloading the traffic being served by them to other BSs which are richer in terms of green energy availability, it does not account for the network latency and thus can lead to quality of service degradation.

Dynamic user association: Since the energy consumption of a BS depends on its traffic load, energy-aware load balancing techniques incorporate the BS traffic load and energy availability in the decision rules for determining which BS a MT would attach itself to. In these strategies, MTs periodically obtain the load and energy information from the BSs in their vicinity and then decide which BS to associate with. However, as MTs associate and direct their traffic at the BSs with higher energy levels, these BSs may experience traffic congestion. Consequently, user association strategies that optimize the energy utilization while avoiding congestion have been proposed (e.g. the GALA scheme discussed in [22]).

Schemes such as those mentioned above are solely based on user-association reconfiguration. They more or less re-distribute the traffic among the BSs thus adjusting their power consumption, but do not bring about significant savings in terms of reducing the overall energy consumption in the network. Additionally, the above mentioned schemes consider a snap-shot problem and do not guide in terms of how to allocate the green energy available over time. Thus to address these issues in this thesis we propose a framework which intelligently allocates the green energy over time and uses green energy and delay

aware downlink power control and user association. This is not only capable of reducing the traffic latency but can also bring down the overall energy consumption of the network. We propose such frameworks for both off-grid as well as grid-connected network of BSs.

- **BS on/off strategies:** Switching off BSs is a powerful way of achieving energy savings in a cellular network. Since cellular networks are provisioned for peak-hour traffic, it may be possible to turn off some BSs during off-peak hours while maintaining coverage and quality. Strategies for saving energy by turning off BSs seek to determine the minimum number of BSs required to serve the area, with the desired quality of coverage (e.g. blocking probability, delay) as a constraint. The problem of minimizing the overall energy consumption of a set of BSs, subject to a limit on the load on any BS, is known to be NP-complete [23]. This problem is equivalent to determining the smallest possible set of active BSs subject to the system load constraint. Heuristics for solving this problem centre on greedily assigning MTs to BSs with higher loads so that the number of the BSs that have no associated MTs (and thus can be turned off) is maximized.

  The existing BS on/off schemes suffer from the drawback that they only consider the load at the different BSs whereas the energy availability at the BSs is not considered while making such switching decisions. Further, the energy savings in the BS on/off schemes are brought at the cost of degradation in the quality of service offered to the users (in terms of increase in the traffic latency). In contrast to this, in this thesis we propose a scheme where the energy savings can be brought while simultaneously improving the traffic latency.

- **Energy and spectrum sharing among BSs:** In any cellular network,

the traffic demand and the harvested energy have spatial and stochastic variations which lead to some interesting possibilities regarding resource usage and sharing. To share resources so that outages are minimized or the quality of service (QoS) of users is improved, solar powered BSs may share energy either directly through electrical cables, or indirectly through power-control/load-balancing/spectrum-sharing mechanisms [24]. Energy sharing between BSs may be achieved by two-way energy flows in a smart grid and strategies to develop such sharing mechanisms may be obtained by modelling the system as an energy-trading system. Spectrum sharing in solar powered BSs is motivated by the fact that for a given rate requirement and channel noise (e.g. in an AWGN channel), the transmit power may be reduced by increasing the bandwidth, and vice-versa. The problem of energy and spectrum sharing may also be considered jointly. The sharing strategies may be developed by modeling the system as a convex optimization problem.

- **Coordinated multipoint (CoMP):** In CoMP, BSs cooperate to jointly serve MTs and is particularly useful in combating inter-cell interference (ICI) in dense deployment scenarios, and enhancing network efficiency and overall QoS for users. Implementation of CoMP requires the formation of clusters of transmit points for CoMP transmissions and the allocation of resources to the transmit points. The extent of cooperation and which BSs should cooperate to serve the MTs is decided based on the resources available at the BSs and the decisions are made with the objective to maximize the system performance or to minimize the energy costs. The cluster formation and resource allocation problems are tightly coupled and optimization problems to

solve them jointly generally lead to non-convex formulations.

1.6 Major contributions and thesis outline

Motivated by the above discussion, this thesis addresses two major challenges in deployment and operation of solar powered base stations namely (a) Resource provisioning for solar powered BSs and (b) Developing operational strategies for resource management for a network of solar powered BSs. Chapters 2 and 3 of the thesis focus on developing frameworks for optimally dimensioning resources (PV panels and batteries) for solar powered BSs whereas Chapters 4 and 5 focus on developing operational strategies for resource management for a network of solar powered BSs.

1.6.1 Major contributions

The major contributions of this thesis are summarized as follows.

1. **Markov models for accurately characterising solar energy**

   In Chapter 2 we present a multi-state Markov model to accurately characterise the solar energy. Specifically, we show how accounting for the day-level weather correlations are critical for dimensioning of resources for applications requiring a high degree of reliability. We characterise the days into good weather and bad weather days and the transition between the two day types is modelled as a two-state Markov process. Also given a day type we consider a Markov model for characterising the hourly harvested solar energy. The model can be used to generate synthetic traces of solar energy data which can be used for resource dimensioning. We show the accuracy of the pro-

posed model by comparing the results against those obtained using empirical traces of solar energy and we also show the superiority of the proposed model over an existing model [21]. In Chapter 3 we propose a simpler model for characterising the solar energy where we characterise the days into 3 day types (i.e. good, bad and very bad weather days) and the day level transitions are modelled as a 3 state Markov process. Contrary to the approach in Chapter 2, for simplicity this model uses the average hourly harvested energy profiles for a given day type for dimensioning purposes. The Markov models presented in the thesis provide an insight that it is the series of bad days coming in succession which predominantly contribute to energy outages and thus modelling bad weather days is important for high-reliability dimensioning applications.

2. **Framework for resource provisioning and dimensioning for solar powered BSs and key insights**

   In Chapter 2, we propose a framework for cost-optimal resource dimensioning for solar powered BSs. Also, based on the analysis from the dimensioning we present insights which may be helpful for cellular operators while dimensioning resources for the solar powered BSs. Some key results presented in this context in the thesis include showing how battery lifetime varies with the number of batteries installed at a BS, how outage probability varies with the number of batteries, and insights from PV-battery configurations for a given outage threshold.

3. **Model for energy outage estimation and battery lifetime evaluation for solar powered base stations.**

Using synthetically generated traces of solar irradiation for evaluation of the energy outage probability and battery lifetime associated with a particular configuration of PV panel and battery size (during resource dimensioning) is computationally very intensive. Additionally, using the same does not give insights into the performance of the system. Thus, in Chapter 3, we present a framework which integrates the modelling of solar energy, network traffic and battery levels and can be used to evaluate the energy outage probability and battery lifetime associated with a PV panel and battery size. The proposed model is simple yet accurate and we test its accuracy by comparing against results from empirical solar energy traces, as well as show its superiority over an existing benchmark.

4. **Green energy and delay aware downlink transmit power control and user association scheme for off grid solar powered BSs.**

   Operating a network of stand-alone solar powered BSs has many challenges associated with them. One of the concerns while operating such BSs is to avoid energy outages. One of the ways to avoid energy outages could be by using BS on/off schemes such as those proposed in [23], but using the same can lead to the degradation of quality of service offered to the users being served by the BSs, in terms of its increasing the traffic latency. One of the ways to manage the traffic latency is to apply user-association reconfiguration which accounts for the green energy availability at the BSs and the delay [22]. However, such an approach is not so effective in brining down the power consumption of the BSs as BSs operate at fixed downlink transmit power levels. To address the above-mentioned issues, we propose green energy and delay aware downlink transmit power control and

user association for the solar powered BSs which is directed towards avoiding energy outages, while simultaneously improving the traffic latency. We show the superiority of the proposed strategy over existing state of art strategies. In addition to this, most of the existing works on BSs powered by renewable energy consider a snapshot problem (i.e. solving a problem for a given instant of time) and do not address the issue of green energy allocation over time. We try to address this issues by proposing an intelligent energy allocation algorithm which allocates green energy in proportion to the load expected in a given hour during the day.

5. **Delay aware resource management for grid energy savings in grid-connected solar powered BSs.**

   Careful management of available green energy at the BSs can increase the grid energy savings. However, during this process, the operator has to carefully account for the increase in the traffic latency. In Chapter 5, we propose a framework which jointly manages the grid energy savings and the traffic latency. The framework uses load proportional energy allocation, downlink transmit power control and optimal user association policy. We show that the proposed framework can lead to around 60% grid energy savings and a lower traffic latency as compared to the traditionally existing scheme. We also compare the performance of the proposed framework with the state of art strategies.

1.6.2 Organization of the thesis

The remainder of this thesis is organized as follows. In Chapter 2, we investigate resource provisioning and dimensioning for solar powered BSs.

Chapter 3 proposes a framework for energy outage estimation and battery lifetime evaluation for solar powered BSs and its application to cost-optimal resource dimensioning for solar powered BSs. In Chapter 4, we propose a temporal green energy allocation scheme, and green energy and delay aware downlink power control and user association for stand alone solar powered BSs whereas in chapter 5 we propose these schemes for a grid connected network of solar powered BSs. Chapter 6 concludes the thesis and discusses potential areas of future work.

1.7 Bibliographical note

Parts of Chapter 1 appear in the following magazine paper

- V. Chamola and B. Sikdar, "Solar Powered Base Stations: Current Scenario, Issues and proposed Solutions," *IEEE Communications Magazine,* . 54, no. 5, pp. 108-114, May 2016.

Parts of Chapter 2 appear in the following journal paper

- V. Chamola and B. Sikdar, " A Multi-State Markov Model for Dimensioning Solar Powered Cellular Base Stations," *IEEE Transactions on Sustainable Energy,* vol. 6, no. 4, pp. 1650-1652, 2015,

and the following conference papers

- V. Chamola and B. Sikdar, " Resource Provisioning and Dimensioning for Solar Powered Base stations", *Proc. IEEE GLOBECOM,* Austin, USA, Dec. 2014,
- V. Chamola and B. Sikdar, "Dimensioning Stand-Alone Cellular Base Station using Series-of-Worst-Months Meteorological Data," *Proc. IEEE ICCS*, Macau, Hong Kong, Nov. 2014,
- V. Chamola and B. Sikdar, "Synthetic Generation of Hourly Solar Irradiance Using a Multi-State Markov Model," *Proc. IEEE/IEIE ICEIC*, Singapore, Jan 2014.

Parts of Chapter 3 appear in the following journal paper

- V. Chamola and B. Sikdar, "Power Outage Estimation and Resource Dimensioning for Solar Powered Cellular Base Stations," *IEEE Transactions on Communications,* Preprint online, pp. 1-12, July 2016 (DOI: 10.1109/TCOMM.2016.2587285)

and the following conference papers

- V. Chamola and B. Sikdar, "Outage Estimation for Solar Powered Cellular Base Stations," *Proc. IEEE ICC*, London, UK, June 2015.
- V. Chamola, P. Narang and B. Sikdar "Battery lifetime estimation for Solar powered Base Stations," *IEEE Symposium on Emerging Topics in Smart and Sustainable Grids*, Singapore, Sept. 2016.

Parts of Chapter 4 appear in the following journal papers

- V. Chamola, B. Krishnamachari and B. Sikdar, "An Energy and Delay Aware Downlink Power Control Strategy for Solar Powered Base Stations", *IEEE Communications Letters*, vol. 20, no. 5, pp. 954-957, May 2016.
- V. Chamola, B. Krishnamachari and B. Sikdar, "Green Energy and Delay Aware Downlink Power Control and User Association for Solar Powered Base Stations," *IEEE Systems Journal* (Under second round of review).

Parts of Chapter 5 appear in the following journal paper

- V. Chamola, B. Sikdar and B. Krishnamachari, "Delay Aware Resource Management for Grid Energy Savings in Green Cellular Base stations with Hybrid Power Supplies,", Accepted for publication in *IEEE Transactions on Communications*.

and the following conference paper

- V. Chamola, P. Narang and B. Sikdar, "Downlink Power Control for Latency Aware Grid Energy Savings in Green Cellular Networks," *Proc. 37th IEEE Sarnoff Symposium*, NJ, USA, Sept. 2016.

Chapter 2

Resource Provisioning and Dimensioning for Solar Powered Base Stations

2.1 Introduction

One of the challenges while deploying a solar powered BS is to appropriately provision resources for harvesting and storing the solar energy. The resources available at the BS for the harvesting and storage of solar energy are PV panels and batteries, which are installed at the BS site. These resources have to be appropriately dimensioned. Over-dimensioning of these resources can lead to un-necessarily high cost of deployment, whereas under-dimensioning can lead to frequent outages which leads to customer dissatisfaction. Taking into account these two aspects, the cellular operator has to carefully provision the resources.

To address this issue, in this chapter we consider the problem of cost-

optimal resource dimensioning for an off-grid solar powered BS. We begin by describing the power consumption of the base station and the solar energy and battery resources used to harvest and store solar energy. We describe the procedure for obtaining the solar energy harvested at a given site and the model for evaluating battery lifetime. For a given PV panel and battery size, we describe the methodology for evaluating the outage probability associated with that resource configuration. The outage probability is evaluated by simulations using long duration traces of BS power consumption and the solar energy. Note that in context of this thesis, we use outage probability to indicate the energy outage probability. Energy outage is defined as an event where the BS does not have enough energy at its disposal and is thus shut off. Next, having obtained the outage probabilities associated with different PV panel and battery configurations, we formulate the problem of cost-optimal resource dimensioning. As described in the introduction to the thesis, we observe the need to accurately model solar irradiation as an important step in dimensioning a solar powered BS. Thus, next we present a multi-state Markov model to characterize the solar energy for a given location. The proposed multi-state Markov model can be used to generate long duration synthetic traces of solar energy data. We use these solar energy traces in the framework for determining the outage of the base station to address the cost optimal PV-battery dimensioning problem for the BS. We compare the cost optimal PV panel and battery dimensions predicted using the solar energy traces generated from our multi-state Markov model with the results predicted through dimensioning using empirical data to verify our model and also show its superiority in dimensioning over results using an existing benchmark model [21]. We also present some key insights into resource dimensioning from the above mentioned analysis.

The rest of this chapter is organized as follows. Section 2.2 presents the literature review. Section 2.3 presents the system model. Section 2.4 presents the system resources and the methodology for outage estimation. Section 2.5 formulates the problem of cost-optimal resource dimensioning. Section 2.6 presents the proposed multi-state Markov model for characterising the solar energy. Section 2.7 presents the numerical results for the dimensioning of resources as well as the key insights from the analysis, while Section 2.8 concludes the chapter.

2.2 Literature review

With the increasing focus on green energy, there have been a number of works that deal with the problem of dimensioning resources for reliable performance of solar powered systems. Guidelines for dimensioning resources for solar powered systems are presented in [25, 26] while [27] proposed the use of the probability of loss of power supply as a reliability index in dimensioning problems. In [28]-[32] the authors propose methodologies for dimensioning of battery size based on the number days of autonomy (i.e. number of consecutive days for which the battery should be able to power the system even if there is no solar energy harvested). The size of the PV panels in such an approach is chosen such that with the average solar irradiation of the worst weather month, the PV panels are able to harvest energy equivalent to the daily average power consumption. The storage dimensions in this method are determined by the product of the days of autonomy and the average daily power consumption. While such methods are simple and provide a rough approximation, they have a number of disadvantages: the solution provided is not necessarily cost-optimal,

the designer has to decide the days of autonomy which requires experience, and it does not provide any guarantees on the outage probability.

The problem of dimensioning of resources for solar powered systems specifically targeting cellular BSs is considered in [3, 34]. The dimensioning in [3, 34] is done through simulations by using long-term solar irradiation data (either real or synthetically generated). However these works do not consider the problem of cost-optimal dimensioning for the solar powered base stations. Thus in our work we address this issue by proposing a framework for cost-optimal resource dimensioning for solar powered BSs.

A critical input that determines the accuracy of the dimensioning results is the solar irradiance data. While historical long-term solar irradiance data is available for certain places, such data is usually not available for much of the developing world where the lack of reliable grid power makes solar powered systems more important. It is noteworthy that many researchers (e.g. [3, 36]) and commercial softwares (e.g. HOMER [37]) use typical meteorological year (TMY) data for dimensioning resources to avoid using long term solar irradiation data. TMY data consists of hourly meteorological data for twelve months and is synthetically generated using long term meteorological data [38]. Since it is generated using long term data and uses averaging of various parameters, bad weather days are reduced in TMY data as compared to real statistical data, thereby leading to more optimistic dimensioning. Thus TMY data is not very suitable when it comes to developing stand-alone systems for telecommunication applications which have strict reliability requirements [39]. Thus there is a need for models which can accurately characterize the solar energy at a given site.

Existing approaches to model the daily/hourly solar irradiance include Markov models [40, 41], autoregressive moving average (ARMA) models

[42] - [44], and models based on artificial neural network approach [45, 46]. The Markovian approach assumes the solar irradiance at a given time (either day or hour) to be dependent only on the solar irradiance at the last time unit. Further, daily or hourly transition statistics are derived to characterise the transition from one solar irradiance level to other. The ARMA approach uses autocorrelation between consecutive days to capture the nature of the solar radiation. The artificial neural network method for characterizing solar irradiance has been developed in the recent past [46]. However, their applicability is for the prediction of solar irradiance based on past observations, and they require long term solar data for training.

It has been shown that Markov models perform better than ARMA models [47, 48]. While most Markov models focus on daily irradiance levels, some models exist for modelling the hourly solar irradiation [21] [48]. However, they lack accuracy since they do not consider the day to day correlations in the solar irradiance. To address this issue, in this chapter we propose a Markov model which captures the solar irradiance characteristics both on an hourly as well as on a daily scale. The proposed model can be used to generate synthetic traces of solar energy data which can be used for resource dimensioning of the solar powered BSs.

2.3 System model

For dimensioning resources for a solar powered base station one requires traces of base station power consumption and the solar energy that can be harvested. Additionally, one needs to understand how the battery lifetime is affected by the charging-discharging patterns that a battery goes through. In this section we describe the methodology for generating traces of BS

power consumption which have been used for dimensioning resources in this chapter. We also present the details of how the solar energy data used in this chapter is obtained and the model adapted to evaluate the battery lifetime.

2.3.1 Base station power consumption

The base station power consumption comprises of two parts: a fixed part which is due to air conditioners, losses in cable feeders etc. and a variable part, which depends on the instantaneous traffic load being handled by the base station. We consider a Long Term Evolution (LTE) macro BS, the power consumption for which is given by [49]

$$L(t) = \mathrm{Y}_{TRX}(P_0 + \Delta K(t) P_{max}), \quad 0 \leq K(t) \leq 1 \tag{2.1}$$

where Y_{TRX} denotes the number of transceivers, P_0 denotes power consumption at zero traffic, Δ denotes slope of load dependent BS power consumption, $K(t)$ is the normalized traffic at time t and P_{max} is the power amplifier output at maximum traffic. Example values of P_0, Δ and P_{max} for a macro BS are 118.7 W, 2.66 and 40 W respectively [49].

The traffic load at a cellular BS consists of a mix of voice and data. Both voice and data traffic show diurnal patterns where the traffic peaks are reached during certain hours of the day and lower levels at nights [50, 51, 52]. In addition, the traffic levels during weekends are lower than weekdays. Given the similarity in their profile, for illustrative proposes we consider a case with only voice traffic and note that the extension to scenarios with data traffic is similar. In addition, we note that off-grid BSs are primarily being deployed in the African and Asian continents due to their

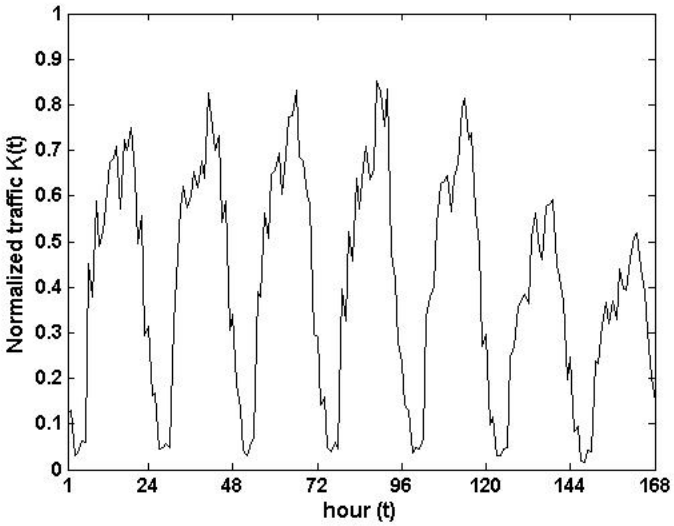

Figure 2.1: Normalized traffic at a BS for a week.

lack of reliable grid-connectivity, and the traffic served by the BSs in these locations is still primarily voice [54].

To model the traffic being served by the BS, we use call based models as proposed in [55] where the call arrival process is Poisson and the call durations are exponentially distributed. Based on this model, calls are generated on a per-minute basis with rate depending on the hour of the day, with average call duration of two minutes [56]. The normalized traffic at a given time, $K(t)$, is obtained by normalizing the instantaneous number of active calls by the maximum number of calls the base station can support. This calculation assumes that at a given point of time, every active voice call utilizes the same amount of radio resources of the BS (and hence equally contributes to the traffic at the BS at that given time instant). The normalized traffic is obtained on a minutely basis (i.e. with a sampling interval of 1 minute) using the above model. However, for simplicity of analysis we consider the average normalized traffic and corresponding BS power consumption on a hourly time scale (i.e. the average value of the traffic during the different minutes in the hour is taken as the traffic value for that hour,

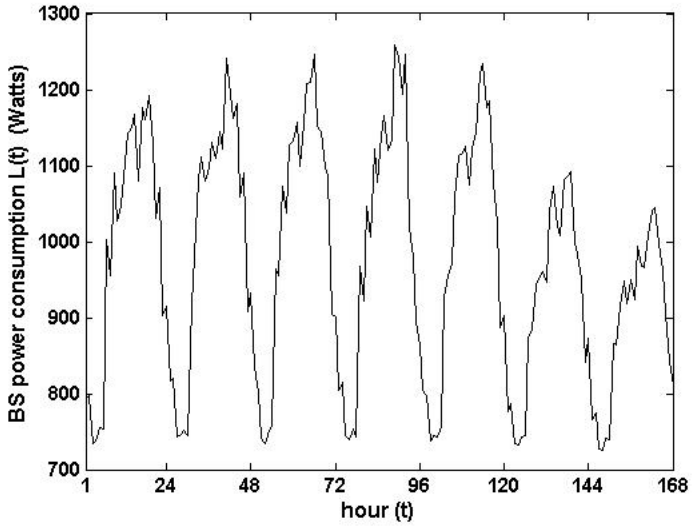

Figure 2.2: BS power consumption for a week.

which is further used to evaluate the power consumption for that hour). Figure 2.1 shows the hourly normalized traffic generated using the above model for a period of one week. The hourly average value of $K(t)$ is used in Equation (2.1) to calculate the average BS power consumption during a given hour.

The above mentioned model can be used to generate traces of hourly BS power consumption for any arbitrary time duration. In such traces, the BS power consumption at time t (where t is the time (in hour) from the beginning of the time-series) is denoted by $L(t)$. An example of the hourly base station power consumption profile for different days in a week is shown in Figure 2.2.

2.3.2 Solar energy resource and batteries

For modeling and evaluation, we use statistical solar irradiation data from the National Renewable Energy Laboratory (NREL), USA [57]. The weather data files are fed into the System Advisor Model (SAM), a tool developed

by NREL which gives the hourly solar power generation for a PV panel with a given rating [58]. We use 10 years of solar data for a given location. For PV panels, we assume default values for the DC-AC loss factor (assumed to be 0.77) and the tilt of the PV panels (assumed to be the latitude for the given location) [59].

We assume that the BS uses lead acid batteries for charge storage due to their popularity and cost advantages over other storage options. The operating conditions of a battery strongly influence the lifetime of a battery and discharging it to very low values can significantly reduce its lifetime. To calculate the battery lifetime, we use a model based on the number of charge cycles to failure for different values of the depth of discharge (DoD) [60]. DoD is defined as the lowest level a battery hits in a given discharging-charging cycle. For modeling the battery lifetime, the entire range of DoD (0-100) is split into M regions. Then, for the operating period (say T years), the number of cycles corresponding to each DoD region is counted. The battery lifetime, L_{Bat} is then

$$L_{Bat} = T/(\sum_{i=1}^{M} \frac{Z_i}{CTF_i}), \tag{2.2}$$

where Z_i is the number of cycles with DoD in region i, and CTF_i is the cycles to failure corresponding to region i [60]. The relationship between the DoD and cycles to failure is generally provided by the battery manufacturer [61] and Figure 2.3 shows the characteristics for a typical lead acid battery [61]. For simplicity we neglect the degradation with time in the PV panel and battery efficiency. Also as the PV panels and batteries are at the BS location, we neglect the leakage in the transmission of energy between the PV panel and the batteries.

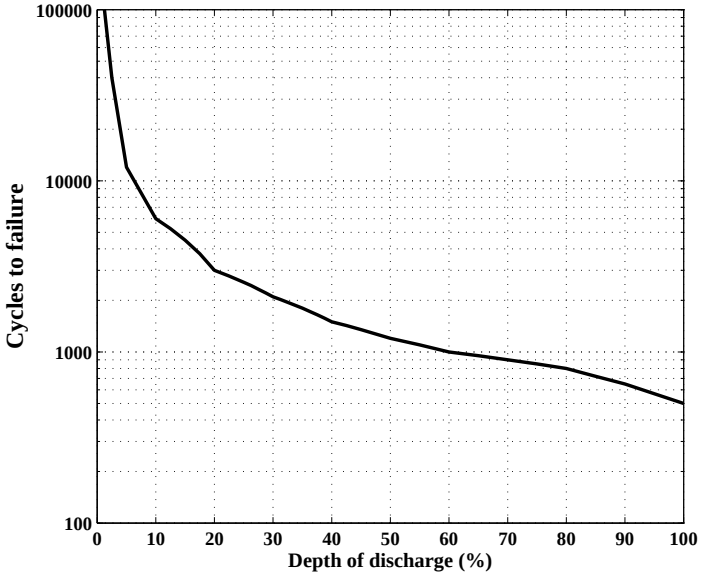

Figure 2.3: Cycles to failure vs DoD for a typical lead acid battery.

2.4 System resources, outage estimation and battery lifetime estimation

Given n_{PV} number of PV panels installed in the BS site, each with DC rating E_{panel}, the overall DC rating of the PV panels for the site, PV_w, is given by

$$PV_w = n_{PV} E_{panel}. \tag{2.3}$$

Similarly, for n_b batteries installed, each with capacity given by E_{bat}, the battery bank capacity B_{cap} is given by

$$B_{cap} = n_b E_{bat}. \tag{2.4}$$

For a particular combination of PV_w and n_b, the outage probability can be calculated by using the energy produced by the PV panels (which depends

on the solar insolation profile at that location), BS power consumption (which is traffic dependent), and the battery charge/discharge dynamics under the influence of the two previous factors. In this work we analyze the solar energy resource, base station power consumption and the energy stored in battery bank on an hourly basis.

For outage and battery lifetime estimation, we require traces of solar energy generated and traces of the BS power consumption. To obtain traces of solar energy generated, the solar irradiation data from NREL is processed through the SAM tool as described in Section 2.3.2. This provides traces of solar energy generated for a solar panel with DC rating of 1 kW. We denote the solar energy generated at time t (where t is the time (in hours) from the begining of the trace) as $S(t)$. For a PV panel with rating PV_w, the energy generated at time t, $\mathcal{E}(t)$, can be expressed as

$$\mathcal{E}(t) = PV_w S(t). \tag{2.5}$$

The model described in Section 2.3.1 is used to generate traces of hourly BS power consumption. In such traces of BS power consumption, we use $L(t)$ to denote the BS power consumption at time t.

We assume that batteries are initially fully charged. To avoid deep discharges which adversely affect the battery life, we disconnect the battery from the system when the overall charge level goes below νB_{cap}. Here ν is the fraction of battery capacity below which the battery is dis-allowed to discharge to avoid battery degradation. We denote the battery level at the end of hour t by $B(t)$. Based on these parameters, the estimated state of the battery power at a given time, B_{est}, is given by

$$B_{est}(t) = B(t-1) + \mathcal{E}(t) - L(t). \tag{2.6}$$

As we have constraints on the battery level which is bound by the limits of battery capacity and minimum state of charge (i.e. νB_{cap}), the battery level at a given time is thus given as

$$B(t) = \begin{cases} B_{cap} & B_{est}(t) \geq B_{cap} \\ B(t-1) + \mathcal{E}(t) - L(t) & \nu B_{cap} < B_{est}(t) < B_{cap} \\ \nu B_{cap} & B_{est}(t) \leq \nu B_{cap} \end{cases} \tag{2.7}$$

with $B(0) = B_{cap}$.

Note that as accounted above, the batteries are not allowed to discharge below νB_{cap} and if the battery level tends to go below that, the batteries are disconnected and the BS is shut down until there is sufficient solar energy harvested to power the BS (and additionally to charge the batteries above that level). Such an occurrence corresponds to energy outage as the BS has shut down due to lack of sufficient energy to operate it.

Telecom operator desire to avoid such energy outages and thus want that the probability of occurence of outage to be very low. In existing literature the outage probability is often captured in terms of the percentage of days during the operational time when such energy outages happen [27], [62]. Thus we consider the outage probability, denoted by Ω, to be given by

$$\Omega = \lim_{D \to \infty} \frac{D_{outage}}{D} \tag{2.8}$$

where D_{outage} is the number of days that have an energy outage and D is the total number of days of operation. Note that although to get an accurate

estimate of the outage probability ideally we require the total number of days D $\rightarrow \infty$. However, in real life scenario we approximate it considering a reasonably large number of days for the outage probability evaluation (e.g. of the order of days in a year or more). The methodology adopted for evaluating the outage probability is explained in the remark at the end of this section.

The battery level values during the different hours (obtained using the operations in Equation (2.7)) can be used to evaluate the battery lifetime L_{Bat}. The methodology for evaluating the battery lifetime was explained in Section 2.3.2 where Equation (2.2) is used to find the value of battery lifetime.

2.5 Cost optimal dimensioning

This section presents a formulation for the cost optimal PV panel and battery dimensioning problem for a solar powered BS. The cost of the system depends on the size of the PV panel and the number of batteries required over the system lifetime. For any given values of PV_w and n_b, the cost also depends on the battery lifetime associated with that configuration. For a target system lifetime of T_{run} years, the total system cost, C, is given by

$$C = N_{Bat}C_B + PV_wC_{PV} \tag{2.9}$$

where C_B is the cost of one battery and C_{PV} is the cost of PV panel per kW. N_{Bat} represents the total number of batteries required over system lifetime of T_{run} years and is given by

$$N_{Bat} = n_b \left\lceil \frac{T_{run}}{L_{Bat}} \right\rceil \tag{2.10}$$

where n_b is the number of batteries powering the base station at any given point in time and L_{Bat} is the battery lifetime for the given PV wattage (PV_w) and number of batteries (n_b).

The cost optimal resource dimensioning problem is then given by

$$\begin{aligned} \underset{PV_w, n_b}{\text{minimize}} \quad & N_{Bat}C_B + PV_wC_{PV} \\ \text{Subject to:} \quad & \Omega < \lambda \end{aligned}$$

where λ is the network operator's specified limit on the tolerable outage probability. Note that PV_w (the PV panel size) and n_b (the number of batteries installed at the BS) are the optimization parameters. The framework to evaluate the outage probability (Ω) corresponding to a certain configuration of PV panel and number of batteries installed at the BS has been already presented in former part of the chapter (Section 2.4) and all one needs to do is to check which PV panel-Battery size configuration has minimum cost while meeting the outage constraint.

Note that in our work we do not have any mathematical expression capturing the functional relationship between the optimization variables and the constraint. However, there is a close functional relationship between the optimization parameters and the outage probability. For example if one increases the PV panel size or number of batteries, generally one can expect the outage probability to reduce by doing so. To solve the optimization problem we propose the following steps

1. We start by assuming a PV panel with rating of 1 kW and evaluate the minimum number of batteies required to ensure that the outage probabiity is below λ. This process is then repeated as the PV panel size is increased in steps of E_{panel}. E_{panel} has been described in Sec-

tion 2.4 and has been taken as 0.5 kW for the results in this chapter. The PV-Battery configurations from this exercise are the prospective configurations to be considered for solving the cost-optimal dimensioning problem. Note that for very low PV panel dimensions (e.g. < 9 kW), generally the number of batteries required to ensure the outage probability below λ (when a realistic value of λ i.e. $\lambda < 1\%$ is taken) is very high, thus increasing the cost associated with the configuration and thus they generally do not turn out to be solution for the cost optimization problem. Also, for large PV dimensions, as one evaluates the minimum number of batteries required to ensure $\Omega < \lambda$, one can observe that after a certain point increasing the PV panel size does not reduce the number of batteries required. Thus, one no longer needs to evaluate the number of batteries required for further configurations of PV panels (since such configuration have a larger PV panel size and it is possible to meet the tolerable outage with the same number of batteries and a smaller PV panel).

2. The battery lifetime associated with the PV-Battery configurations obtained in the previous step is evaluated and the cost associated with each of these configurations is computed using Equation (2.9).

3. The configuration with the lowest cost is chosen as the solution for the cost-optimal resource dimensioning problem.

Note that the parameters used in our modeling and dimensioning framework may change over time. Traffic volumes tend to increase with time while the efficiency of hardware such as PV panels decreases [64, 65]. Since cellular network infrastructure is deployed with an intended lifetime of multiple years, it is standard practice during cellular network planning and deployment to account for forecasts of the expected rise in traffic and

other parameter changes. Thus in the proposed dimensioning framework, the projected traffic at the end of the system lifetime may be used for modeling the system load. Similarly, the projected efficiency of the PV panels may be used to compute the harvested energy and classify the day types. Note that this approach means that the system will be over-provisioned during the initial years of operation. If the network operator desires to avoid such over-provisioning, an alternative is to repeat the dimensioning exercise every few years and install additional PV panels and batteries as needed.

2.6 Multi-state Markov model for characterising hourly harvested solar energy

In this section we describe our proposed multi-state Markov model [16, 63] to characterize the hourly solar energy harvested at a given location. The multi-state Markov model is based on a model that combines daily correlations in weather conditions affecting the solar irradiation with finer-grained, hourly transitions in solar irradiance levels. Using the proposed model for solar energy, one can generate synthetic traces of solar energy harvested which can be used for resource dimensioning.

2.6.1 Model description

The PV panels harvest solar energy during the daytime. While part of the harvested energy is used to supply the instantaneous power demand of the BS, the excess energy is stored in the battery bank. During the time of low or no solar energy which may be either due to bad weather or at night, the

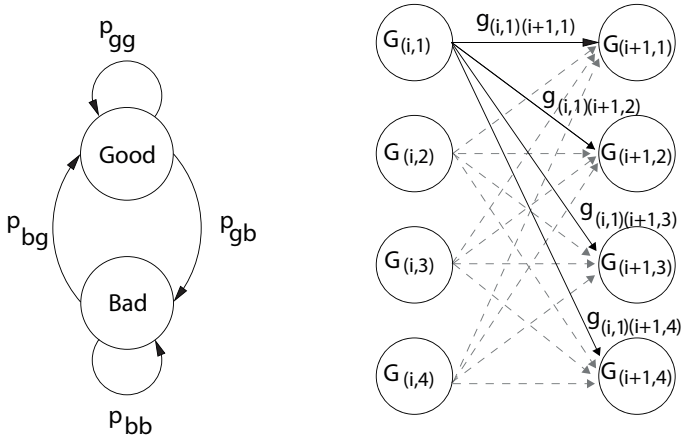

Figure 2.4: (Left:) Transition between good and bad days. (Right:) Hourly transition in a good day.

BS is powered by the batteries. The BS load profile and the solar energy profile play key roles in dimensioning the PV panel and battery resources. We assume that the telecom operator has a model for the load profile as well as the historical data to characterize the solar energy profile for a given location.

It has been shown in previous work that the solar energy profile of any location may be modelled as a Markov process [21, 48]. This work refines such models by proposing a multi-state Markov model for the solar energy resource. In the proposed model, any day is classified as either a "good" or a "bad" weather day based on the level of energy that is harvested. For example, sunny days would be classified as good days. The fraction of all days that are classified as bad is denoted by ξ. Given that a day is either good or bad, the next day may be either good or bad, depending on the weather conditions. To capture the occurrence of consecutive good or bad weather days, the transition is modeled as a two-state, discrete time Markov process (as shown in Figure 2.4 (Left)). The transition probability

matrix of this Markov process is given by

$$\mathbf{T} = \begin{bmatrix} p_{gg} & p_{gb} \\ p_{bg} & p_{bb} \end{bmatrix} \tag{2.11}$$

where p_{gg} (resp. p_{bb}) is the probability of transition from a good (bad) day to a good (bad) day, and $p_{gb} = 1 - p_{gg}$ (resp. $p_{bg} = 1 - p_{bb}$) is the probability of transition from good (bad) day to bad (good) day.

Next, to capture the hourly variations in the solar energy, we categorize each hour to belong to one of four possible regions. Each region is characterized by its energy level and the four regions for each hour of good and bad days are different. The overall state of the process representing the solar energy harvested at any time t is denoted by

$$S_t : S_t \in \{G_{x,y}, B_{x,y}\}, \qquad x \in \{1, 2...24\}, y \in \{1, 2, 3, 4\} \tag{2.12}$$

where G and B correspond to the state of solar energy for the good and bad weather days respectively, x is the hour of the day and y denotes the region of the solar energy for that hour. Each state has a corresponding solar energy value which is the average hourly solar energy in that state as obtained from the empirical data, and is denoted by E_{S_t}. An example of the four regions for each hour of good and bad weather days is shown in Figure 2.5 and the methodology for obtaining the values of E_{S_t} and the other parameters used in our model is described in Section 2.6.2. Please note that in Figure 2.5 (left), we show $G_{12,1}$ which indicates that the solar energy state corresponds to a good day type (indicated by the use of G in $G_{12,1}$), the hour number is 12 ($x = 12$) and the region of solar energy within the hour is 1 ($y = 1$).

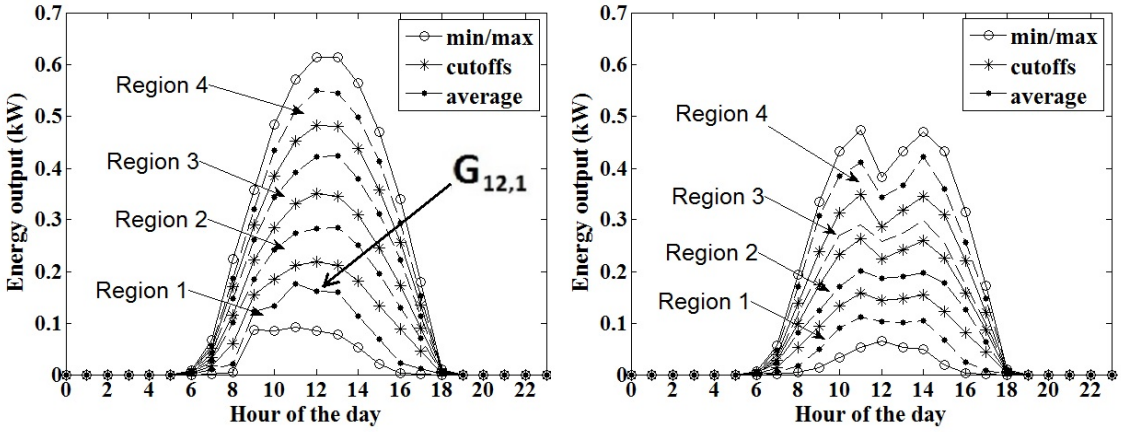

Figure 2.5: Analysis for (Left) good day (Right) bad day

Remark: Note that while more than four states may be used to categorize any hour of the day, our experimental results show that the marginal improvement in accuracy by including additional states does not justify the increased complexity of the model. Also our experimental results showed that when less than four states are used to characterize the hourly solar energy, there is significant loss of accuracy in the subsequent outage estimation using the traces thus generated. Additionally, note that the multi-state Markov model can be used to generate long-duration traces of solar energy data to be used for resource dimensioning. In the time series of data generated using the model, t denotes the time (in hours) of a particular entry in this data from the begining of the time-series. S_t denotes the state of the solar energy at time t (in hours). Please note that t may vary from 1, 2, $\cdots, \infty$ based on the number of days under consideration; whereas x just denotes the hour of the day for that time. Say we generate 3000 days worth of data using the proposed model and let us consider time $t = 4000$ (i.e. the 4000^{th} hour in the time series). This time corresponds to the 16^{th} hour on the 167^{th} day. Thus, for this hour we have $x = 16$. Now, if the 167^{th} day turns out to be good day type and the solar irradiation during the 16^{th} hour belongs to the 4^{th} region, then the state for this time is denoted by

$G_{16,4}$.

According to the Markovian assumption for the solar energy, the state of solar energy at any hour only depends on the state of the solar energy in the previous hour and the transition probability of going from the previous state to the current state. Thus,

$$P[S_t|S_{t-1}, S_{t-2}, ...S_0] = P[S_t|S_{t-1}]. \tag{2.13}$$

Given that the solar energy is currently in a given state, in the next hour, the state may transition to any of four states in the next hour (for both bad and good weather days). This Markov process has been depicted in Figure 2.4 (Right). For a good weather day, the transition probability matrix is given by

$$\mathbf{G} = \begin{bmatrix} g_{(1,1)(1,1)} & \cdots & g_{(1,1)(24,4)} \\ \vdots & \ddots & \vdots \\ g_{(24,4)(1,1)} & \cdots & g_{(24,4)(24,4)} \end{bmatrix} \tag{2.14}$$

with

$$g_{(i,j)(k,l)} = \begin{cases} r_{(i,j)(k,l)} & k = (i) \bmod 24{+}1;\ j,l \in \{1,2,3,4\} \\ 0 & \text{otherwise} \end{cases} \tag{2.15}$$

where $g_{(i,j)(k,l)}$ is the probability of transition from the j-th region in the i-th hour to the l-th region in k-th hour on a good weather day. Note that from a particular region in a given hour, the solar energy can just go to one of the regions in the next hour. $r_{(i,j)(k,l)}$ denotes the numerical value of the transition probability and satisfies

$$\sum_{l=1}^{4} r_{(i,j)(k,l)} = 1, \qquad k = (i) \bmod 24{+}1, j \in \{1,2,3,4\}. \tag{2.16}$$

The transition probability matrix for a bad weather day is defined similarly.

The solar energy model defined above provides the solar energy harvested by a 1 kW PV panel at any given point of time. Thus the solar energy harvested by a PV panel with capacity PV_w for a given state S_t of the solar energy at time t is given by

$$\mathcal{E}(t) = PV_w E_{S_t}. \tag{2.17}$$

2.6.2 Parameter estimation

To obtain the parameters for the model described above, we use historical data of solar energy, such as that provided by NREL. Due to seasonal variations, different months in the year have different values for the various parameters in the model. To find the parameters for a given month, we consider the series of data corresponding to the days of that particular month from all years in the historical solar energy data. This data is then fed to the SAM tool [17] developed by NREL to generate the hourly harvested solar energy by a PV module with DC rating 1 kW. The daily solar power output for each day in a given month is computed and the days are sorted as per the total power generated in the day. ξ fraction of the days with the lowest energy are termed " bad " days while the remaining are termed "good" days. The data is then used to calculate the transition probabilities of going from a bad day to bad day, and good day to good day, in order to obtain the transition probabilities p_{gg}, p_{gb}, p_{bb} and p_{bg} for Equation (2.11).

To obtain the average energy harvested in each of the four possible regions of each hour, we first analyze the data to record the hourly minimum and

maximum values of solar energy generated for both good and bad weather days (Please refer Figure 2.5). The space between the minimum and maximum solar energy generated for each of these hours is divided by defining cutoffs that uniformly partition the space into four regions. Each of the four regions specifies a state of solar energy at that hour and the average hourly solar energy in each of those states is then obtained from the empirical data.

2.6.3 Resource provisioning and dimesnioning using multi-state Markov model for solar energy

The multi-state Markov model described in the previous section can be used to generate long duration traces of harvested solar energy for a given location which can be further used for the dimensioning of solar powered BS. The solar energy harvested by the BS at time t is denoted by E_t and is given by Equation (2.17).

Recall that in Section 2.4 we described the system model for PV panel size and battery dimensioning. We use the framework described there but now instead of using the empirical data of the harvested solar energy (from the NREL website), we use the harvested solar energy traces generated from our multi-state Markov model. To show the accuracy of the multi-state Markov model as well as this dimensioning approach, we compare the various statistical results relating to the PV panel and battery sizing from harvested solar energy traces from our model against those obtained using empirical traces. These results have been presented in the following subsection.

2.7 Numerical results

In this section we present the numerical results for the dimensioning of resources for the solar powered BSs. We also validate the accuracy of the proposed multi-state Markov model for characterising the solar energy by comparing the results obtained using the same against those obtained using empirical solar energy traces. We also show its superiority over an existing benchmark model [21].

For simulations, we consider a LTE base station system with 10 MHz Bandwidth and 2×2 Multi Input Multi Output (MIMO) configuration with capacity to support 300 calls at any given time instant. We assume 3 sectors for our macro BS, each with 2 transceivers, thus giving us $Y_{TRX} = 6$. We model the traffic using the methodology described in Section 2.3.1. We consider call arrival rates during the different hours for different days as shown in Figure 2.6. Note that the traffic on weekends is lower than that on weekdays (which has been shown in large scale cellular traffic studies like [50], [53]). Additionally, as described in Section 2.3.1, we assume the average call duration of two minutes [56]. We assume E_{panel} as 0.5 kW. We assume that the BSs use 12 V, 205 Ah flooded lead acid batteries, each having a rating 2.46 kWh. ν, the fraction of total battery capacity below which the battery is dis-allowed to discharge has been taken as 0.3. To validate the methodology presented in herein, we consider two locations: Kolkata (India) and Miami (USA). The solar data for these locations was obtained from the NREL database and used in the SAM tool to obtain hourly values of the solar power generated. The various parameters for the solar energy model are obtained using the statistical solar energy data from NREL database and the methodology described in Section 2.6.2. We used $\xi = 0.15$ for both

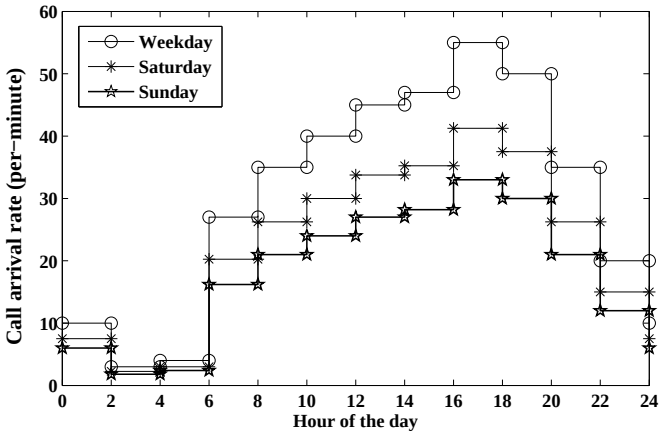

Figure 2.6: Call arrival rate considered during the different hours of the day.

the locations. We use seven years of data (2000-2006) for parameter estimation and evaluate the performance using data for years 2007-2009. For the cost-optimization problem we choose two values of λ (the threshold outage probability) as 0.5% and 1%.

Following is a brief description of how the results are obtained using the above-mentioned information.

- For the proposed multi-state Markov model and the model proposed in [21], we estimate the various modeling parameters using the solar energy data for year 2000-2006. After obtaining these parameters, the multi-state Markov model and the model in [21] are used to generate solar energy data for 50 years. For results using empirical solar energy traces, we consider the solar energy data for 3 years (2007-09). A different year range is taken for estimating the modeling parameters for the proposed model (as compared to that used to obtain resuts with empirical solar energy traces) to avoid using the same dataset for model-training and evaluation.

- The traffic model proposed in Section 2.3.1 is used to generate long-duration traces of BS traffic which further gives the BS power con-

sumption traces for the outage probability evaluation. For the results using empirical solar energy traces, we generate 3 years worth of hourly BS power consumption data using the methodology presented in Section 2.3.1. For the results using the proposed multi-state Markov model and the model in [21], BS power consumption for 50 years is generated.

- With the solar energy data and the BS power consumption for the various methodologies in place, we can use the framework proposed in Section 2.4 to estimate the outage probability for different configurations of PV panel size and the number of batteries.
- As our ojective is to find the cost-optimal PV panel and battery configuration, we use the solution methodology described in Section 2.5 to find the solution of the optimization problem.

Next we present the simulation results to show the efficacy of the proposed methodology in estimating various key parameters required for cost-optimal dimensioning of resources (i.e. the battery lifetime, outage probability, PV panel-battery configuration for a given outage constraint, and finally the cost-optimal configuration).

2.7.1 Battery lifetime

We begin with evaluating how the battery lifetime varies with the number of batteries installed for a given PV panel size. Please note that the battery lifetime is an important variable to be estimated for resource dimensioning and it appears in Equation (2.10) of Section 2.5 (Cost optimal dimensioning). For these results, for a given PV panel size, we vary the number of batteries and observe the resulting battery lifetime. Figure 2.7

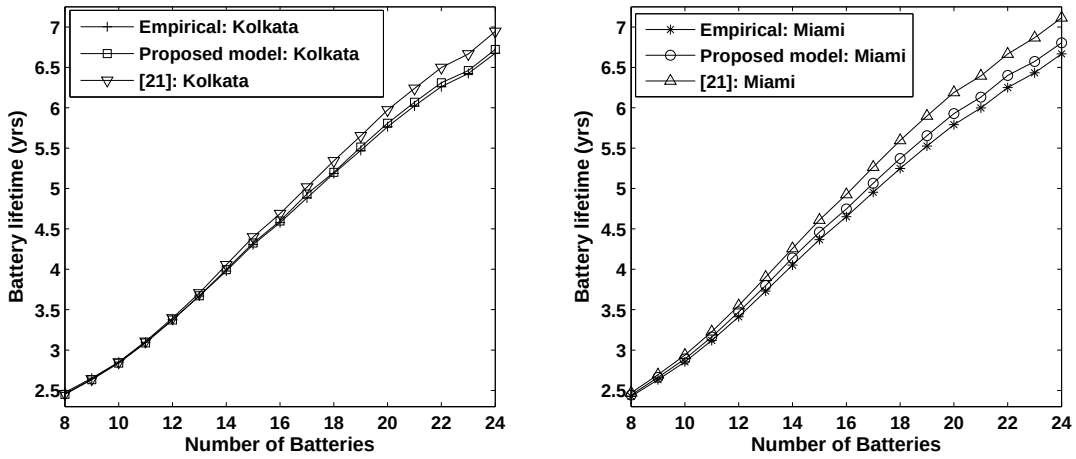

Figure 2.7: Number of batteries vs battery lifetime for the two locations for PV wattage of 12 kW.

shows the battery lifetime obtained for a PV wattage of 12 kW. We note that our model predicts the battery lifetime quite accurately for both the locations. From Figure 2.7 we note that the prediction of the battery lifetime for the proposed model has accuracy above 98% for Miami and above 95% for Kolkata (whereas for [21] these values are 95% and 85% respectively). We also observe that as the number of batteries decreases, the battery lifetime decreases. This is because with fewer batteries, the batteries are more likely to go through deeper discharge cycles, which reduces their lifetime. In Figure 2.8 we show the battery lifetime for two different PV panel sizes for Kolkata to show the effect of PV panel size on the battery lifetime. The nature of result for Miami is similar. We note that for a lower PV panel size, the battery lifetime is lower than that for a higher PV panel size. The intuition behind this is that with a lower PV panel size, the energy harvested is less and thus the batteries go through deeper discharges.

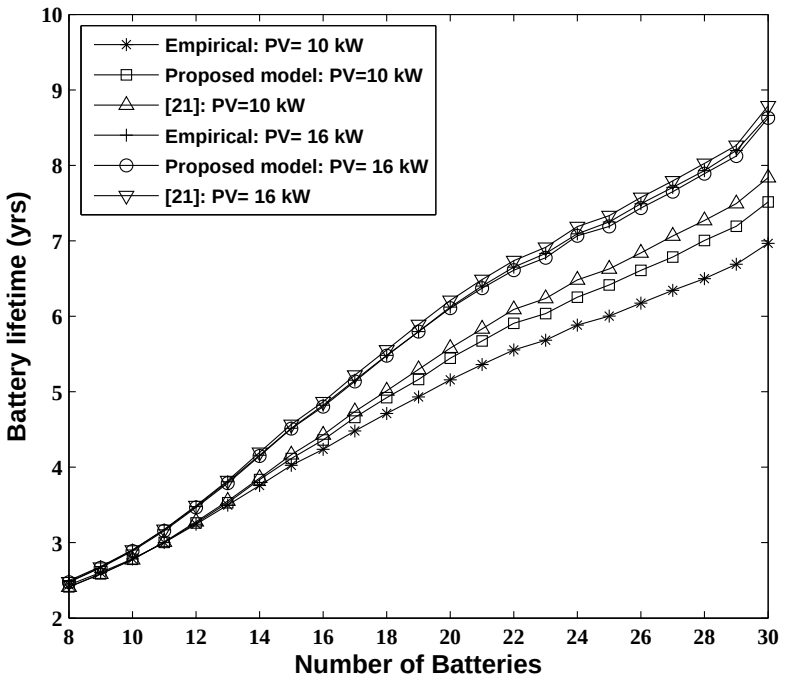

Figure 2.8: Battery lifetime for two different PV panel sizes: Kolkata.

2.7.2 Battery sizing

Next, we evaluate the battery requirements for achieving a given outage probability. Note that as described in Section 2.5, for a given PV panel rating, finding the number of batteries required to ensure the outage probability being below a certain threshold is an important step in cost-optimal resource dimensioning. We begin with considering a PV panel of rating 12 kW and show the battery requirements for various outage probabilities which is shown in Figure 2.9. We note that for very low outage probabilities, the number of batteries required grows very large. This is because a location may occasionally have very bad weather days in sequence and to avoid outages during these periods, the BSs require a very big battery bank size. Next, for two different PV panel sizes (10 kW and 16 kW), we analyse the outage probability for different number of batteries. The results for the two locations have been shown in Figure 2.10 and 2.11 respectively. Note

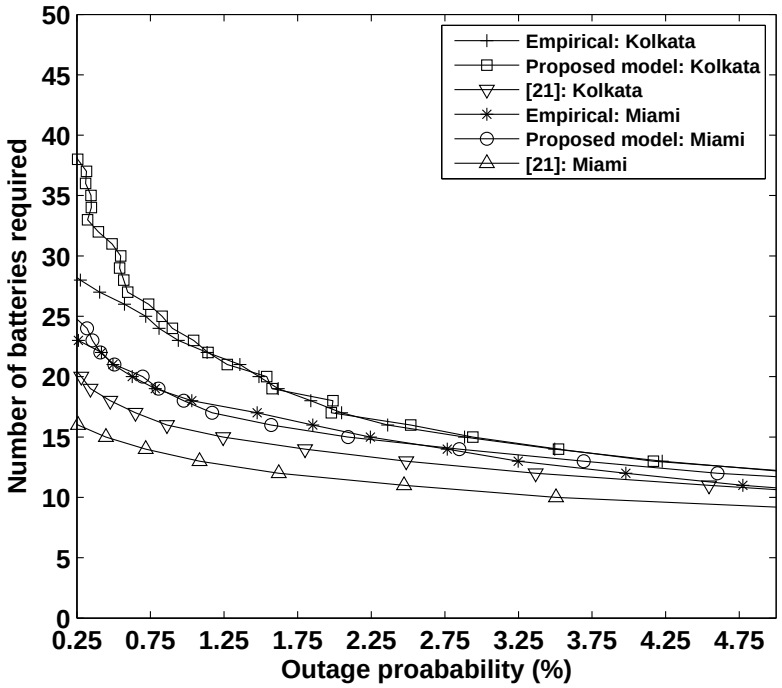

Figure 2.9: Number of batteries required for a given outage for the two locations for PV wattage= 12 kW.

that as expected, for a PV panel size of 16 kW, one is able to ensure a particular outage probability with a fewer number of batteries as compared to the number of batteries required when the PV panel size is 10 kW. This is because for a higher PV panel size, the energy harvested is higher and thus fewer number of batteries are required to ensure the outage probability to be below a certain value.

2.7.3 PV Wattage requirements

Next we study the the PV wattage requirement as a function of the number of batteries and outage probability. For Kolkata, Figure 2.12 shows the required PV wattage for outage probabilities of 0.5 and 1% for various battery sizes. The nature of the results for Miami is similar. The results show that as expected, the required PV wattage increases when the number

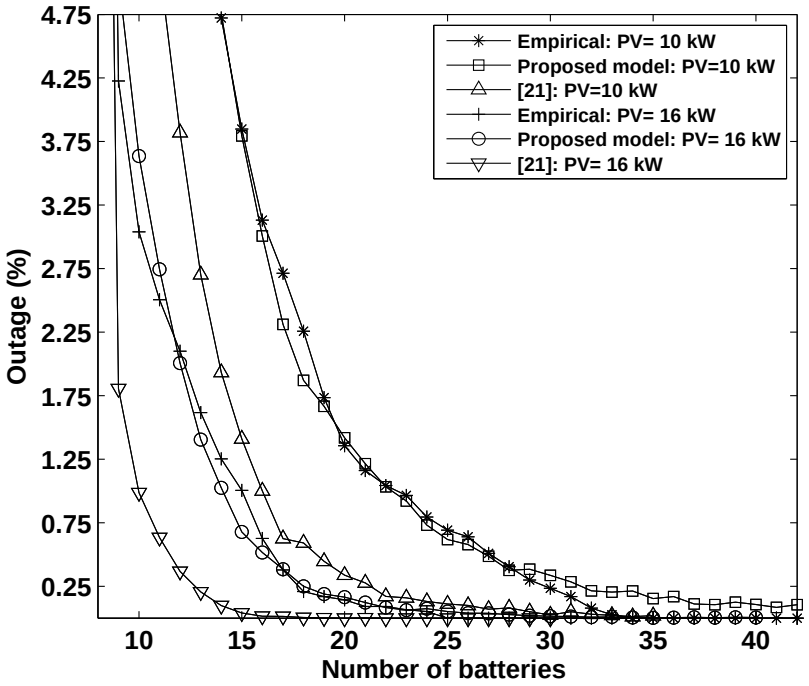

Figure 2.10: Energy outage vs number of batteries required for different PV panel sizes: Miami.

of batteries is reduced. Also, when the number of batteries is reduced beyond a certain point, the required PV wattage tends to infinity. This is because while an increase in the PV wattage increases the solar energy harvested during the day, the small number of batteries implies that there are not enough batteries to store the energy. Consequently, outages occur frequently and it is not possible to keep the outage rates below the desired limit.

2.7.4 PV-Battery configuration for a given outage constraint

For various PV panel dimensions, the number of batteries required to achieve 0.5% and 1% outage rates for the two locations are shown in Figure 2.13 and 2.14. Note that an outage probability of 1% corresponds to outage events in roughly 4 days in a year. The PV-battery configurations shown

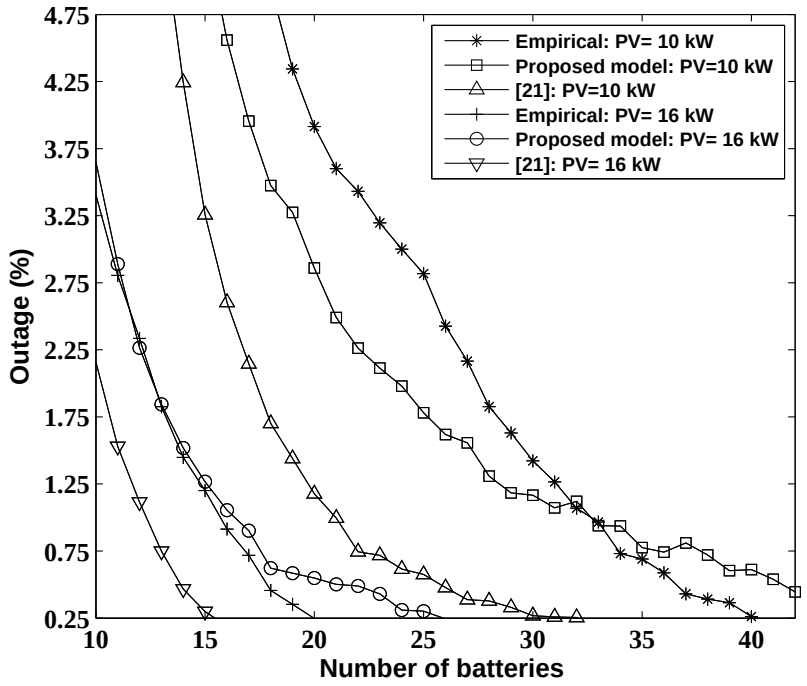

Figure 2.11: Energy outage versus number of batteries required for different PV panel sizes: Kolkata.

in Figure 2.13 and 2.14 are the prospective solutions for the cost-optimal resource provisioning problem presented in Section 2.5. The results predicted using our model have a close match with the results from the empirical data. We observe that for smaller PV panel sizes, the number of batteries required for a given outage is very high. We also observe that the number of batteries required for a given outage probability decreases as the PV wattage increases, and after a certain point the required number of batteries starts saturating. This is because once we have sufficient energy harvested and stored in the batteries to meet an outage constraint, adding more batteries is pointless. Thus in these cases if the PV size is further increased, the energy is wasted. Also, as expected, the required number of batteries increases as the limit on the outage probability is decreased.

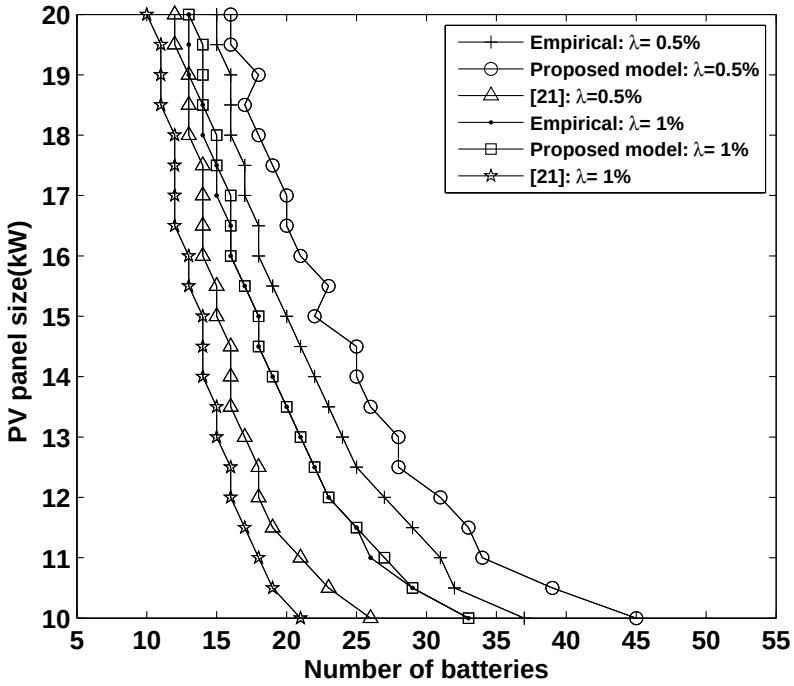

Figure 2.12: Number of batteries vs PV panel size required for different outage probabilities (λ): Kolkata.

2.7.5 Cost optimal configuration

Finally we consider the problem of cost-optimal resource provisioning for the solar powered BS. Note that in Section 2.7.1, we presented the battery-lifetime estimation results which are an important step in determining the optimal-cost configuration (it is specifically used in Equation (2.10)). We also presented results for the number of batteries required for a given PV panel size in Section 2.7.2 and the prospective candidates for cost-optimal resource provisioning problem in Section 2.7.4. Next, we consider two target operational times of $T_{run} = 5$ years and $T_{run} = 10$ years for the cost-computation. Also, based on the market statistics, we assume the cost of PV panels C_{PV} as US$ 1000/kW and the cost of the lead acid batteries C_B has been assumed as US$ 280 [66]. The cost associated with the prospective PV-battery configurations which meet the target outage prob-

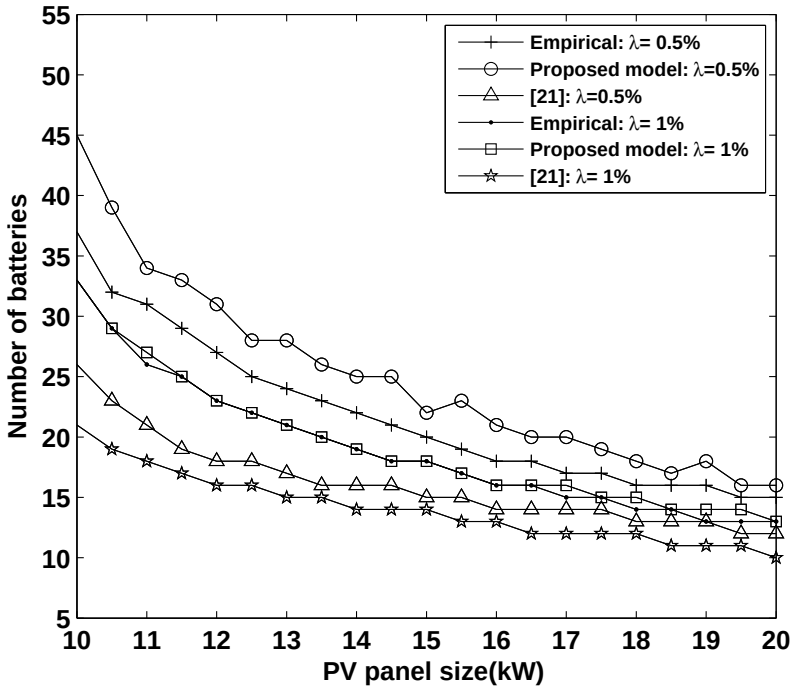

Figure 2.13: PV panel size vs number of batteries required for different outage probabilities (λ): Kolkata.

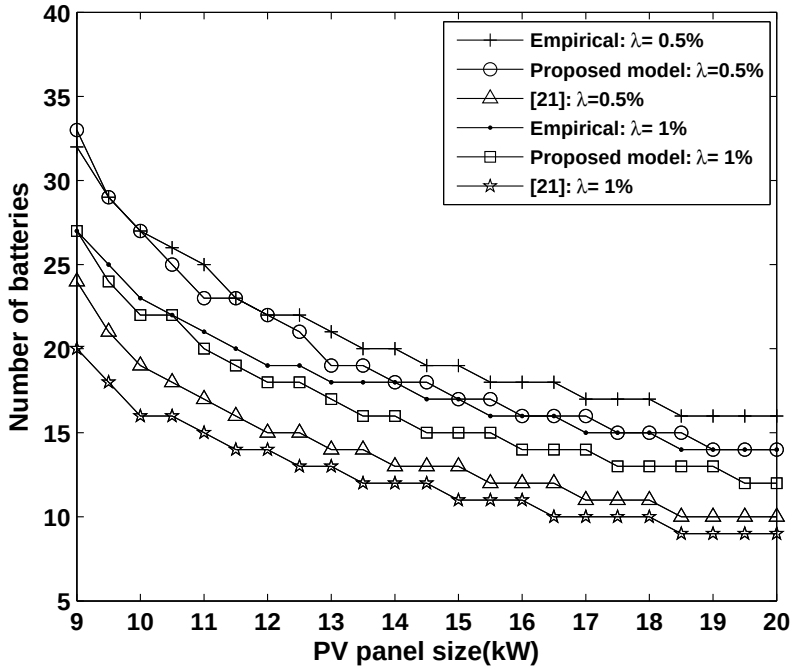

Figure 2.14: PV panel size vs number of batteries required for different outage probabilities (λ)): Miami.

Table 2.1: Optimal Configuration for $T_{run} = 5$ years.

Location	Empirical		[21]		Proposed model	
	PV_w	n_b	PV_w	n_b	PV_w	n_b
$\lambda = 0.5\%$						
Kolkata	12.5	25	11.5	19	12.5	28
Miami	10	27	10	19	11	23
$\lambda = 1\%$						
Kolkata	11	26	10.5	19	12	23
Miami	10	23	9.5	18	10	22

Table 2.2: Optimal Configuration for $T_{run} = 10$ years.

Location	Empirical		[21]		Proposed model	
	PV_w	n_b	PV_w	n_b	PV_w	n_b
$\lambda = 0.5\%$						
Kolkata	16	18	12	18	15	22
Miami	12	22	11	17	13	19
$\lambda = 1\%$						
Kolkata	14.5	18	11	18	14.5	18
Miami	12	19	9.5	18	12	18

ability (obtained as results in Section 2.7.4) were calculated as described in Section 2.5 (using Equation (2.9)). The cost optimal configuration for the two different target operational times (for two target outage probabilities of 0.5% and 1%) has been tabulated in Table 2.1 and 2.2. We note that the results from the proposed model closely match the optimal configuration using simulations with empirical data, and outperforms the benchmark model from [21]. From Tables 2.1 and 2.2 we observe that considering a larger operational lifetime results in a bigger PV panel size in the cost optimal solution. This is because for optimization over a larger operational time, the cost of replacement of the batteries starts dominating the overall cost and thus configurations with higher PV panel size that need smaller number of batteries tend to be more cost optimal.

Remark: As mentioned in Chapter 1 (Section 1.2.2), the size of a PV panel with rating 1 kW is typically 5 m^2. Thus, PV panels with an overall rat-

Figure 2.15: Off-Grid Solar base station at Sangatta (a. front view, b. side view) [67]

ing of 10 kW would require an installation area of around 50 m^2. Such dimensions of PV panels for off-grid BSs are not uncommon (e.g. a solar powered BS owned by the telecom operator Telkomsel in Sangatta, Indonesia as shown in Figure 2.15 has a PV panel with an overall rating of 12.3 kW (See Section 1.4 for details). Additionally, existing works which study resource dimensioning for PV panels also suggest similar dimensions of the PV panel for off-grid solar powered BS (e.g. [3], [33],[63], [74]).

Also note that the cost optimal resource configuration is chosen considering the contribution of both the cost of the PV panels and the batteries. Thus, at times it is possible that for higher outage probabilities, a configuration with smaller PV panel size but with larger number of batteries may turn out to be solution for the cost-optimal resource dimensioning problem. For example in Table 2.2, in the results for [21] for Miami, one can see that although the PV panel size required for $\lambda = 1\%$ is less than that required for $\lambda = 0.5\%$, the number of batteries required for $\lambda = 1\%$ is more as compared to that required for $\lambda = 0.5\%$.

2.8 Conclusion

In this chapter we considered the problem of cost optimal PV panel and battery sizing for solar powered cellular base stations and we presented a framework for determining the same. The proposed framework is based on our model for evaluating the outage probability associated with a base station that uses historical solar irradiance data as the input. Also we proposed a multi-state Markov model to accurately characterize the solar energy. The proposed model was evaluated through data collected for two different geographical locations. Numerical results showed that for a given PV panel size, the battery lifetime increases as the number of batteries installed at the BS is increased. Also, the number of batteries required for very low outage probabilities tends to be very high, thus leading to a high cost; thus it is advisable for operators to plan resources while allowing for some outage probability (like 0.5% or 1% as considered in this chapter). Further we see that for very low PV panel sizes, the number of batteries required to meet low outage probabilities is very high which leads to a very high cost for such configurations. We show the cost-optimal configuration for two different operational periods and the results provide the insight that considering a larger operational time increases the contribution of the battery replacements in the cost computation and thus relatively higher PV panels with fewer batteries tend to be more cost optimal.

Chapter 3

Energy Outage and Battery Lifetime Estimation for Solar Powered Cellular Base Stations

3.1 Introduction

In the previous chapter the problem of cost-optimal resource dimensioning for a solar powered BS was discussed. The fundamental step in such dimensioning is to evaluate the outage probability and battery lifetime associated with a particular configuration of PV panel and battery size. Although the approach for outage estimation and dimensioning resources using the solar energy data traces generated using the multi-state Markov model described in the last chapter has good accuracy, its data complexity is quite high (because of the need to generate long duration traces of solar energy data). Additionally it lacks an analytic model for the BS power consumption and the batteries. To address this issue, in this chapter we propose an analytic model which consists of simpler models to character-

ize the solar energy, BS traffic as well as the states for the battery bank (energy) levels, so as to obtain accurate results while avoiding the need to generate traces of solar energy data (as required in the previous chapter). The proposed model accounts for hourly as well as daily variation in the harvested solar energy as well as the load dependent BS power consumption. The model evaluates the steady state probability of the battery level which is then used to estimate the outage probability. Simulation results with empirical solar irradiance and BS power consumption for two geographically diverse locations are used to validate the proposed model and to demonstrate its accuracy. We also show the superiority of the proposed model over an existing benchmark [21].

The rest of the chapter is organized as follows. In Section 3.2 we present the related work and in Section 3.3 we present the background material and system model. Section 3.4 presents the model for evaluating the energy outage probability. Section 3.5 presents the methodology for obtaining the steady state probabilities of the system states and the outage probability. Section 3.6 describes the problem of cost optimal dimensioning. Finally, Section 3.7 presents simulation results to validate our methodology and Section 3.8 concludes the chapter.

3.2 Literature review

The problem of dimensioning of resources for solar powered systems specifically targeting cellular BSs is considered in [3, 34]. The dimensioning in [3, 34, 16, 63] is done through simulations by using long-term solar irradiation data (either real or synthetically generated). An overview of commercial software tools used for simulation based dimensioning solar

powered systems is presented in [68]. Simulation based approaches are not only computationally intensive, but also do not provide any insights into the performance of the system. Literature on modeling of solar powered systems includes [69] and [70] that model solar energy using Beta and log-normal distributions, respectively, and use these models to dimension resources for a solar powered system. A Markov chain based model for energy storage is proposed in [71], but it considers solar irradiation with an exponential distribution thus assuming the solar irradiation to be memoryless. Existing literature has shown that the solar energy is better modeled as a Markov process and these models have been used to dimension storage for solar powered systems in [72, 62]. Further, [21] proposes a Markov model for solar energy which is used to dimension cost optimal PV panel and battery sizes. However, a greater accuracy than that offered by the model in [21] is required in cellular network planning (as also shown by the results in this chapter).

While existing literature has addressed various individual aspects of dimensioning solar-powered systems, there is no work which integrates the modeling of solar energy, network traffic, and battery levels while being simple and accurate. Thus in this chapter we present a framework which incorporates all these factors into the model in order to evaluate the system performance, and the framework is tailored specifically for dimensioning resources for solar powered cellular BSs.

3.3 System description

3.3.1 Base station power consumption

We use the same model for BS power consumption as used in the previous chapter (Section 2.3.1). We consider a Long Term Evolution (LTE) macro BS, the power consumption for which is given by [49]

$$L(t) = \Upsilon_{TRX}(P_0 + \Delta K(t) P_{max}), \quad 0 \leq K \leq 1 \tag{3.1}$$

where Υ_{TRX} denotes the number of transceivers, P_0 denotes power consumption at zero traffic, Δ denotes slope of load dependent BS power consumption, K is the normalized traffic at time t and P_{max} is the power amplifier output at maximum traffic.

3.3.2 Solar energy resource and batteries

For modelling and evaluation, we use statistical solar irradiation data from the National Renewable Energy Laboratory (NREL), USA [57]. The methodology for obtaining the hourly solar power generation using the statistical data has been described in Section 2.3.2 of the last chapter. Additionally, we consider that the BS uses lead acid batteries for charge storage and details for the same (like the method for battery lifetime evaluation) has been described in Section 2.3.2 of the last chapter.

3.4 Model for evaluating BS outage probability

In this section, we present the framework to evaluate the outage probability of a solar powered BS.

3.4.1 System resources

We denote the number of PV panels installed at the BS by n_{PV}, where each panel has a DC rating denoted by E_{panel}. The overall DC rating, PV_w, is then given by

$$PV_w = n_{PV} E_{panel}. \tag{3.2}$$

Also, let n_b denote the number of batteries used by the BS, each with a storage capacity denoted by E_{bat}. Thus the overall battery storage capacity, B_{cap}, is given by

$$B_{cap} = n_b E_{bat}. \tag{3.3}$$

To prevent deep discharges, the batteries are disconnected when the charge level drops below νB_{cap} where ν denotes the fraction of the battery capacity below which batteries are dis-allowed to discharge. Such events correspond to energy outages at the BS. To calculate the enegy outage probability, we use discrete time Markov chains to model the solar energy, load, and the battery level on a daily basis [73], [74]. Next we describe these models in detail.

3.4.2 Model for harvested solar energy

Daily variations in the solar energy at a location have been shown to be well modeled as a Markov process [75, 76]. We classify any given day into one

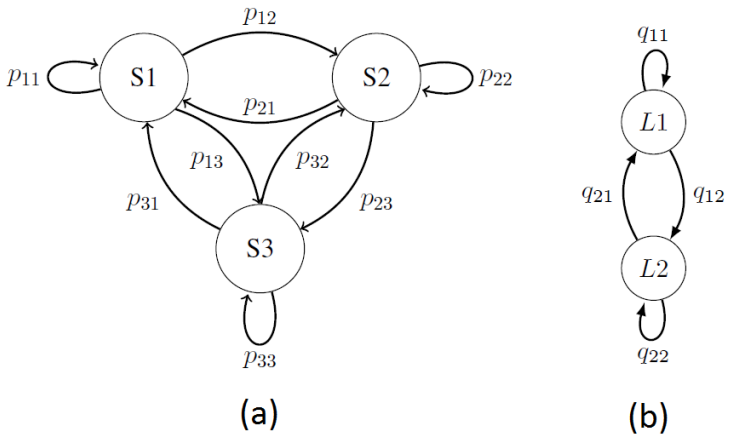

Figure 3.1: a. Transition between different Solar day types. b. Transition between different states for BS load

of three solar day types: $S1$, $S2$ and $S3$. Among these, $S1$ and $S2$ represent very bad weather and bad weather days, respectively, while $S3$ denotes a good weather day. A given day is classified as one of the three day types based on the solar energy harvested on that day using a standard PV panel size (taken as 1 kW in this chapter). Days with daily harvested energy below γ_1 are classified as $S1$, between γ_1 and γ_2 are classified as $S2$, and all other days are classified as $S3$. The transition probabilities between the three day types for a given location is calculated using historical statistical weather data. The Markov process for the state transitions is shown in Figure 3.1(a). The transition probability matrix for this Markov process is given by

$$T_S = \begin{bmatrix} p_{11} & p_{12} & p_{13} \\ p_{21} & p_{22} & p_{23} \\ p_{31} & p_{32} & p_{33} \end{bmatrix} \tag{3.4}$$

where p_{11} is the probability of a day of type $S1$ remaining the same on the next day, whereas p_{12} (resp. p_{13}) is the probability of transition from a day type $S1$ to day type $S2$ (resp. $S3$) on the next day. The other variables are defined similarly.

We also calculate the average hourly solar energy harvested for each of the day types using the statistical weather data (assuming a PV panel with DC rating 1 kW). The average harvested energy value for the day is denoted by the vector $\mathcal{H}_\alpha$ which is given as:

$$\mathcal{H}_\alpha = (h_{\alpha,1}, h_{\alpha,2}, \cdots, h_{\alpha,24}); \quad \alpha \in \{1,2,3\} \tag{3.5}$$

where α denotes the solar day type. $\alpha = 1,2$ and 3 denote S1, S2 and S3 solar day types, respectively. $h_{\alpha,1}$ denotes the solar energy harvested for the first hour of the α day type and so on. Note that based on the above notation, $\mathcal{H}_1$, $\mathcal{H}_2$ and $\mathcal{H}_3$ are the average harvested energy profiles for day types $S1$, $S2$ and $S3$, respectively. The procedure for estimating the transition probabilities and the average solar profile has been presented in Section 3.5.3. For a PV panel of size PV_w, the profile of harvested solar energy, $\mathcal{E}$ is given by

$$\mathcal{E} = PV_w \mathcal{H}_\alpha. \tag{3.6}$$

Remark: We have used 2 states for bad day types since they are the ones which have a greater impact on the outage probability. Note that when just 2 states are used for the solar energy (i.e. just bad day type and good day type) there is an inherent problem. If the threshold to decide whether the day is a bad day or good day is kept high, then the average solar energy for bad days becomes large thus leading to a lower outage probability in the outage estimation process. On the other hand, if the threshold to decide the bad day is kept very low, there are very few bad weather days and the transition probability to the bad day type becomes very small. This again leads to a lower outage probability during the outage estimation process. We have addressed this issue by using 2 day types for the bad weather days,

where one of the day types, S1, represents very bad weather day whereas S2 represents bad weather day. Also, in this chapter three states (S1, S2 and S3) have been used to classify a particular day in terms of the solar energy harvested. Note that although more than three states can be used to classify a particular day, through simulations we have observed that the improvement in the estimation accuracy is outweighed by the increase in complexity due to the additional states.

3.4.3 Model for BS load

Previous studies have shown that the traffic load at a base station follows diurnal patterns, and the overall load levels are lower on the weekends when compared to weekdays [50, 51, 52, 53]. Thus our model considers two load types: low ($L1$) and high ($L2$), that depend on the day of the week. In this chapter we use the term *load* to denote the BS power consumption which is given by Equation (3.1). The transitions between the load day types is approximated as a two-state Markov process, as shown in Figure 3.1(b). The transition probability matrix of this Markov process is given by

$$T_L = \begin{bmatrix} q_{11} & q_{12} \\ q_{21} & q_{22} \end{bmatrix} \tag{3.7}$$

where q_{11} (resp. q_{22}) is the probability of transition from a low load (high load) day to a low load (high load) day, and $q_{12} = 1 - q_{11}$ (resp. $q_{21} = 1 - q_{22}$) is the probability of transition from low load day to a high load day. The transition probabilities for the Markov process are chosen such that on an average, five weekdays are followed by two weekend days.

Similar to the solar energy profile $\mathcal{H}_\alpha$, we define the 24 hour load profile

vector $\mathcal{L}_\beta$ as the average load during each hour of the day and it is given as

$$\mathcal{L}_\beta = (l_{\beta,1}, l_{\beta,2}, \ldots, l_{\beta,24}); \quad \beta \in \{1, 2\} \tag{3.8}$$

where β denotes the load day type. $\beta = 1$ and 2 denote $L1$ and $L2$ load day types, respectively. $l_{\beta,1}$ denotes the average base station load for the first hour of β load day type and so on. Based on the above notation, $\mathcal{L}_1$ and $\mathcal{L}_2$ are the average load profile vectors for a low load and a high load day, respectively. We present the methodology for estimating $\mathcal{L}_\beta$ and the transition probabilities (i.e. q_{11}, q_{12} etc.) in Section 3.5.3.

3.4.4 Model for battery level

For modeling the battery level at a BS, the overall battery bank capacity, B_{cap}, is rounded off to the closest integer value above it. For mathematical tractability, the possible battery levels are discretized into blocks of 1 kWh. Thus the number of levels in the battery model, N, is given by

$$N = \lceil B_{cap} \rceil \tag{3.9}$$

and the battery may be in any one of the N possible levels at any given point in time.

3.4.5 BS outage probability

There are three important factors which decide if there is an outage on a given day. These factors are: the solar energy harvested on the day, the BS power consumption during the day and the battery level when the day begins. Thus for the estimation of outage probability, we consider the

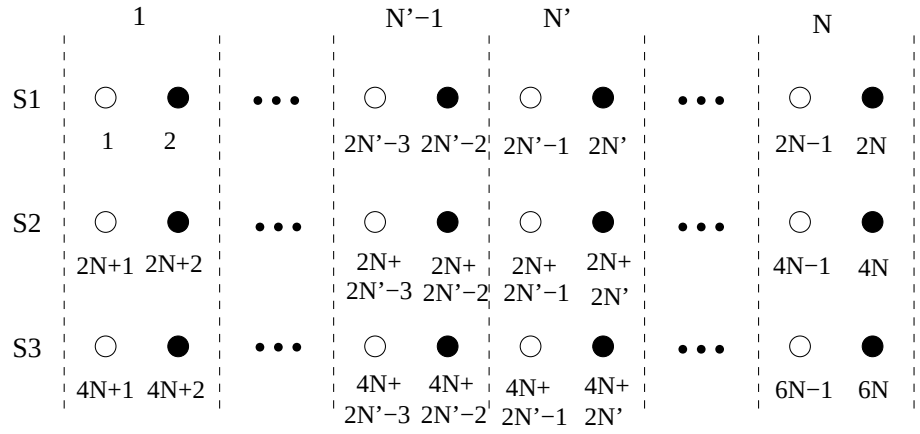

Figure 3.2: States of the system

state of the system defined as a 3-tuple consisting of: the solar day type, the load type and the battery level. Note that a state characterizes the system's condition during a day's period (i.e. a 24 hour period). The solar day type and the load type determine the solar energy and load profile during the different hours of the day for the state. Additionally, the battery level at the beginning of the day is termed as the battery level of the state. For notational simplicity, the state of the system is denoted by U which is defined as

$$U = 2N(\alpha - 1) + \beta + 2(b - 1) \tag{3.10}$$

where $\alpha \in \{1, 2, 3\}$ is the solar day type ($\alpha = 1$ for $S1$, $\alpha = 2$ for $S2$ and $\alpha = 3$ for $S3$), $\beta \in \{1, 2\}$ is the load day type ($\beta = 1$ for low load and $\beta = 2$ for high load) and $b \in \{1, 2, ..., N\}$ is the battery level. The state space is shown in Figure 3.2.

Proposition 3.4.1: *The state notation given in Equation (3.8) results in a unique state number for a day with given day type, load type and battery level.*

Proof: The proof of this proposition is given in Appendix A.

The notation in Equation (3.10) gives a uniue state number for a day with given day type, load type and battery level as shown above. For example let

us consider a day with solar day type S3, load type as high load and battery level as 1 kW. Then the state for this day is given by $U = 2N(3-1)+1$ $+2(1-1) = 4N+1$. Note that this state can also be seen as the first state in the third row in Figure 3.2. There are $6N$ possible states since there are three, two and N choices for the solar day type, load type and the battery level, respectively. Further, each column in the figure (separated by dashed lines) represents states with a particular battery level (indicated on the top of the figure). As per our notation defined in Equation (3.10), the first, second and the third rows corresponds to day type $S1$, $S2$ and $S3$ respectively. Also, the odd positions in each row (shown by empty circles) denote low load days while the even positions (shown by dark circles) denote high load days.

The transition in system state is modeled at the beginning of each day (i.e. every 24 hour period). The state on a given day only depends on the battery level, solar day type (i.e. energy harvested) and the load day type (i.e. power consumption) of the previous day. Thus the system state can be modeled as discrete time Markov chain, whose transition probability matrix is denoted as

$$T_B = \begin{bmatrix} \sigma_{(1,1)} & \cdots & \sigma_{(1,6N)} \\ \vdots & \ddots & \vdots \\ \sigma_{(6N,1)} & \cdots & \sigma_{(6N,6N)} \end{bmatrix} \tag{3.11}$$

where $\sigma_{(U,V)}$ is the probability of transition from state U to V.

The batteries are disconnected from the load when the charge level goes below νB_{cap}, to prevent deep discharges and the consequent battery degradation. Thus the battery level never goes below νB_{cap} and the states below this level are not visited in our model. This boundary battery level which

we denote by N' is shown in Figure 3.2, and is given by

$$N' = \lceil \nu B_{cap} \rceil. \tag{3.12}$$

Algorithm 1 Battery level evaluation (BLC) Algorithm

function $BLC(U)$
  if $1 \leq U \leq 2N$ **then** ▷ Extracting solar energy & battery level information for state U
    $\mathcal{E} = PV_w \mathcal{H}_1$;
    $b = \lceil U/2 \rceil$;
  else if $2N + 1 \leq U \leq 4N$ **then**
    $\mathcal{E} = PV_w \mathcal{H}_2$;
    $b = \lceil (U - 2N)/2 \rceil$;
  else
    $\mathcal{E} = PV_w \mathcal{H}_3$;
    $b = \lceil (U - 4N)/2 \rceil$;
  end if
  if $U\%2 == 1$ **then** ▷ Extracting load day type information
    $W = \mathcal{L}_1$;
  else
    $W = \mathcal{L}_2$;
  end if
  initialize: $b' = b$, $\Gamma(U) = 0$
  $\mathcal{E} = PV_w \mathcal{H}$; ▷ Profile of energy harvested for the state
  for $t = 1 : 24$ **do** ▷ Evaluating hour by hour battery level
    $b' = b' + \mathcal{E}(t) - W(t)$; ▷ next battery level
    if $b' > B_{cap}$ **then** ▷ ensuring battery level $\leq B_{cap}$
      $b' = B_{cap}$;
    else if $b' < \nu B_{cap}$ **then** ▷ ensuring battery level > νB_{cap}
      $b' = \nu B_{cap}$; $\Gamma(U) = 1$; ▷ noting outage event in vector Γ
    end if
    $b_{tracker}(t) = b'$; ▷ storing hourly battery level in $b_{tracker}$
  end for
  $l_{Bat}(U) = LE(b_{tracker})$; ▷ calling LE algorithm for lifetime evaluation
  Return: round(b') ▷ Returning battery level after system in state U
end function

For a given state U, the next battery level depends on the initial battery level b, the solar day type α, and the load type β, and can be computed using function $BLC(U)$ shown in Algorithm 1. The $BLC(U)$ function has 3 purposes as stated below:

- It gives the battery level of the states to which the state transition from state U) occurs.
- It stores the information whether state U is an outage state or not (i.e. is there any energy outage during the day in the given state).
- For state U, it stores the hourly battery level (charging-discharging) profile which is used later on to evaluate the battery lifetime (which is required for estimating the cost associated with the particular PV panel and battery configuration).

The BLC function accepts the state of the system (U) and uses it to extract the information regarding its battery level (b), solar energy profile ($\mathcal{E}$) and the load profile (denoted in the algorithm by W). W is $\mathcal{L}_1$ if U is a low load day and is $\mathcal{L}$ otherwise. Lines 2-16 in the algorithm extract the information regarding b, $\mathcal{E}$ and W. Specifically, note that as shown in Figure 2.2, the states from 1 to $2N$ have solar-day type S1 (and hence the solar energy harvested profile for them is $\mathcal{H}_1$). Additionally, for these states the battery levels can be given by the simple formula $\lceil U/2 \rceil$. This is becuase for S1 day type $\alpha = 1$ and substituting it in Equation (3.10) we get $b = \frac{U+(2-\beta)}{2}$. Now becuase β has only two feasible values given as $\beta \in \{1,2\}$, b can be found using the simple expression $\lceil U/2 \rceil$. Further, note that the odd states correspond to low load days whereas the even states correspond to high load days. We use this fact (using $U\%2$) to infer the load type for a given state. Further, we store the hourly load profile for that particular day type in the vector W. The solar energy profile, battery levels and the load type for the remaining states can be found using similar intuition. Note that b' is initialized to the battery level b and then updated for each hour of the next 24 hour period (line 20; note that the sampling interval for this operation is 1 hour). To prevent battery degradation, we avoid deep discharges by

preventing b' from going below a threshold νB_{cap} by disconnecting the battery (lines 23, 24). Thus if in any hour b' drops below νB_{cap}, we mark the state as an *outage state*, and record it in a vector Γ. Also, the charge level does not exceed the battery capacity B_{cap} (lines 21, 22). The function $BLC(U)$ returns b' rounded off to the closest integer, since our model only allows discrete battery levels (line 29). The next battery level can thus be obtained as

$$b' = BLC(U). \tag{3.13}$$

For any given battery level, there are six possible states (based on the solar day and load type). Thus the next state can be one of six states with that battery level. The next battery level is completely determined by the current state U (using the BLC algorithm). With α and β denoting the solar day and load type of state U, respectively, the transition probability from state U to state V is given by

$$\sigma(U,V) = \begin{cases} p_{\alpha 1} q_{\beta 1} & V = 2BLC(U) - 1 \\ p_{\alpha 1} q_{\beta 2} & V = 2BLC(U) \\ p_{\alpha 2} q_{\beta 1} & V = 2BLC(U) + 2N - 1 \\ p_{\alpha 2} q_{\beta 2} & V = 2BLC(U) + 2N \\ p_{\alpha 3} q_{\beta 1} & V = 2BLC(U) + 4N - 1 \\ p_{\alpha 3} q_{\beta 2} & V = 2BLC(U) + 4N \\ 0 & \text{otherwise.} \end{cases} \tag{3.14}$$

Figure 3.4 shows the 6 different state transitions from state U. The

Remark: Note that given a state U as input, the BLC algorithm returns the battery level of the states to which the state transition occurs. So, say this battery level is 10, then $(2BLC(U) - 1)$ would simply be $(2 * 10 - 1 = 19)$,

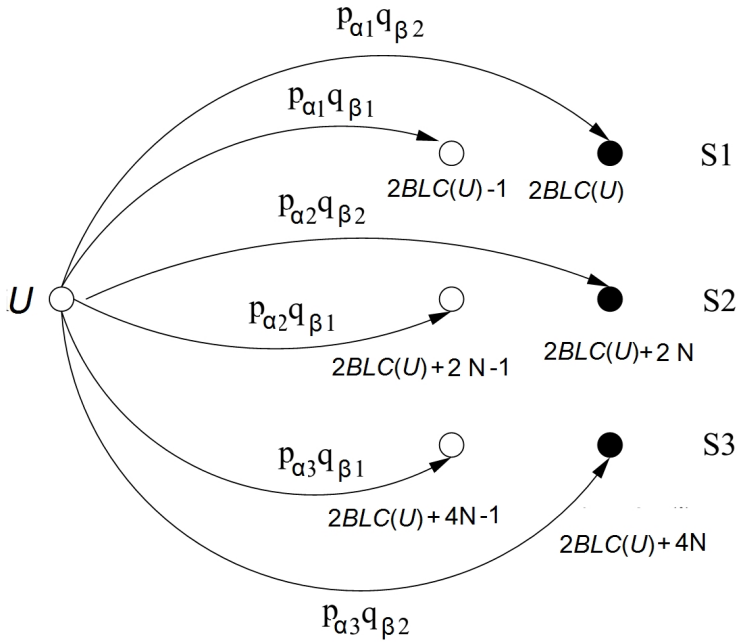

Figure 3.3: Transition from a given state U.

i.e. the transition is to state 19. Additionally, as described before, α and β in the state transition probabilies of Equation (3.12) are the solar day type and load day type for state U.

The steady state probability vector is denoted by π and is computed in the next section. The vector π can be given as $\pi = [\pi_1, \pi_2...., \pi_{6N}]^T$, where π_1 is the steady state probability of state 1 and so on. Recall that $BLC(U)$ computes and stores the outage status (0 for no outage and 1 for outage) for each state in the vector Γ. The outage probability, Ω can be written as

$$\Omega = \Gamma\pi \tag{3.15}$$

We also evaluate the battery lifetime associated with a given state. As it has been discussed earlier in Section 2.5, estimating the battery-lifetime associated with a particular PV panel and battery configuration is an important step in solving the cost-optimal resource provisioning problem (which

Algorithm 2 Lifetime Evaluation (LE) Algorithm

1: **function** $LE(b_{tracker})$
2: $b_{old} = b_{tracker}(1)$, $dod = null$;
3: **for** $t = 1 : 24$ **do**
4: **if** $b_{tracker}(t) > b_{old}$ **then** ▷ Capture depth-of-discharge (DoD) points
5: $dod = dod \ || \ \left(1 - \frac{b_{old}}{B_{cap}}\right)$; ▷ Store DoD points in vector dod
6: **end if**
7: $b_{old} = b_{tracker}(t)$;
8: **end for**
9: $l_{battery} = \frac{1}{365} / \left(\sum_{q=1}^{length(dod)} \frac{1}{cycles\_to\_failure(dod(q))}\right)$ ▷ evaluating battery lifetime using formula presented in Section 2.3.2
10: Return: $l_{battery}$ ▷ Returning battery lifetime corresponding to the state
11: **end function**

is motivation for the outage estimation analysis presented in this chapter). In our model, we have different states and we estimate the battery lifetime given that the system is in a particular state. Further, after finding the steady state probability of being in different states (as discussed in subsequent sections in the chapter) which is denoted by π, we can estimate the battery lifetime associated with the particular configuration of PV panel and battery size, L_{Bat}, which is given as

$$L_{Bat} = l_{Bat}\pi \tag{3.16}$$

where l_{Bat} is the vector which stores the battery lifetime for the different states in the BLC algorithm (line 28). The battery lifetime for a given state is calculated as follows. The battery lifetime is computed in the BLC algorithm by storing the battery level profile in the variable $b_{tracker}$ (see line 26) which is used to evaluate the battery lifetime associated with that state. The battery lifetime is calculated using the Lifetime Evaluation (LE) Algorithm (Algorithm 2) (the algorithm is called at line 28 in the BLC algorithm).

Note that this algorithm uses the methodology for evaluating the battery lifetime as described in Section 2.3.2. For the given battery level profile (stored in $b_{tracker}$), it notes the depth of discharge points which are stored in the vector dod (please see line 5 in the LE algorithm; note that the symbol $||$ denotes the concatenation operator). As described in earlier chapters, Depth of discharge (DoD) refers to the lowest level the battery reaches in a discharge-charge cycle. Further using the cycles to failure corresponding to the entries in the vector dod, using Equation (2.2) we calculate the battery lifetime $l_{battery}$ (in years) for the given state (line 9 in the LE algorithm). Note that as a state denotes the system's state during a day's time, T in Equation (2.2) has been taken as $1/365$ years. The relationship between the DoD and the cycles to failure is generally provided by the battery manufacturer and the function cycles_to_failure provides a mapping for the cycles to failure corresponding to the DoD points stored in the vector dod. For example, if Figure 2.3 is considered to represent the relationship between DoD and cycles to failure; and if $dod(1)$ is 0.6 (i.e. 60% depth of discharge), then the cycles to failure corresponding to it will be 1000.

For any choice of PV_w and n_b, the associated outage probability and battery lifetime may be evaluated by using the methodology presented above. Then, for an operator specified tolerable outage probability λ, the feasible dimensioning solutions are all configurations of PV_w and n_b that satisfy

$$\Omega \leq \lambda. \tag{3.17}$$

Section 3.6 addresses the problem of obtaining the cost optimal configuration that selects the PV panel and battery sizes that satisfy the required outage constraint with minimum cost.

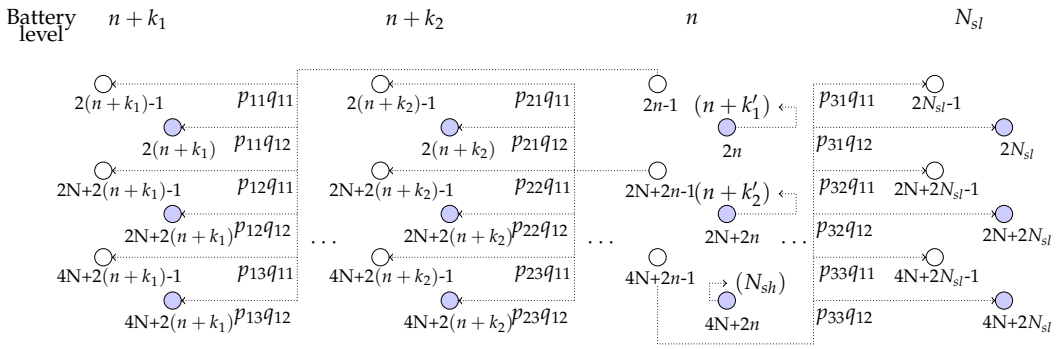

Figure 3.4: State diagram showing transition from states having battery level n (for clarity only transition from low load states are shown)

3.5 Steady state probability estimation

This section presents a methodology for obtaining closed form solutions for the steady state probability of the different states in the system which is required for evaluating the outage probability and battery lifetime as explained in the previous section. In the model presented in Section 3.4, there are different levels of change (i.e. "jumps") in the battery levels when there is a transition from one state to another, depending on the solar day type $(S1, S2 \text{ or } S3)$, load day type $(L1, L2)$, and PV panel and battery sizes. These transitions are shown in Figure 3.4 for states with battery level n. To avoid cluttering, we only show the state transitions for the low load states. For high load states, we only show the battery levels of the final states for each transition. The changes in the battery levels when the load day type is low $(L1)$ for solar day type $S1$ and $S2$ are denoted by k_1 and k_2, respectively, whereas the changes when BS traffic is high $(L2)$ for solar day types $S1$ and $S2$ are denoted by k_1' and k_2', respectively. The magnitudes of these changes depend on the PV panel size and can be obtained using Algorithm 1 by considering a scenario where the change is not bound by the lower or upper limits. The change in the battery level on a $S1$ day type (k_1, k_1') are negative for realistic PV panel sizes.

Table 3.1: Cases for steady state probability estimation of critical states

Case	k_2	k_2'	Case	k_2	k_2'
1	< -1	< -1	5	0	< -1
2	> 0	> 0	6	0	-1
3	> 0	0	7	-1	< 0
4	> 0	< -1	8	> 0	-1

To simplify the model and reduce the state space, we first note that the battery level does not go below $N' = \lceil \nu B_{cap} \rceil$ or above $N = \lceil B_{cap} \rceil$. In addition, the impact of the day and load types on the operation of the BS results in additional simplifications on the state transitions. To visualize these simplifications, we consider practical deployment scenarios where the BSs are provided with sufficient battery capacity and PV panels to endure occasional periods of sustained bad weather. For realistic resource dimensions, on a $S3$ (i.e. good) day, the PV panels harvest enough energy to power the BS and fully charge the batteries (irrespective of the initial battery level on that day). Thus in the evenings of $S3$ days, the battery starts discharging after being charged to N and at the end of the day, the final battery level depends on whether it is a high or low load day. We denote the final battery level at the end of 24 hours to be N_{sh} and N_{sl} for high and low load days, respectively. Since $S3$ days are the best in terms of energy generation, N_{sh} and N_{sl} act as the upper limits of the battery level at the end of a high/low load day for $S1$ and $S2$ days also, and states with higher energy levels can be eliminated from the state space. The states with battery level N_{sl} and N_{sh} play a critical role in determining the steady state probabilities of the other states. Therefore they are termed *critical* states in the rest of the chapter, and all other states are *non-critical* states.

3.5.1 Steady state probability of critical states

To evaluate the steady state probabilities of the critical states, we consider the structure of the state transition diagram, as shown in Figure 3.4. While k_1 and k_1' are always negative for realistic PV panel dimensions, k_2 and k_2' may be positive or negative depending on the PV panel size. The various possibilities for the values of k_2 and k_2' that lead to different structures of the state transition diagram are shown in Table 4.1. Next we present the analysis for these cases.

Before considering each case, we present general results on the steady state probability of being in states with solar day type $S1$, $S2$ and $S3$, denoted by P_1, P_2 and P_3, respectively. From Figure 3.2 we have

$$\begin{aligned} P_1 &= \pi_1 + \pi_2 + \pi_3 + \cdots + \pi_{2N-1} + \pi_{2N} \\ P_2 &= \pi_{2N+1} + \pi_{2N+2} + \pi_{2N+3} + \cdots + \pi_{4N-1} + \pi_{4N} \\ P_3 &= \pi_{4N+1} + \pi_{4N+2} + \pi_{4N+3} + \cdots + \pi_{6N-1} + \pi_{6N}. \end{aligned}$$

Let Q_1 and Q_2 be the steady state probability of being in states with low and high load days, respectively. We then have

$$\begin{aligned} P_1Q_1 &= \pi_1 + \pi_3 + \pi_5 + \cdots + \pi_{2N-1} \\ P_1Q_2 &= \pi_2 + \pi_4 + \pi_6 + \cdots + \pi_{2N} \\ P_2Q_1 &= \pi_{2N+1} + \pi_{2N+3} + \pi_{2N+5} + \cdots + \pi_{4N-1} \\ P_2Q_2 &= \pi_{2N+2} + \pi_{2N+4} + \pi_{2N+6} + \cdots + \pi_{4N} \\ P_3Q_1 &= \pi_{4N+1} + \pi_{4N+3} + \pi_{4N+5} + \cdots + \pi_{6N-1} \\ P_3Q_2 &= \pi_{4N+2} + \pi_{4N+4} + \pi_{4N+6} + \cdots + \pi_{6N}. \end{aligned}$$

Note that P_1, P_2, P_3, Q_1 and Q_2 are obtained from empirical solar irradiation and traffic load data as described in Section 3.5.3.

- **Case 1:** $k_2 < -1,\ \ k_2' < -1$

  The structure of the state transitions for this case is shown in Figure 3.5. The figure shows states with battery levels between N' and N_{sl}, and their state transitions. To avoid cluttering the figure with a large number of states, we denote all non-critical states using a representative battery level n. The transition probabilities have been marked on the respective lines except for the cases where it is 1. Recall that all states with solar day type $S3$ transition to a state with battery level N_{sl} or N_{sh}, depending on the load day type. We use this fact to simplify our analysis. The summations at the bottom of the figure show the addition of these probabilities which populate the various critical states. Recall that the probabilities of low and high loads for a solar day of type $S3$ are P_3Q_1 and P_3Q_2, respectively, and indicated at the summation symbols in Figure 3.5. To avoid clutter, the transitions from any state to a battery level, say a, which has non-critical states, have not been drawn completely and are marked by (a).

  Considering the balance equations at various boundaries around the critical states (denoted by the dotted circles marked A-L in Figure 3.5), the steady state probability for the critical states can be shown to

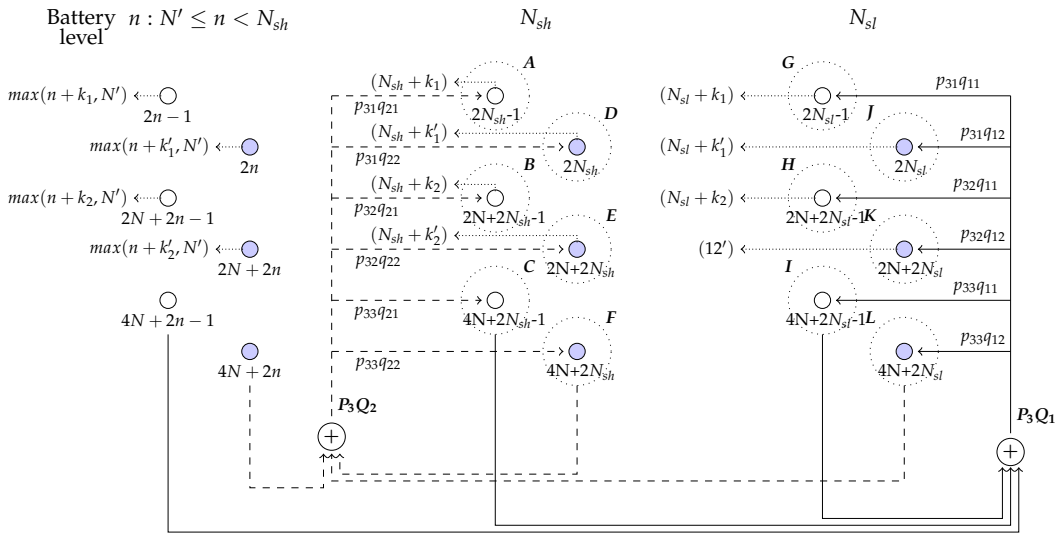

Figure 3.5: State diagram for case 1.

be:

$$
\begin{aligned}
\pi_{2N_{sl}-1} &= p_{31}q_{11}P_3Q_1 \\
\pi_{2N_{sl}} &= p_{31}q_{12}P_3Q_1 \\
\pi_{2N+2N_{sl}-1} &= p_{32}q_{11}P_3Q_1 \\
\pi_{2N+2N_{sl}} &= p_{32}q_{12}P_3Q_1 \\
\pi_{4N+2N_{sl}-1} &= p_{33}q_{11}P_3Q_1 \\
\pi_{4N+2N_{sl}} &= p_{33}q_{12}P_3Q_1 \\
\pi_{2N+2N_{sh}-1} &= p_{32}q_{21}P_3Q_2 \\
\pi_{2N+2N_{sh}} &= p_{32}q_{22}P_3Q_2 \\
\pi_{2N_{sh}-1} &= p_{31}q_{21}P_3Q_2 \\
\pi_{2N_{sh}} &= p_{31}q_{22}P_3Q_2 \\
\pi_{4N+2N_{sh}-1} &= p_{33}q_{21}P_3Q_2 \\
\pi_{4N+2N_{sh}} &= p_{33}q_{22}P_3Q_2.
\end{aligned}
$$

- **Case 2:** $k_2 > 0, k'_2 > 0$ **and Case 3:** $k_2 > 0\ k'_2 = 0$

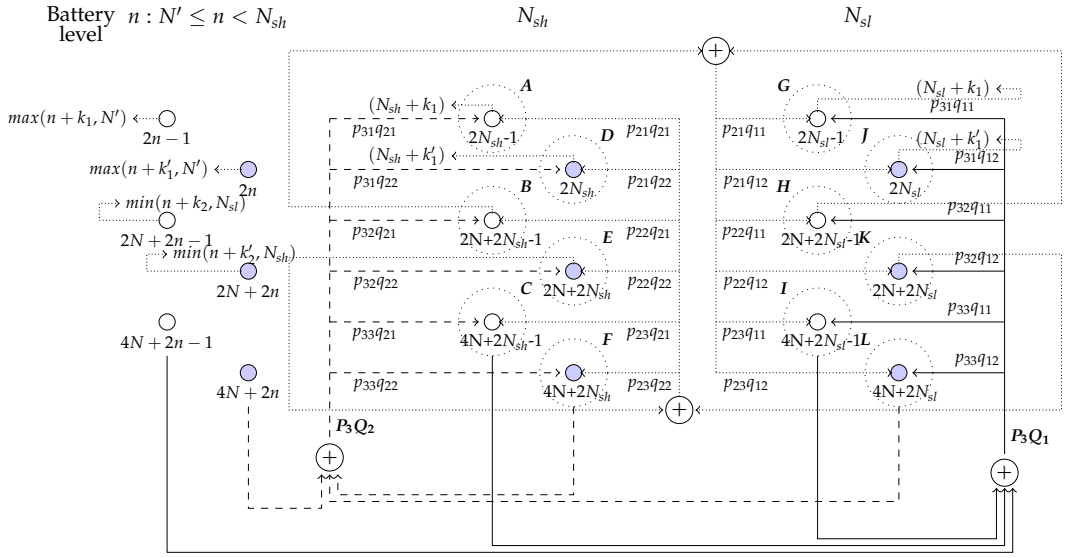

Figure 3.6: State diagram for case 2 and case 3.

We consider Case 2 and Case 3 together because their state transition diagrams have the same structure. Since k_2 and k'_2 are non-negative in these two cases, the critical states with solar day type $S2$ can also result in transitions to critical states. More specifically, high load states with battery level N_{sh} and N_{sl} and solar day type $S2$ may result in transitions to any of the critical states with battery level N_{sh}. Similarly, low load states with battery levels N_{sh} and N_{sl} and solar day type $S2$ may have transitions to critical states with battery level N_{sl}.

To obtain the steady state probabilities of the critical states for these cases, we consider the boundaries shown by dotted circles in Figure 3.6. The balance equations for boundaries H and K around states $2N + 2N_{sl} - 1$ and $2N + 2N_{sl}$ can be written as

$$\pi_{2N_{sl}+2N-1} = p_{32}q_{11}P_3Q_1 + (\pi_{2N_{sh}+2N-1} + \pi_{2N_{sl}+2N-1})p_{22}q_{11} \quad (3.18)$$

$$\pi_{2N_{sl}+2N} = p_{32}q_{12}P_3Q_1 + (\pi_{2N_{sh}+2N-1} + \pi_{2N_{sl}+2N-1})p_{22}q_{12}. \quad (3.19)$$

From the previous two equations we can conclude that

$$\frac{\pi_{2N_{sl}+2N-1}}{\pi_{2N_{sl}+2N}} = \frac{q_{11}}{q_{12}}. \tag{3.20}$$

Similarly, balance equations around boundaries B and E around states $2N + 2N_{sh} - 1$ and $2N + 2N_{sh}$ can be written as

$$\pi_{2N_{sh}+2N-1} = p_{32}q_{21}P_3Q_2 + (\pi_{2N_{sh}+2N} + \pi_{2N_{sl}+2N})p_{22}q_{21} \tag{3.21}$$

$$\pi_{2N_{sh}+2N} = p_{32}q_{22}P_3Q_2 + (\pi_{2N_{sh}+2N} + \pi_{2N_{sl}+2N})p_{22}q_{22} \tag{3.22}$$

which in turn imply

$$\frac{\pi_{2N_{sh}+2N-1}}{\pi_{2N_{sh}+2N}} = \frac{q_{21}}{q_{22}}. \tag{3.23}$$

From Equations (3.18)-(3.23), we have

$$\begin{aligned}
\pi_{2N_{sh}+2N-1} &= \frac{p_{32}q_{21}P_3(Q_2 - p_{22}q_{11}Q_2 + p_{22}q_{12}Q_1)}{(1 - p_{22}q_{22} - p_{22}q_{11} + p_{22}^2q_{11}q_{22} - p_{22}^2q_{12}q_{21})} \\
\pi_{2N_{sl}+2N-1} &= \frac{p_{32}q_{11}P_3(Q_1 - p_{22}q_{22}Q_1 + p_{22}q_{21}Q_2)}{(1 - p_{22}q_{22} - p_{22}q_{11} + p_{22}^2q_{11}q_{22} - p_{22}^2q_{12}q_{21})} \\
\pi_{2N_{sh}+2N} &= (q_{22}/q_{21})\pi_{2N_{sh}+2N-1} \\
\pi_{2N_{sl}+2N} &= (q_{12}/q_{11})\pi_{2N_{sl}+2N-1}.
\end{aligned}$$

Using the steady state probabilities above, the steady state probabili-

ties of the other critical states can be obtained as

$$\pi_{2N_{sh}-1} = p_{31}q_{21}P_3Q_2 + (\pi_{2N_{sh}+2N} + \pi_{2N_{sl}+2N})p_{21}q_{21}$$
$$\pi_{2N_{sh}} = p_{31}q_{22}P_3Q_2 + (\pi_{2N_{sh}+2N} + \pi_{2N_{sl}+2N})p_{21}q_{22}$$
$$\pi_{2N_{sl}-1} = p_{31}q_{11}P_3Q_1 + (\pi_{2N_{sh}+2N-1} + \pi_{2N_{sl}+2N-1})p_{21}q_{11}$$
$$\pi_{2N_{sl}} = p_{31}q_{12}P_3Q_1 + (\pi_{2N_{sh}+2N-1} + \pi_{2N_{sl}+2N-1})p_{21}q_{12}$$
$$\pi_{2N_{sh}+4N-1} = p_{33}q_{21}P_3Q_2 + (\pi_{2N_{sh}+2N} + \pi_{2N_{sl}+2N})p_{23}q_{21}$$
$$\pi_{2N_{sh}+4N} = p_{33}q_{22}P_3Q_2 + (\pi_{2N_{sh}+2N} + \pi_{2N_{sl}+2N})p_{23}q_{22}$$
$$\pi_{2N_{sl}+4N-1} = p_{33}q_{11}P_3Q_1 + (\pi_{2N_{sh}+2N-1} + \pi_{2N_{sl}+2N-1})p_{23}q_{11}$$
$$\pi_{2N_{sl}+4N} = p_{33}q_{12}P_3Q_1 + (\pi_{2N_{sh}+2N-1} + \pi_{2N_{sl}+2N-1})p_{23}q_{12}.$$

In Cases 2 and 3, some of the non-critical states with day type $S2$ may also transition to critical states due to k_2 and k_2' being non-negative. However, these transitions have been neglected due to the following reasons: (i) the number of non-critical states with solar day type $S2$ contributing to critical states is very small (due to k_2 and k_2' being small even for large PV panels) and (ii) the overall probability, P_2, of states with solar day type $S2$ is typically much smaller than those with solar day type $S3$. Thus the contribution of the few non-critical states with solar day type $S2$ is negligible in comparison of those with solar day type $S3$ (where all states contribute to the steady state probability of critical states). Further, our simulation results show that this approximation does not have any appreciable effect on the accuracy of the model. The steady state probabilities of the critical states for Cases 4-8 can similarly be obtained as shown below.

Note that the steady state probability analysis for the other cases (i.e. cases 4-8) have been presented in Appendix B.

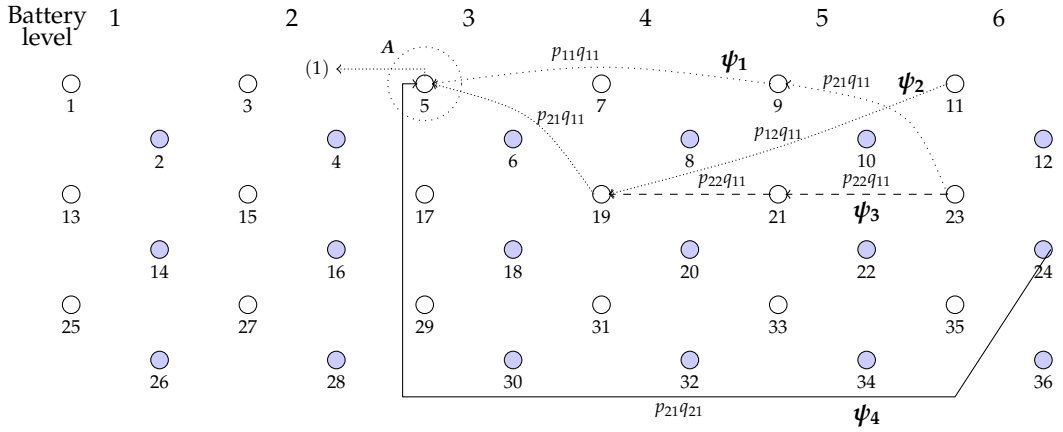

Figure 3.7: State diagram for sample example. Only the transitions of interest to state 5 are shown.

3.5.2 Calculating steady state probability of non-critical states

To obtain the probabilities of the non-critical states, we first define *seed* states as $[\pi_{2N_{sl}}, \pi_{2N_{sl}-1}, \pi_{2N_{sl}+2N}, \pi_{2N_{sl}+2N-1}, \pi_{2N_{sh}}, \pi_{2N_{sh}-1}, \pi_{2N_{sh}+2N}, \pi_{2N_{sh}+2N-1}]$ (i.e. critical states with day type $S1$ and $S2$). The seed states are the critical states whose steady state probabilities may be used to obtain the steady state probabilities of all non-critical states. Note that critical states with solar day type $S3$ are not seed states for they do not lead to transition into non-critical states. To present an intuitive idea of our methodology, consider a simple scenario with just six possible battery levels, as shown in Figure 3.7. For illustration, we assume $k_1 = -2$, $k_1' = -4$, $k_2 = -1$ and $k_2' = -3$. For simplicity, let us assume that the states with battery level 6 are the critical states and states 11, 12, 23 and 24 are the seed states.

To obtain the steady state probability of a non-critical state, we consider the balance equations around its boundary. As an example, consider boundary A around state 5 in Figure 3.7. There may be transitions into state 5 from states 9, 19 and 24. However, states 9 and 19 (non-critical states) are visited only as a result of transitions from states 11, 12, 23 and 24 (seed states). The

probability of all transitions into state 5 (or any non-critical state) can be expressed in terms of the steady state probabilities of the seed states. For example, we have

$$\begin{aligned}
\pi_5 &= p_{11}q_{11}\pi_9 + p_{21}q_{11}\pi_{19} + p_{21}q_{21}\pi_{24} \\
\pi_9 &= p_{21}q_{11}\pi_{23} \\
\pi_{19} &= p_{12}q_{11}\pi_{11} + p_{22}q_{11}\pi_{21} \\
\pi_{21} &= p_{22}q_{11}\pi_{23}.
\end{aligned}$$

Using the equations above, π_5 may be expressed in terms of the steady state probability of the seed states as

$$\pi_5 = p_{21}p_{12}q_{11}^2\pi_{11} + p_{21}q_{11}((p_{22}q_{11})^2 + p_{11}q_{21})\pi_{23} + p_{21}q_{21}\pi_{24}.$$

Thus, in order to obtain the steady state probability of any non-critical state, we need to find all possible transition paths to that state, starting from any of the seed states. To achieve this, we propose a path tracking algorithm shown in Algorithm 3: $PATR(N_s, n, k, \phi(\cdot), f(\cdot), g(\cdot), N_{sl}, N_{sh})$. The inputs to the algorithm include N_s (the battery level of the seed states, typically N_{sl} or N_{sh}), n (the battery level of the target non-critical state), $k = [k_1, k_1', k_2, k_2']$, and the functions $\phi(\cdot)$, $f(\cdot)$ and $g(\cdot)$ that track the battery level, solar energy state and BS load state, respectively, of the intermediate states in the paths from the seed states to state with battery level n.

Recall that there are no transitions from states with solar day type $S3$ to the non-critical states. Thus we have only four state transitions of interest from a given battery level (from states with solar day type $S1$ and $S2$) and these transitions are to states whose battery levels are different by any

of the values in $k = [k_1, k_1', k_2, k_2']$. The algorithm uses the vectors ϕ', f' and g' to track the battery level, solar day type and load day type of the intermediate states in a path from a seed state to states with battery level n. The vectors ϕ, f and g serve as inputs with the (incomplete) paths discovered so far, and ϕ, f and g are null vectors when the function $PATR$ is initially called. From the current state in the path, we consider all four possible transitions (based on k), and T denotes the battery level after the transition (line 2). Note that as mentioned earlier, the vectors ϕ', f' and g' which are vectors to track the path save the information regarding the battery level, solar day type and the load day type of the intermediate states corresponding to a given transition (i.e. one among the four transitions corresponding to the different values of k (as $k \in \{k_1, k_1', k_2, k_2'\}$)) (lines 3-9). Next we ensure that boundary conditions are not violated (lines 11-19). Specifically, if the intermediate state is a low load state then the next battery level cannot exceed N_{sl} whereas if it is a high load state then it cannot exceed N_{sh}. Additionally N cannot go below N'. Now, if the resulting battery level after the transition is n, we add the entire path as an entry in the global path indicator variables (i.e. Φ, F and G, see lines 20-24). Note that we also evaluate the number of transitions that have been made in the current path (stored in variable t, see line 25 in the PATR algorithm). Once the number of transitions becomes large (typically > 4), the likelihood of occurrence of that path (which equals the product of the state transition probabilities between all intermediate states) becomes very small and thus can be neglected. Thus while the path length is smaller than a threshold t_{max}, the $PATR$ algorithm is iteratively called with T as the current battery level (line 27).

We denote the number of possible paths by s and Ψ denotes all possible

Algorithm 3 Path Tracking (PATR) Algorithm

function $PATR(N_s, n, k, \phi, f, g, N_{sl}, N_{sh})$
  for $i = 1$ to 4 **do** ▷ Different transition paths from given battery level
    $\phi' = [\phi\ N_s]$; ▷ Capture battery level of intermediate state
    $f' = [f\ ceil(i/2)]$; ▷ Capture solar day type of intermediate state
    if $i = 1$ or $i = 3$ **then**
      $g' = [g\ 1]$; ▷ Capture load day type of intermediate state
    else
      $g' = [g\ 2]$;
    end if
    $T = N_s + k(i)$; ▷ next battery level after intermediate state
    if $T > N_{sl}$ and $(i = 1$ or $i = 3)$ **then**
      $T = N_{sl}$; ▷ Ensuring T$\leq N_{sl}$ if intermediate state has low load
    end if
    if $T > N_{sh}$ and $(i = 2$ or $i = 4)$ **then**
      $T = N_{sh}$; ▷ Ensuring T$\leq N_{sh}$ if intermediate state has high load
    end if
    if $T \leq N'$ **then** ▷ Ensuring T $\geq$ N′
      $T = N'$;
    end if
    if $T = n$ **then** ▷ saving path identifiers if $T = n$
      $\Phi = [\Phi; \phi']$;
      $F = [F; f']$;
      $G = [G; g']$;
    end if
    $t = length(\phi')$; ▷ storing transition path length at current stage
    if $(T < N_{sl}$ and $T \geq N'$ and $t < t_{max})$ **then**
      $PATR\ (T, n, k, \phi', f', g', N_{sl}, N_{sh})$;
    end if
  end for
end function

paths from the seed states to states with battery level n. Each element of Ψ represents a path that is uniquely characterized by the values of Φ, F and G as

$$\Psi = \{\psi_1, \psi_2..., \psi_l, ..., \psi_s\}; \quad \psi_l = (\Phi_l, F_l, G_l). \tag{3.24}$$

The vectors Φ_l, F_l and G_l are of the form

$$\begin{aligned} \Phi_l &= \{\phi_{l1}, \phi_{l2}...\phi_{lu}\} \\ F_l &= \{f_{l1}, f_{l2}., ..., f_{lu}\} \\ G_l &= \{g_{l1}, g_{l2}..., g_{lu}\} \end{aligned}$$

where u is the number of intermediate stages in the l-th path and ϕ_{l1}, f_{l1} and g_{l1} denote the battery level, solar day type, and load day type of the initial state, and so on. For example, considering the states with battery level $n = 3$ in Figure 3.7, the solution for Ψ is given as

$$\Psi = \{\psi_1, \psi_2, \psi_3, \psi_4\} \tag{3.25}$$

with $\psi_1 = (\Phi_1, F_1, G_1)$ and so on. Note that the different paths are also indicated in Figure 3.7 for clarity. The various parameters (e.g. Φ_1, F_1 etc.) for Figure 3.7 are as follows

$$\Phi_1 = \{6, 5\} \quad F_1 = \{2, 1\} \quad G_1 = \{1, 1\} \tag{3.26}$$

$$\Phi_2 = \{6, 4\} \quad F_2 = \{1, 2\} \quad G_2 = \{1, 1\} \tag{3.27}$$

$$\Phi_3 = \{6, 5, 4\} \quad F_3 = \{2, 2, 2\} \quad g_3 = \{1, 1, 1\} \tag{3.28}$$

$$\Phi_4 = \{6\} \quad F_4 = \{2\} \quad G_4 = \{2\}. \tag{3.29}$$

Now, let Λ_l denote the steady state probability of the seed state of the l-th

path. Then the steady state probability of a state U with battery level n, solar day type α and load day type β, can be written as

$$\pi_U = \sum_{l=1}^{s} \Lambda_l p_{f_{l1}f_{l2}} q_{g_{l1}g_{l2}} p_{f_{l2}f_{l3}} q_{g_{l2}g_{l3}} \cdots p_{f_{lu}\alpha} q_{f_{lu}\beta}. \tag{3.30}$$

Finally, the steady state probabilities of all the states may be used in Equation (3.15) to obtain the overall outage probability.

Remark: Our model implicitly assumed that N_{sl} and N_{sh} are separated by a unit difference in the charge levels, which, to a large extent, is a result of the granularity in the battery levels being taken to be 1 kW. However, based on the base station type/size, this difference may not be around 1 kW (and can be, say 0.5 kW or 2 kW etc.). In that case, to use the proposed model, the granularity of the system would need to be adjusted so that N_{sl} and N_{sh} are still separated by a unit charge. Also, the model assumes that all states with solar day type $S3$ transition to a state with battery level N_{sh} or N_{sl}. While this assumption is valid in most realistic scenarios, it does not hold for very small PV panels (e.g. 7 kW or smaller for macro base stations). However, such small PV panels are not used in practical scenarios, since the number of batteries required for such scenarios tends to be too large to be economically and spatially feasible [16]. This can also be observed from Figures 3.14 and 3.15 which show that as the PV panel size decreases, the number of batteries required for a given threshold on the outage probability increases sharply, thereby increasing the capital cost. Also, note that for every non-critical state, the PATR algorithm starts from a critical state (which are 8 in number) and searches if the battery level corresponding to the non-critical state is achieved within t_{max} hops. Thus the worst-case computational complexity of the PATR algorithm for estimating the steady state probability of the non critical state is $O(t_{max}N)$.

3.5.3 Parameter estimation

The state transition probabilities and solar energy profiles for the solar energy model described in Section 3.4.2 are obtained using historical solar irradiation data. The solar irradiation data is fed to NREL's SAM tool which gives the hourly harvested solar energy for a PV panel with DC rating 1 kW as an output. Due to seasonal variations, different months in the year have different values for the various parameters in the model. To find the parameters for a given month, we consider the series of data corresponding to the days of that particular month from all years in the historical solar energy data. This data is then fed to the SAM tool to generate the hourly harvested solar energy. Next we calculate the solar energy generated for each day, and use it for categorizing the day into a given type ($S1$, $S2$ or $S3$). The values of γ_1 and γ_2 to categorize the days are estimated for a given PV panel size based on the energy harvested in a day compared to the average daily BS power consumption, L_{avg}. For a PV panel with rating PV_w, γ_1 and γ_2 are given by

$$\gamma_1 = \frac{0.5 L_{avg}}{PV_w}, \qquad \gamma_2 = \frac{L_{avg}}{PV_w}. \tag{3.31}$$

The intuition behind the choice of thresholds γ_1 and γ_2 is that $S1$ and $S2$ denote very bad and bad weather days, respectively, where the solar energy harvested during the day is less than the energy required to power the BS for a day. With this choice of γ_1 and γ_2, the energy harvested in $S1$ days is less than half of the energy required to power the BS over the day, and while $S2$ days harvest more energy than $S1$ days, it is still less than that required to power the BS during the entire day.

Next, we obtain the hourly harvested solar energy profile for the three day types by calculating the average hourly harvested energy of the days with

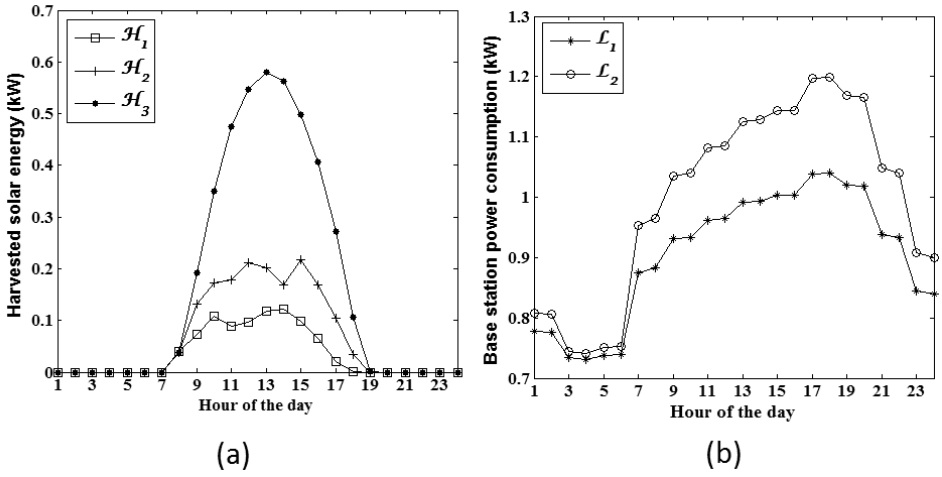

Figure 3.8: a. Average harvested energy profile for 3 day types for Jaipur (September, PV_w =12 kW) b. Average load profiles for the 2 load day types.

that day type. Figure 3.8(a) shows example values of the average harvested energy profiles for the different day types for Jaipur, India for the month of September and for $PV_w = 12$ kW. Also, from the statistical data we compute the transition probabilities $p_{ij}, 1 \leq i, j \leq 3$, of going from one day type to another. These state transition probabilities are used to calculate the steady state probabilities of being in a given solar day type (i.e. the probabilities P_1, P_2 and P_3). After the parameter estimation is done individually for every month of the year, the corresponding outage probability for that month for a given PV-battery configuration may be evaluated using the framework developed in this chapter. The outage probability for each month is averaged to obtain the overall outage probability for the given PV-battery configuration.

For generating the load profiles we use the model described in Section 2.3.1 to generate call arrivals and their call durations on a per-minute basis. The call volumes thus obtained are normalized by the maximum number of users which can be supported by the BS at a given time to give the normalized traffic. This is used in Equation (2.1) to calculate the BS power

consumption. Note that the call arrival rates are lower on a low load day thus leading to lower BS power consumption. The traces of BS power consumption (load) thus obtained are averaged on an hourly basis to calculate the hourly BS load profile for the days. Next, the BS power consumption profile for a significant number of days (of the order of years) is used to find the average load profile during a high load day (by averaging the load on weekdays) and low load day (by averaging the load on weekends). Figure 3.8(b) shows the average load profiles used in this chapter for the two load days. The traces are also used to obtain the state transition probability between a low load day and a high load day (i.e. $q_{ij}, 1 \leq i, j \leq 2$), and the steady state probabilities Q_1 and Q_2.

3.6 Cost optimal dimensioning

The formulation for the cost optimal PV panel and battery dimensioning problem for a solar powered BS is as follows

$$\begin{aligned} \underset{PV_w, n_b}{\text{minimize}} \quad & N_{Bat} C_B + PV_w C_{PV} \\ \text{Subject to:} \quad & \Omega < \lambda \end{aligned}$$

The details of the problem has been described in the previous chapter in Section 2.5, and is thus omitted. The relationship between Ω (the outage probability) and the optimization variables (PV_w and n_b) is explained as follows. In the model proposed in this chapter, for higher PV panel sizes (PV_w), the probability of days being S3 (good weather days) is higher. Thus the steady state probability of the states with solar day type S3 is higher. States with the solar day type as S3 correspond to good weather days and

thus have lower outage probability. Therefore, for larger PV panel sizes the outage probability turns out to be lower. Further, for a given PV panel size, when the battery dimensions (n_b) are lower, there is a higher chance of a state transition occurring from a given state to the cut-off battery level (N') during the bad weather days ($S1$ and $S2$ days). This contributes to the higher outage probability when the number of batteries is lower. However, when the battery dimensions are large, such a probability of transition to the cut-off battery is lower, thus leading to a lower outage probability.

The way the optimization problem is solved in this chapter is similar to that described earlier in Section 2.5. However, the difference in the solution methodology is as follows. In Section 2.5 we had used simulations with traces of BS power consumption and solar energy for estimating the outage probability and battery lifetime corresponding to a particular configuration of PV panel size and number of batteries. However, in this chapter we use the model proposed in this chapter to estimate these parameters for a given configuration of PV panel size and number of batteries.

3.7 Numerical results

This section presents results to verify the proposed outage estimation and battery lifetime evaluation model and the framework for cost optimal system dimensioning of solar powered BSs.

We consider a LTE macro base station with 10 MHz bandwidth and 2×2 Multi Input Multi Output (MIMO) configuration with capacity to support 300 calls at any given time instant. We assume that the BS has three sectors and each sector has two transceivers (thus, $Y_{TRX} = 6$). To validate the proposed framework, we consider two geographically diverse locations:

San Diego (USA) and Jaipur (India). The various parameters for the solar energy model are obtained using the statistical solar energy data from NREL database and the methodology described in Section 3.5.3. We use seven years of data (2000-2006) for parameter estimation and evaluate the performance using data for years 2007-2009. We assume E_{panel} as 0.5 kW. We assume that the BSs use 12 V, 205 Ah flooded lead acid batteries, each with a capacity of 2.46 kWh. ν, the fraction of total battery capacity below which the batteries are not allowed to discharge has been taken as 0.3. For modelling the load profiles we use the methodology described in Section 2.3.1 and the various parameters were calculated as described in Section 3.5.3. We considered call arrival rates during the different hours for the different days as shown in Figure 2.6 and the average call duration was taken as 2 minutes [56]. The average BS power consumption during a day, L_{avg}, was taken as 22.8 kWh. t_{max} for the PATR algorithm was taken as 6. As benchmarks for comparison, we consider results obtained using simulations with empirical traces for the solar energy and the traffic load, as well as the model proposed in [21].

Following is a brief description of how the results are obtained using the above-mentioned information:

- The description of how results are obtained using empirical traces and the benchmark model [21] has been already described in the results section of the previous chapter (Section 2.7).
- For the model proposed in the paper, we estimate the various modeling parameters (e.g. the solar energy profiles for the different day types, load profiles for the different load day types, and the transition probabilities between different solar day and load day types) as described in Section 3.5.3. Note that the solar energy data for year

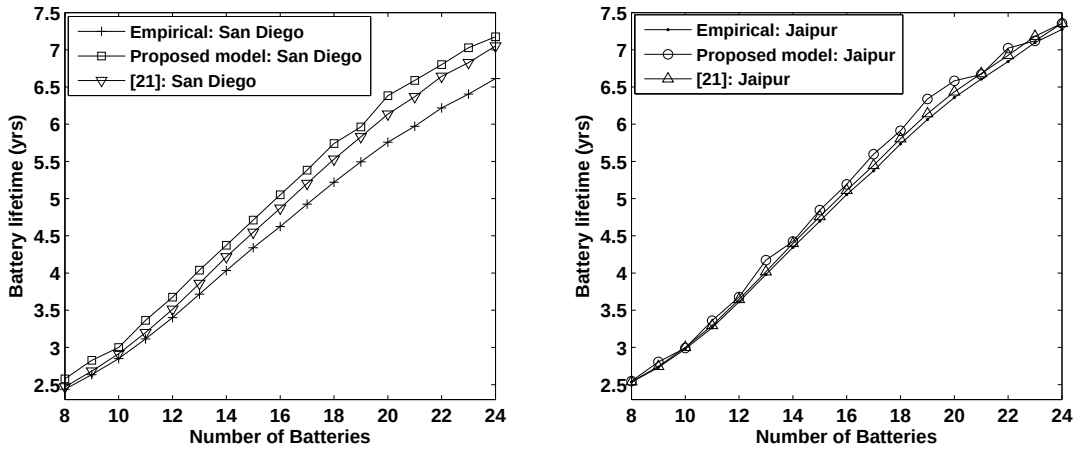

Figure 3.9: Number of batteries vs battery lifetime for the two locations for PV wattage of 12 kW.

2000-2006 was used for estimating the solar energy parameters.

- With the solar energy and BS load profiles, and the transition probabilities in place, we can use the framework proposed in this chapter to estimate the outage probability and battery lifetime for a given configuration of PV panel size and number of batteries.
- As our ultimate ojective is to find the cost-optimal PV panel and battery configuration, we use the detailed solution methodology described in Section 2.5 to find the solution of the optimization problem.

3.7.1 Battery lifetime

We begin with analyzing how the battery lifetime varies with the number of batteries. Please note that the battery lifetime is an important variable to be estimated for resource dimensioning and it appears in Equation (2.10) of Section 2.5 (Cost optimal dimensioning). Figure 3.9 shows the battery lifetime obtained for a PV panel size of 12 kW installed at the BS site for the two locations. We note that our model predicts the battery lifetime quite

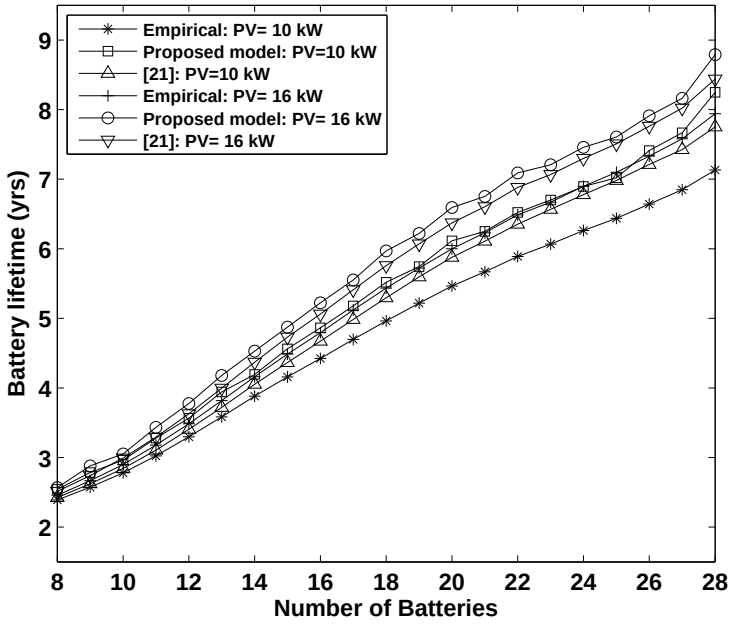

Figure 3.10: Battery lifetime for two different PV panel sizes for San Diego.

accurately for both the locations. From Figure 3.9, we note that the prediction of the battery lifetime for the proposed model has accuracy above 90% for San Diego and above 95% for Jaipur (whereas for [21] these values are 94% and 98% respectively). Note that although the proposed model has lower accuracy than [21] in terms of predicting the battery lifetime, it by and large outperforms [21] in terms of outage estimation as shall be shown in Section 3.7.2. From Figure 3.9 note that as the number of batteries decreases, the battery lifetime decreases. This is because with fewer batteries, the batteries are more likely to go through deeper discharge cycles, which reduces their lifetime. In Figure 3.10 we show the battery lifetime for two different PV panel sizes for San Diego to show the effect of PV panel size on the battery lifetime. The nature of result for Jaipur is similar. We note that for a larger PV panel size, the battery lifetime is higher than that for a lower PV panel size. The reason for this is that for a larger PV panel size, the energy harvested is also larger and thus the batteries go through fewer deep discharges. Also, the values for the battery lifetime prediction

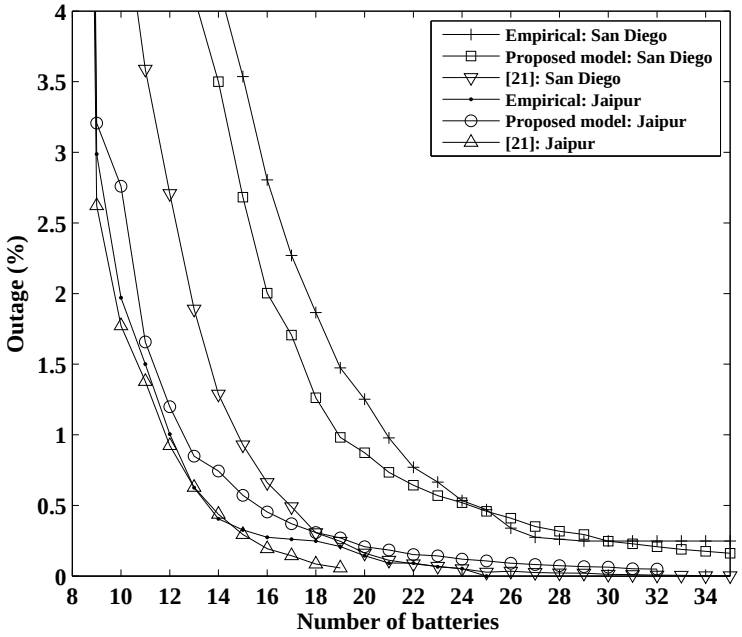

Figure 3.11: Outage probability vs number of batteries (PV panel size: 12 kW).

accuracy for these two PV panel sizes for the proposed scheme (as well as the benchmark scheme) is similar to those discussed while commenting on the battery lifetime prediction accuracy for Figure 3.9 discussed earlier in this section.

3.7.2 Energy outage analysis

Next we analyze how the outage probability is affected by the number of batteries. For both locations, we consider a PV panel with DC rating 12 kW installed at the BS site. The variation in the outage probability with respect to the number of batteries is shown in Figure 3.11. It can be seen that the outage probability estimated using our model has a close match with that obtained using simulations with empirical data. Also, the proposed model outperforms the model proposed in [21] in predicting the outage probability. Note that when the number of batteries becomes very small, the outage probability rises sharply. This is on account of batteries being

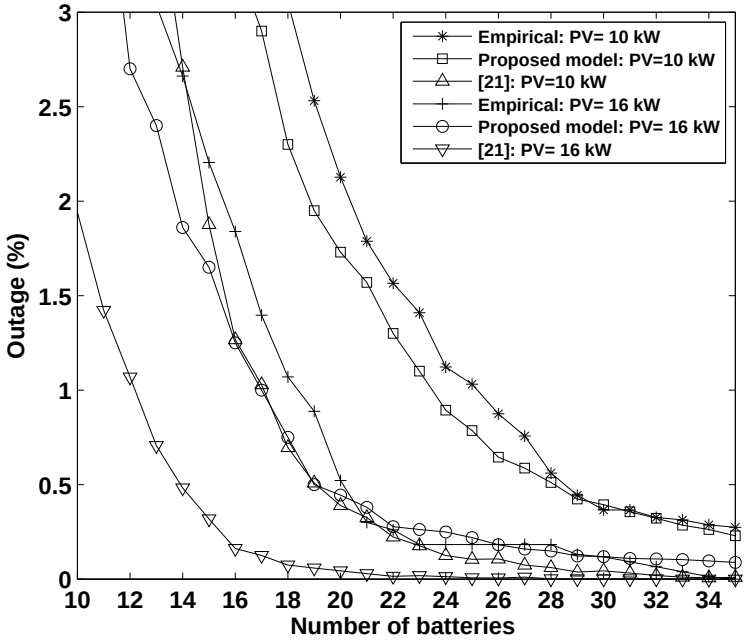

Figure 3.12: Outage probability versus number of batteries required for different PV panel sizes: San Diego.

too small to hold sufficient charge to power the BS even when there is sufficient energy harvested. Further, we can also observe that the number of batteries required to meet very low outage probabilities ($< 0.25\%$) becomes very large. This is because for any location, the outages are usually caused when there are many bad days at a stretch. These periods of consecutive bad weather days determine the required battery size and ensuring very low outage probabilities requires a large number of batteries.

3.7.3 Effect of PV panel size on outage

We consider two PV panel sizes: 10 kW and 16 kW to study the impact of the PV panel size on the outage probability. The outage probability corresponding to the different PV panel sizes with respect to the number of batteries have been shown in Figures 3.12 and 3.13 for San Diego and

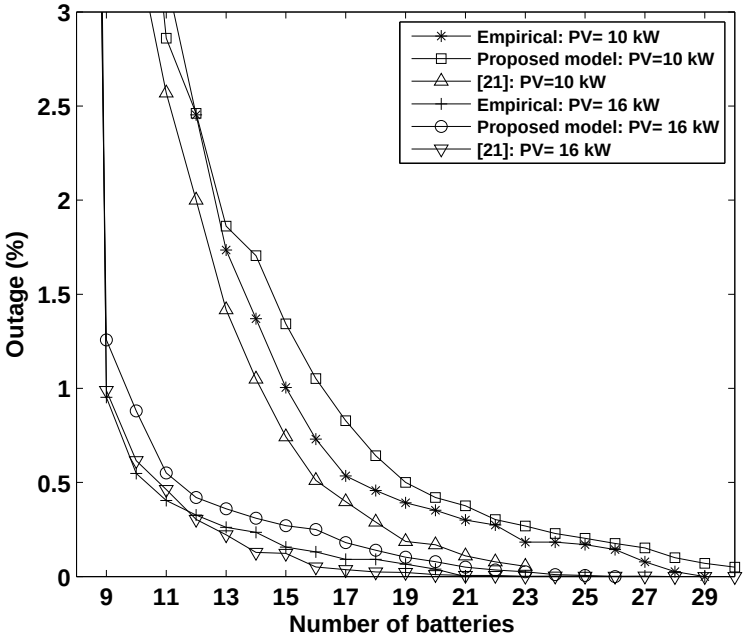

Figure 3.13: Energy outage vs number of batteries required for different PV panel sizes: Jaipur.

Jaipur, respectively. Note that for a larger PV panel size, the same outage probability can be met with a lower number of batteries, as compared to the case of smaller PV panel size. Again, from the plots we can see that proposed model outperforms the benchmark model from [21] in terms of predicting the outage probability for a given battery size.

3.7.4 PV-Battery configuration for a given outage constraint

Given a outage constraint, a network operator is usually interested in the minimum number of batteries required for different PV panel sizes. Note that these configurations of PV panel and battery sizes are prospective candidates for resource dimensioning for the BS, and the configuration with the lowest cost is selected by the operator. We consider two target outage values: 0.5% and 1%. Figures 3.14 and Figure 3.15 show these PV panel-

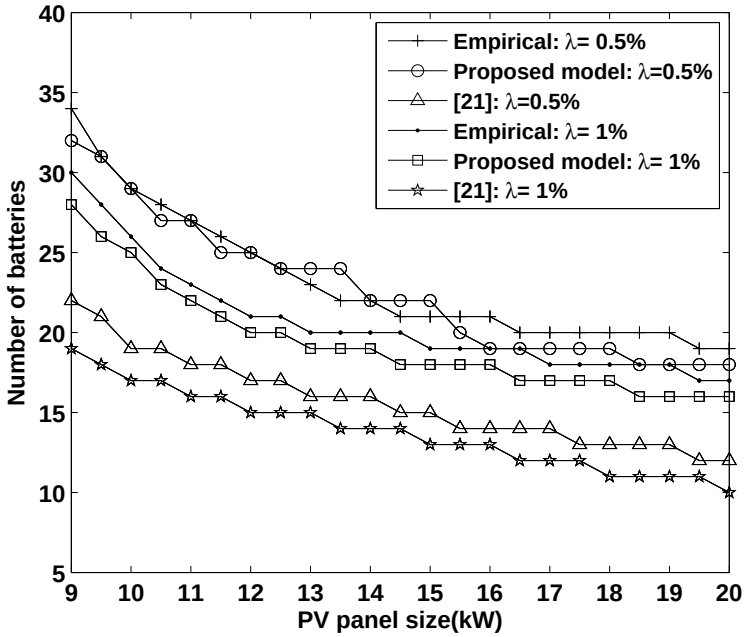

Figure 3.14: PV panel size vs number of batteries required for different outage probabilities (λ): San Diego.

battery configurations for achieving the two target outage values for the two locations.

3.7.5 Cost optimal configuration

In Section 3.7.1 we presented the battery-lifetime estimation results which are an important step in determining the optimal-cost configuration (it is specifically used in Equation (2.10)). We also presented results showing the accuracy of the proposed model in terms of estimating the outage probability in Sections 3.7.2 and 3.7.3. Outage probability is an important parameter to estimate because the cost-optimal resource dimensioning is done so as to ensure the outage to be below a certain threshold outage value (λ). Next, results concerning the prospective candidates for cost-optimal resource provisioning problem were presented in Section 2.7.4. This section presents results for the cost-optimal PV and battery configuration.

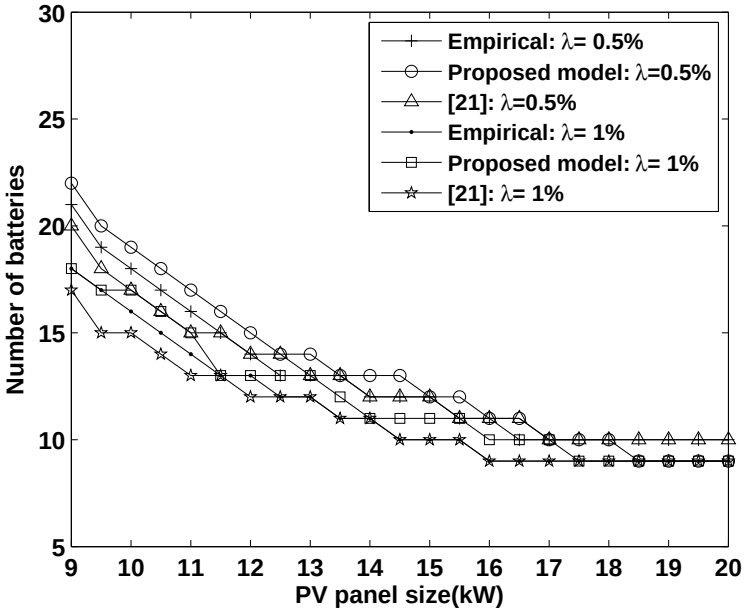

Figure 3.15: PV panel size vs number of batteries required for different outage probabilities (λ)): Jaipur.

Table 3.2: Optimal Configuration for $T_{run} = 5$ years.

Location	Empirical		[21]		Proposed model	
	PV_w	n_b	PV_w	n_b	PV_w	n_b
$\lambda = 0.5\%$						
San Diego	10	29	9	22	10.5	27
Jaipur	9.5	19	9.5	18	9.5	20
$\lambda = 1\%$						
San Diego	10.5	24	9	19	10.5	23
Jaipur	9	18	9	17	9	18

The cost associated with the prospective PV-Battery configurations which meet the target outage probability can be calculated as described in Section 3.6. We consider two target operational times $T_{run} = 5$ years and $T_{run} = 10$ years. Also, based on the market statistics, we assume the cost of PV panels C_{PV} as US$ 1000/kW and the cost of the lead acid batteries C_B has been assumed to be US$ 280 [66]. The cost optimal configuration for the two target operational times (for two target outage probabilities of 0.5% and 1%) has been tabulated in Tables 3.2 and 3.3. We note that the results from the proposed model closely match the optimal configuration using simulations

Table 3.3: Optimal Configuration for $T_{run} = 10$ years.

Location	Empirical		[21]		Proposed model	
	PV_w	n_b	PV_w	n_b	PV_w	n_b
$\lambda = 0.5\%$						
San Diego	13.5	22	10	19	14	22
Jaipur	10.5	17	10.5	16	10.5	18
$\lambda = 1\%$						
San Diego	12	21	9.5	18	12	20
Jaipur	9.5	17	9	17	9.5	17

using empirical data and outperforms the benchmark model [21]. From Tables 3.2 and 3.3 we observe that considering a larger operational lifetime results in a bigger PV panel size in the cost optimal solution. This is because for optimization over a larger operational time, the cost of replacement of the batteries starts dominating the overall cost and thus configurations with larger PV panel sizes that need smaller number of batteries tend to be more cost optimal.

Remark: From the above numerical results, we see that for San Diego, the proposed model has significantly better accuracy than the model proposed in [21]. This is because our model specifically models the correlations in the weather patterns of successive days. The analysis shows the importance of carefully accounting for the bad weather days while developing models for dimensioning resources for applications requiring high degree of reliability. We also note that the predictions from the benchmark models are reasonably accurate for Jaipur, which is a location that has very good solar insolation. Thus, since Jaipur only has very few bad weather days in a year, there is limited improvement in the accuracy by using our proposed model. However, [21] relies on the generation of long term synthetic traces of solar energy data which is computationally very intensive. Additionally, [21] does not model the system load and the battery levels. These factors also contribute to the superiority of our proposed model over the model

proposed in [21].

Note that the results and trends for the model proposed in this chapter are similar to those using the model proposed in the previous chapter. For example, in Figure 3.16 we show the results for the battery lifetime, and PV panel and number of batteries required for a tolerable outage probability for the model proposed in chapter 2 and chapter 3. Ch2 and Ch3 in the legend of Figure 3.16 denote Chapter 2 and Chapter 3, respectively. The left figure shows the battery lifetime for the location Kolkata for PV panel size 12 kW. The right figure shows the PV panel and number of batteries configuration to ensure outage to be below 1%. Note that the model proposed in chapter 3 has slightly lower accuracy as compared to that of model proposed in chapter 2. However, the model proposed in Chapter 3 has a lower complexity which is primarily because of using fewer states for solar energy. In Chapter 2 we have a multi-state markov model, where the solar energy can be in one of 192 possible states (2 day types $\times$ (24 hours $\times$ 4 solar state categories per hour)). However in Chapter 3 we have just 3 day types (and the average value of the solar energy profile is considered for those days). Additionally Chapter 3 simplifies the outage estimation process in the sense that the proposed framework finds the steady state probability of being in the different states in the model and identifying which states are the outage states; and thus it does not require long term simulation using solar energy traces and BS power consumption like that required in the model proposed in Chapter 2 and [21].

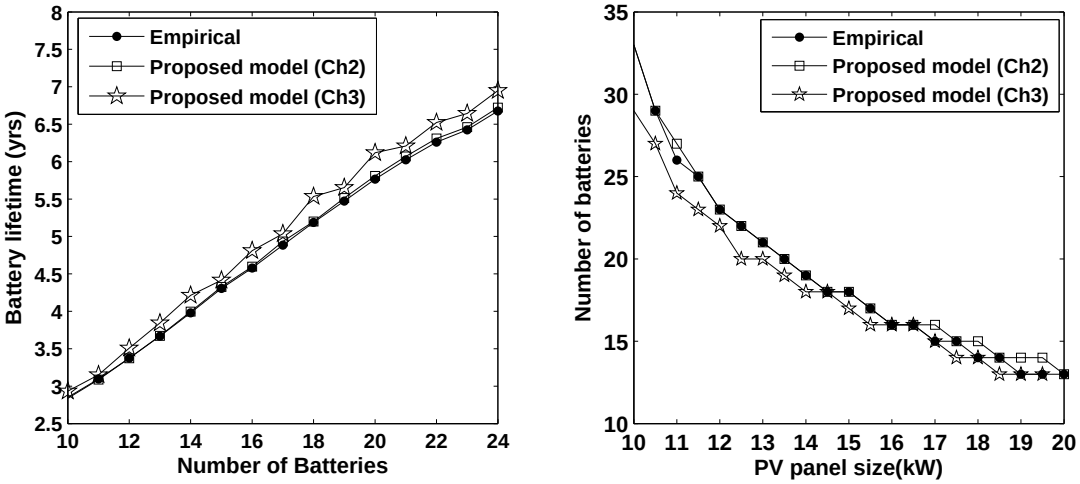

Figure 3.16: (Left) Number of batteries vs battery lifetime for Kolkata for PV wattage of 12 kW, (Right) PV panel size vs number of batteries required for outage probability $\lambda = 1\%$: Kolkata.

3.8 Conclusion

In this chapter we proposed an analytic model for estimating the outage probability and battery lifetime for cellular BSs powered by solar energy. The harvested solar energy, base station load and the battery levels were modeled as discrete time Markov processes. We modeled the solar energy for a given day as a three state markov process whereas the BS load was modeled as a two state Markov process. The battery level was discretized for reducing the state space. These models were further used to estimate the outage probability and battery lifetime associated with a given PV panel size and battery configuration. Using this estimate, the problem of obtaining the cost optimal PV panel-battery configuration for a solar powered BS was addressed. The proposed model was verified by comparing against simulation using empirical traces of solar energy and load data, and was shown to outperform the current state of the art.

Chapter 4

Green Energy and Delay Aware Downlink Power Control and User Association for Off-Grid Solar Powered Base Stations

4.1 Introduction

Using renewable resources like solar energy to power the base stations (BSs) has emerged as a promising solution for greening cellular networks [77]-[79]. In the last two chapters we addressed the issues related to resource provisioning for solar powered BSs. Next in this chapter and in Chapter 5 we study operational strategies for a network of solar powered BSs. In this chapter we consider a network of off-grid solar powered BSs. Such solar powered BSs are carefully provisioned with resources like PV panels and batteries, taking into account the trade-off between the CAPEX

(capital expenditure) and quality of service performance (QoS) [16]. Due to cost constraints, the BSs cannot be over-provisioned beyond a certain degree and thus they require additional effort for managing the green energy available to them, specifically during bad weather periods. In the absence of such energy management, the network can experience critical energy outages during these times. Another key challenge in operating a network of such BSs is to intelligently manage the green energy available to the BSs while ensuring low traffic latency. This chapter presents a methodology for minimizing the traffic latency, given the constraints on the energy availability at the solar-powered BSs. In contrast to existing approaches based on just user association reconfiguration or BS on/off strategies, our methodology uses a combination of intelligent energy allocation, and green energy and delay aware BS downlink power control and user association. We show the performance gains of the proposed methodology over existing benchmarks through simulations using a real BS deployment scenario from United Kingdom (UK).

The rest of this chapter is organized as follows. Section 4.2 presents the literature review. Section 4.3 presents the system model. Section 4.4 presents the problem formulation. Section 4.5 presents the solution methodology. Section 4.6 presents the numerical results and Section 4.7 summarizes the chapter.

4.2 Literature review

Reducing the network energy consumption is one of the ways of solving the problem of avoiding energy outages at the BSs during bad weather periods [80]. In related work, [81] introduces the concept of energy saving

in a network by BS switching (i.e. switching off some of the BSs to reduce network energy consumption). Some basic issues in dynamic BS switching are described in [82], [83] and [84]. A framework for BS switching and transmit power control with the objective of minimizing the energy used in the network is proposed in [85]. In [86], the authors propose a scheme (named SWES) for dynamic switching of BSs to minimize the overall energy consumption. This scheme saves energy by turning off BSs and it is a greedy heuristic which seeks to determine the minimum number of BSs required to serve the area, with the desired quality of coverage. The authors in [87] propose cell breathing techniques for bringing down the network energy consumption. Cell breathing refers to BSs dynamically reconfiguring the area being served by them based on the network traffic. The authors in [87] achieve cell breathing by adjusting the transmit power levels of the BSs. The author in [88] proposes a rate and power control based energy-saving technique for orthogonal frequency division multiple access (OFDMA) systems. The authors in [89] propose a scheme which uses the adaptation of BS transmit power levels and coverage area (based on the channel condtions and traffic load) to improve the energy efficiency performance of an OFDMA system. An energy-efficient scheme for resource allocation in OFDMA systems with hybrid energy harvesting BSs is proposed in [90] where a dynamic programming approach for power allocation is used to minimize the network energy consumption. Further, [91] proposes an algorithm, named ICE, for green energy aware load balancing to minimize the overall energy consumption, achieved by tuning the beacon levels of the BSs.

The studies above are primarily focused on minimizing the network energy consumption. However, these studies do not consider the impact

of the energy minimization on the network delay performance. Studies which address network delay performance include [92] which proposes a distributed user association scheme using a primal-dual formulation for traffic load balancing. Authors in [93] propose an α-optimal user association policy for flow level cell load balancing with the objective of maximising the throughput or minimizing the system delay. However the above-mentioned schemes ([92],[93]) consider BSs powered by the grid and thus do not account for the green energy availability at the BSs. Methodologies which consider the green energy availability in addition to the delay performance of the system include [94] and [95]. The authors in [94] propose the GALA scheme which accounts for the green energy availability at the BS while making user-association decisions. The authors formulate the problem of minimizing the sum of weighted latency ratios of the BSs where the weights are chosen to account for the green energy availability at the BSs. Authors in [95] consider BSs powered by hybrid supplies and formulate the problem of minimizing the weighted sum of the cost of average system latency and the cost of on-grid power consumption. The approach in [94] and [95] to manage the available energy and network latency is by reconfiguring the BS-MT (mobile terminal) user-association. In contrast to such an approach, this chapter presents a methodology for energy and latency management based on downlink transmit power control in addition to user association reconfiguration, and demonstrates its performance gains over existing approaches.

Also, the above-mentioned studies solve the problem of latency management and green energy utilization for a given instant of time and do not deal with the allocation of the available green energy over time. Thus, in addition to downlink power control and user association reconfiguration,

our methodology uses a temporal energy allocation algorithm to intelligently manage the green energy available to the BSs so as to maximize the benefit derived from it. With this energy allocation in place, this chapter presents a comprehensive framework for the operation of an off-grid BS, guiding the energy allocation, downlink power control, as well as user-association which has been missing in existing literature [98], [99].

An emerging alternative for improving the performance of cellular networks is through the use of distributed antennas wherein multiple BSs use joint transmission and reception [96], [97]. This approach requires a setup where all baseband signal processing is done at a central processor (the setup of Cloud-Radio Access Network (C-RAN)), whereas the BSs only perform the radio frequency (RF) operations. The BSs transfer the information to the central processor through high-capacity backhaul links which is further transferred back to the BSs after signal processing. However, this paper does not consider such a setup as it requires high capacity back-haul links to be setup between the BSs and the central processor which may not be viable due to various geographic and economic reasons, specifically for off-grid scenarios (e.g. mountainous terrains or developing nations with a communication infrastructure in its budding phase).

4.3 System model

In this section we describe the traffic model considered in the chapter. We also describe the formulation of the BS load and the network latency.

4.3.1 Traffic model, BS load and Network latency

We consider a network of cellular BSs offering coverage to a geographical region $\mathcal{R}$. We denote the set of the BSs as $\mathcal{B}$ and the user locations are denoted by $x \in \mathcal{R}$. For simplicity, in this chapter, we focus only on downlink communication (i.e. BSs to MTs). We denote the downlink transmit power vector of the BSs by P. The BSs can only operate at discrete values of transmit power levels which are denoted by $P(j) \in \{0, \omega, 2\omega, \cdots, P_{max}\}$, where $P(j)$ denotes the power level of the j-th BS, ω is the granularity of power control, and P_{max} is the maximum transmit power level at which the BSs can operate. We assume that file transfer requests at location x arrive following a Poisson point process with arrival rate $\lambda(x)$ per unit area and an average file size of $\frac{1}{\mu(x)}$. We define the traffic load density at location x as $\gamma(x) = \frac{\lambda(x)}{\mu(x)}$, where $\gamma(x)$ captures the spatial traffic variability. Assuming BS j is serving the users at location x, the rate offered by the BS to the users can be generally given using the Shannon-Heartley theorem [93] as

$$c_j(x) = BW_j \log_2(1 + SINR_j(x)) \tag{4.1}$$

where BW_j is the total bandwidth offered by the j-th BS and $SINR_j(x)$ is given by

$$SINR_j(x) = \frac{g_j(x)P(j)}{\sigma^2 + \sum_{m \in I_j} g_m(x)P(m)} \tag{4.2}$$

where $g_j(x)$ denotes the channel gain between BS j and the user at location x and it accounts for the shadowing loss and path loss, σ^2 denotes the noise power level, and I_j is the set of interfering BSs for BS j. This chapter assumes perfect information of the channel gain which may be estimated given the topological details of the terrain, and drive-through site surveys. Next, we introduce a user association indicator function $u_j(x)$ which spec-

ifies the user association between the BSs and the MTs. This value is 1 if users at location x are served by BS j and is 0 otherwise. We now define the BS load ρ_j, which denotes the fraction of time BS j is busy serving its traffic requests and is given by [94]

$$\rho_j = \int_{\mathcal{R}} \frac{\gamma(x)}{c_j(x)} u_j(x) dx. \tag{4.3}$$

Definition 4.3.1: *The feasible set of the BS loads $\rho = (\rho_1, \cdots, \rho_{|\mathcal{B}|})$ is denoted by $\mathcal{F}_1$ and can be defined as*

$$\begin{aligned}\mathcal{F}_1 = \Big\{ \rho \;\mid\; & \rho_j = \int_{\mathcal{R}} \frac{\gamma(x)}{c_j(x)} u_j(x) dx, \\ & 0 \le \rho_j \le 1 - \epsilon, \;\; \forall j \in \mathcal{B}, \\ & u_j(x) \in \{0, 1\}, \;\; \forall j \in \mathcal{B}, \;\; \forall x \in \mathcal{R}, \\ & \sum_{j=1}^{|\mathcal{B}|} u_j(x) = 1, \;\; \forall j \in \mathcal{B}, \;\; \forall x \in \mathcal{R} \Big\},\end{aligned}$$

where ϵ is an arbitrarily small positive constant.

The MTs attach to the BS based on the scheme described later in the chapter in Section 4.5.3. Since file transfer arrivals are Poisson processes, the sum of transfer requests arriving at the BSs is also a Poisson process. Since the service process at a BS follows a general distribution, the BSs may be modeled as a M/G/1-processor sharing queue. The average number of flows at BS j can thus be given by $\frac{\rho_j}{1-\rho_j}$ [95]. According to Little's law, the delay experienced by a traffic flow is directly proportional to the average number of flows in the system [100]. Thus we take the total number of the flows in the network as the network latency indicator, $\mathcal{D}(\rho)$, which is given

by [95]

$$\mathcal{D}(\rho) = \sum_{j \in \mathcal{B}} \frac{\rho_j}{1 - \rho_j}. \tag{4.4}$$

The indicator above has been used in several contemporary studies to quantify the network latency performance (e.g. [22], [86] [93], [94]).

4.3.2 BS power consumption

The base station power consumption consists of a fixed part and a traffic dependant part. This chapter considers a network of macro BSs. The power consumption of BS j is denoted as $L(j)$, and is given as [101]

$$L(j) = P_0(j) + \Delta P(j)\rho_j, \;\; 0 \leq \rho_j \leq 1, 0 \leq P(j) \leq P_{max} \tag{4.5}$$

where P_0 is the power consumption at no load (zero traffic) and Δ is the slope of the load dependent power consumption.

4.3.3 Solar energy resource and batteries

We use statistical weather data provided by National Renewable Energy Laboratory (NREL) [17]. This is fed to NREL's System Advisor Model (SAM) tool which yields the hourly energy generated by a PV panel with a given rating. The BSs are assumed to use lead acid batteries to store the excess energy harvested by the PV panels. These are a popular choice in storage applications on account of their lower cost and being more time tested than other alternatives.

4.4 Problem formulation

Our objective is to maximize the benefit derived from the green energy available to the BS, in terms of improving the system level latency. While doing so, we desire to avoid energy outages at the BSs. Thus, we consider the problem, [P1], as minimizing the total system level latency during the day, given the harvested solar energy available to the BSs. The problem can be formulated as

$$\begin{aligned} \textbf{[P1]} \ \underset{E_t,\ P_t,\ \rho^{(t)}}{\text{minimize}} \quad & \sum_{t=1}^{24} \mathcal{D}_t(\rho^{(t)}) \\ \text{subject to:} \quad & \rho^{(t)} \in \mathcal{F}_1, \qquad \forall t \\ & \sum_{t=1}^{24} L_t(j) \leq \mathcal{G}(j), \ \ \forall j \in \mathcal{B} \end{aligned}$$

where the network latency for the t-th hour of the day is denoted by $\mathcal{D}_t$, $L_t(j)$ denotes the BS j's power consumption for the t-th hour, and $\mathcal{G}(j)$ denotes the green energy budget available to the j-th BS during the day. The methodology for evaluating $\mathcal{G}(j)$ is discussed in Section 4.5.1. Note that the design variables in the above problem are the green energy allocation (denoted by E), the transmit power levels (P) and the BS loads (ρ). E_t, P_t and $\rho^{(t)}$ denote the value of these variables at time t.

4.5 Solution methodology

To solve the problem formulated in Section 4.4, we propose the Green energy and delay Aware User association and Resource Allocation (GAURA) scheme which consists of three parts: (a) temporal energy allocation (b) BS downlink power control and (c) user association reconfiguration. In

Section 4.5.1 we propose an algorithm for intelligently allocating the green energy budget over time. Further, given the energy allocation, in Sections 4.5.2 and 4.5.3 we address the optimization problem by suitably adjusting the downlink transmit power levels of the different BSs and applying user association reconfiguration, respectively.

4.5.1 Temporal energy provisioning

The energy available to power the BS on a given day comes from two sources: (a) the solar energy harvested by the BS during the day and (b) the charge remaining in the batteries from the previous day. This energy needs to be intelligently used during the day. Note that it is not advisable to use up all of this energy as the BSs require some charge in the batteries to power them during the early morning hours on the next day, as the solar energy is only available after sunrise. Therefore it is required that the battery level does not go below a certain level at the end of the day, which we denote by B_{cr}. Thus the energy budget which is actually available to the j-th BS for use is given by $\mathcal{G}(j)= B_{ini}(j) - B_{cr}(j) + \sum_{t=1}^{24} \mathcal{H}_t(j)$ where $B_{ini}(j)$ denotes the battery level of the j-th BS at the beginning of the day, and $\mathcal{H}_t(j)$ denotes the solar energy harvested by BS j in the t-th hour of the day. To allocate this energy budget available to the BS during the day, we propose the TEA (Temporal Energy Allocation) algorithm (Algorithm 4). The green energy allocated to BS j in the t-th hour is given as $E_t(j)$. Note that the green energy is allocated to a given hour in proportion to the BS power consumption during that hour. Let B_{cap} denote the battery capacity. To avoid battery degradation, we assume that the batteries are disconnected from the BS if the battery level goes below a certain threshold state of charge, $B_c = \nu B_{cap}$, at any point of time.

Algorithm 4 The TEA Algorithm

1: $\mathcal{G}(j)= B_{ini}(j) - B_{cr}(j) + \sum_{t=1}^{24} \mathcal{H}_t(j), \quad \forall j \in \mathcal{B}$;
2: **for** $t = 1 : 24$ **do**
3: $\quad E_t(j) = \mathcal{G}(j) \frac{L_t(j)}{\sum_{h=1}^{24} L_h(j)}$;
4: **end for**

The proposed algorithm requires the information of the solar energy expected to be harvested during the day. There exist many methodologies to predict the solar energy generation, usually days and hours in advance. These could be integrated with weather forecasts to give a more accurate prediction. Some models for the prediction of solar energy include [102] and [103]. Additionally, with the increasing number of applications using renewable energy, there exist many such companies which specialise in the field of solar energy prediction for such applications (e.g. [104], [105], [106]). Note that the proposed framework only needs an hourly estimate of the solar energy generation which makes the task even simpler. We also assume that the information of traffic profile from previous weeks is available, which is used to generate the predicted BS power consumption (L) for the initial energy allocation. Note that this energy allocation is only an initialization step and is later updated as shown in Section 4.5.2. We assume that there is a central server which does these operations at the beginning of the day and the decisions made by it guide the temporal energy allocation during the day.

4.5.2 Green energy and delay aware transmission power control

We begin this section by with the following proposition that affects downlink power control.

Proposition 4.5.1. *The network latency ($\mathcal{D}$) is a non-convex function of the BS power levels.*

We use simulations to show that the network delay ($\mathcal{D}$) is a non-convex function of the BS power levels. We consider a network of BSs as shown in Figure 4.3, and the simulation settings are as described in Section 4.6. We consider the BSs operating at 3 p.m. in the afternoon and with BSs 2, 4, 5 and 6 operating at transmit power level 20 W. Next, we vary the power levels of BS 1 and BS 3 and study the effect of doing so on the network latency. Figure 4.1 shows the network latency for different values of power levels for BS 1 and BS 3. From the figure we can easily conclude that the network latency is a non-convex function of BS power levels.

The problem of power level control of a set of BSs to address the objective function in [P1] is thus a non-convex optimization problem with respect to the BS power levels. Finding the global minima of the optimization problem requires a search over the whole search space of possible power levels, which has very high computational complexity. For $\mathcal{B}$ BS's, the computational complexity is given by $O(Z^{|\mathcal{B}|T})$ where Z denotes the number of power levels a BS can operate at and T denotes the number of hours under consideration. Thus to address the power control problem, next we propose a greedy heuristic with very low computational complexity.

We assume that a central server does the power control operations at the beginning of the day and the decisions made by it guide the power levels of the BSs during the day. The power control decisions are made for a time granularity of a hour. To facilitate the power control operations, we assume that the central server has the information of the average hourly traffic profile at a given location which is used for evaluating the underlying user-association based on the user association policy proposed in Section

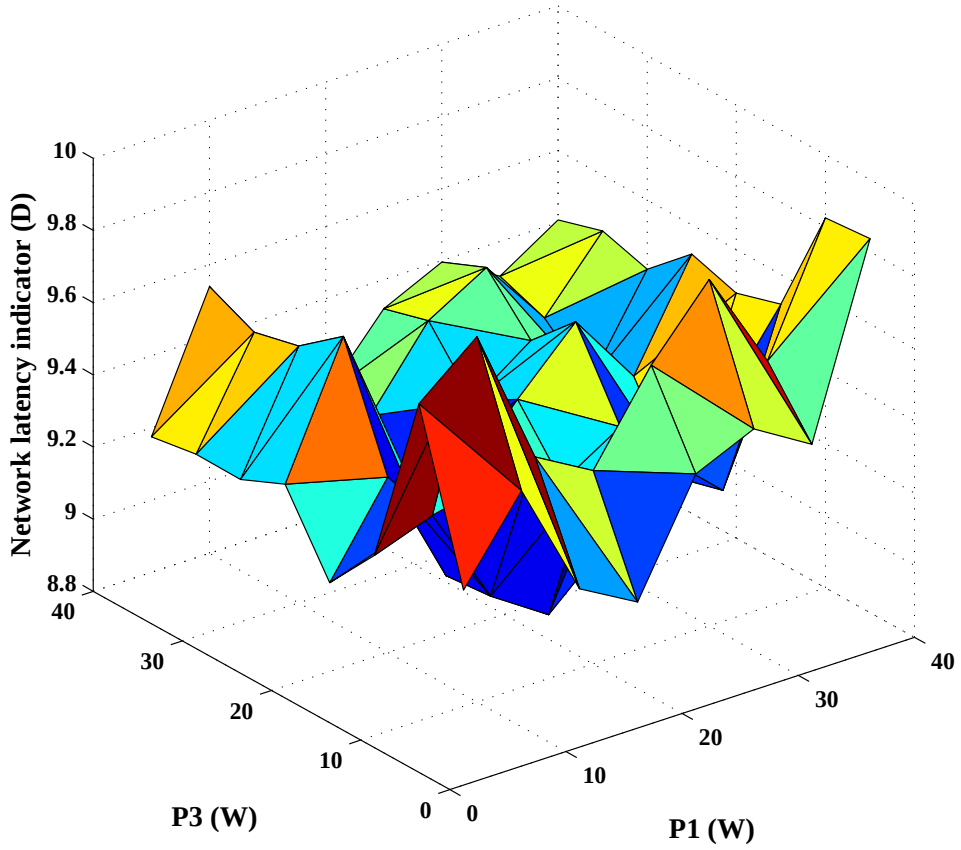

Figure 4.1: Latency variation with power control operations on BS 1 and BS 3.

4.5.3. In existing literature, there exist many papers which study, model and predict traffic in cellular networks (e.g. [53], [107], [108] and [109]). These models can be used for the real time implementation of the proposed power control algorithm. Note that such an assumption is not uncommon and has been considered in many contemporary works like [110] and [111].

The BS load, BS power consumption and the traffic served by a BS are affected by its transmit power level. For the transmit power level control operations, it is important to capture the information whether a BS is energy constrained or not. In order to do so, we define *deficiency ratio* of BS j during hour t, $\Theta_t(j)$, as

$$\Theta_t(j) = \frac{L_t(j)}{E_t(j)}. \tag{4.6}$$

Note that the case when $L_t(j) > E_t(j)$ corresponds to a situation where the power consumption of the j-th BS in the t-th hour is more than the green energy allocated for that given hour, which indicates that the BS is energy constrained. While determining power levels for the BSs, two concerns regarding the operations of the BSs need to be accounted for which are (a) to avoid energy deficinecy (i.e. $\Theta_t(j) > 1$) and (b) to avoid traffic overload at a BS (i.e. $\rho_j^{(t)} > 1$). To capture the intensity of these problems faced by a BS, we define a term *strain index* which is given by

$$\Psi_t(j) = \max(0, \Theta_t(j) - 1) + \max(0, \rho_j^{(t)} - 1). \tag{4.7}$$

Next, we propose the green energy and delay aware power control algorithm (Algorithm 5) which is aimed at eliminating the strain index and improving the network latency performance. The proposed algorithm is sequentially carried out for each hour of the day beginning with the first hour of the day. For a given hour, the BS power control begins by trying to eliminate the strain index for the BSs. To achieve this, the BS with the largest value of strain index is identified at every step every step (using $\max(\Psi)$, line 5) and its transmit power level is reduced by ω (line 6). This reduction in transmit power level contributes to relieving the strain of the BS in terms of energy deficiency as well as traffic overload. The reason for this is as follows. When the transmit power level of a BS is reduced, some of its users are offloaded to nearby BSs which reduces the BS load (ρ). Further, as the BS load is reduced, the power consumption of the BS which is dependent on the BS load (as shown in (4.5)) is also reduced. After all the BSs

Algorithm 5 Green Energy and Delay Aware Power Control Algorithm

Initialize: $P_t(j) = P_{max}, \quad \forall j \in \mathcal{B}$
Compute $\Psi_t(j), \quad \forall j \in \mathcal{B}$
$\Psi_t(j) = max(0, \Theta_t(j) - 1) + max(0, \rho_j^{(t)} - 1)$
while $max(\Psi_t) > 0$ **do** ▷ Loop to eliminate strain index
    a. g : $\arg\max_{j \in \mathcal{B}} \Psi_t$
    b. $P_t(g) = max(0, P_t(g) - \omega)$;
end while
$Latency\_reduction = True$;
while $Latency\_reduction = True$ **do** ▷ Power control for latency improvement
    Γ_{old}= network latency with power vector P.
    for $j = 1 : |\mathcal{B}|$ **do**
        $P_{curr} = P_t$
        $P_{curr}(j) = max(0, P_t(j) - \omega)$
        Compute network latency for power vector P_{curr} and store in $\Gamma_{pc}(j)$
        if $\max(\Theta_t) > 1$ **then**
            $Poss(j)$= $False$
        else $Poss(j)$= $True$
        end if
    end for
    a. h : index of BS having $Poss = True$ for which power control leads to minimum network latency (Γ_{pc})
    b. Set $\Gamma_{new} = \Gamma_{pc}(h)$
    if $\Gamma_{new} < \Gamma_{old}$ **then**
        $P_t(h) = max(0, P_t(h) - \omega)$;
    else
        Set $Latency\_Improvement = False$
    end if
end while
for $j = 1 : |\mathcal{B}|$ **do** ▷ Carrying over left-over energy
    $L_t(j) = P_0(j) + \Delta P_t(j) \rho_j^{(t)}$
    $\mathcal{Y}_t(j) = E_t(j) - L_t(j)$
    for $h = t + 1 : 24$ **do**
        $E_h(j) = E_h(j) + \mathcal{Y}_t(j) \frac{L_h(j)}{\sum_{m=t+1}^{24} L_m(j)}$
    end for
end for

have zero strain index, the power control operations are done so as to minimize the overall system latency. For this, one by one the BSs reduce their transmit power by ω and the system latency with the new set of power levels is stored in the vector Γ_{pc} (lines 10-19). The BS for which the reduction of power level leads to the largest reduction in the system latency, while allowing all BSs to have $\Theta_t(j) > 1$ (which is tracked by the vector *Poss*), updates its transmit power level. This process is continued until there is no further improvement in the system latency by powering down any of the BS (lines 20-26). The latency improvement is checked through the status variable *Latency_reduction* which is true if the latency reduces as a result of the power control operation and is set to false otherwise. Note that the latency improvement brought by the power control operations is because of the load balancing effect and interference management.

For a given hour, for the transmit power levels determined by the proposed algorithm, the BSs may not be using all of the energy allocated to them for that hour. We denote the leftover energy by $\mathcal{Y}$ in the algorithm and this energy is distributed to the subsequent hours in proportion to their respective traffic loads (lines 28-34). For each hour, the worst case computational complexity of the proposed algorithm is $O((Z-1)|\mathcal{B}|^2)$. The scenario for the power control operations with the worst case computational complexity is the one where power levels of all BSs fall to 0, starting from an initial power level of P_{max}. We have $\mathcal{B}$ BSs and each BS has $(Z-1)$ transmit power level transitions possible (i.e. from P_{max} to $(P_{max}-\omega)$, $(P_{max}-\omega)$ to $(P_{max}-2\omega)$, $\cdots$, ω to 0). While deciding any of these power level transitions, the value of the objective function for each of the $\mathcal{B}$ BSs is evaluated. This gives the overall computational complexity for the proposed power control algorithm for a given hour as $O((Z-1)|\mathcal{B}|^2)$. Note that with each

iteration of the power control operations, the load levels at each BS change. Thus after each iteration (consisting of Algorithm 4 followed by Algorithm 5) we use the new load levels at each BS as the input to Algorithm 1 for the next iteration. After a few iterations (typically 3-4), solution for transmit power levels converges. The worst case computational complexity of the proposed algorithm for T hours of operation is given by $O(T(Z-1)|\mathcal{B}|^2)$.

Remark: The power control operations begin with addressing the energy outage and the traffic overload issue. Once that is addressed, power level control is done to bring down the network latency. As the problem of minimizing the network latency by power control operations is a non-convex optimization problem, the proposed algorithm obtains a local optimal solution. The proposed algorithm has the rationale of a greedy descent approach where the BS whose power level decrement leads to the largest reduction in the delay is powered down. Thus the power levels at any subsequent iteration of power control operation has delay performance better than that before it. Further, when decrementing the power level of none of the BSs leads to a reduction in the delay, we return that set of power levels as the solution of the power level values for that hour.

4.5.3 Green energy and delay aware user association policy

The user-association policy determines the MT-BS association at any point of time. In this section we propose a green energy and delay aware user association policy. For any given value of power levels (coming from the power control algorithm) and green energy allocation at a given time, the proposed user association policy contributes to achieving the global optimal of value of the objective function (for that set of power levels). The

user association policy operates in an iterative way. The BSs periodically measure their traffic loads and use it to determine their coalition factors (defined later in this subsection) which are advertised to the MTs. These coalition factors are used by the MTs to associate with the BSs so as to minimize the objective function. The BSs and MTs update their association until convergence. Note that this can be easily implemented in a distributed manner where the BSs have to just periodically broadcast their coalition factors which can be embedded in the beacon signals of the BSs [112]. Note that the coverage regions of the BSs are overlapping and a user can choose to associate with any one of the multiple BSs in its reception range.

For the user-association problem we consider the transformed problem [P2.1], with an intentionally added barrier function in the problem [P1] to have delay and energy aware user association. User association is a continuous phenomenon where the set of active users in the network keeps changing and the users associate with the BSs based on the proposed user-association policy. The proposed user-association policy is applicable at all times and thus we omit the time index t in this subsection. Additionally, we use $D(\rho_j)$ to denote the delay indicator for the j-th BS (i.e. $D(\rho_j) = \frac{\rho_j}{1-\rho_j}$). Note that the constraint corresponding to the energy availability at the BS has been indirectly incorporated in the transformed objective problem through the barrier function $e^{\Theta(\rho_j)}$. The problem [P2.1] is defined as follows

$$\textbf{[P2.1]} \quad \underset{\rho}{\text{minimize}} \quad X(\rho) = \sum_{j \in \mathcal{B}} \left(D(\rho_j) + e^{\Theta(\rho_j)} \right)$$

$$\text{subject to:} \quad \rho \in \mathcal{F}_1$$

and its solution involves finding the optimal BS loads (ρ) which minimizes the value of $X(\rho)$. Note that the value of Θ for BS j is a function of ρ_j,

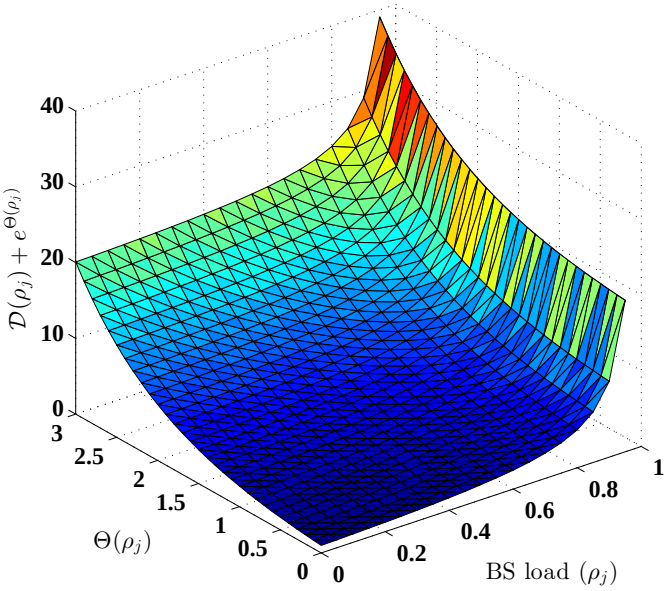

Figure 4.2: Variation of components in the objective problem [P2.1] with its respective parameters.

as $\Theta(j) = \frac{L(j)}{E(j)} = \frac{P_0 + \Delta P(j)\rho_j}{E(j)}$. Thus in this subsection, for notational clarity we denote it by $\Theta(\rho_j)$. The intuition behind choosing the particular barrier function (i.e. $e^{\Theta(\rho_j)}$) is as follows. While deciding the user association policy, we not only want the user association policy to bring about delay improvement in the network, but also want it to account for the green energy available at the BS. $\Theta(\rho_j)$, has been defined previously as $\frac{L(j)}{E(j)}$. When a BS is running low on energy, the value $\Theta(\rho_j)$ grows large and thus the users will be discouraged to join that BS (as it increases the value of the objective function sharply). Further, the barrier function is exponential with respect to the value of $\Theta(j)$. Thus after a certain point when the BS starts running very low on energy, its contribution to the objective function increases sharply. Figure 4.2 shows how the two parts in the objective function in problem [P2.1] vary with their respective parameters for BS j.

Since $u_j(x) \in \{0, 1\}$, the set $\mathcal{F}_1$ is not convex. To formulate our problem [P2.1] as a convex optimization problem, we begin with relaxing the user-

association indicator function to $0 \leq u_j(x) \leq 1$, where u_j can be interpreted as the probability that a user at location x associates with BS j. We denote the relaxed set of BS loads as $\tilde{\mathcal{F}}_1$ and it is given as

$$\begin{aligned}\tilde{\mathcal{F}}_1 = \Big\{\rho \;\mid\; \rho_j = &\int_{\mathcal{R}} \frac{\gamma(x)}{c_j(x)} u_j(x)dx, \\ &0 \leq \rho_j \leq 1-\epsilon, \;\; \forall j \in \mathcal{B}, \\ &0 \leq u_j(x) \leq 1, \;\; \forall j \in \mathcal{B}, \;\; \forall x \in \mathcal{R}, \\ &\sum_{j=1}^{|\mathcal{B}|} u_j(x) = 1, \;\; \forall j \in \mathcal{B}, \;\; \forall x \in \mathcal{R}\Big\}.\end{aligned}$$

Theorem 4.5.1: The feasible set $\tilde{\mathcal{F}}_1$ is convex.

Proof. This proof has been taken from [93] and is included here for completeness. Let us consider two BS load vectors ρ^a and ρ^b with $\rho^a \neq \rho^b$. There exists an associated $u^a(x) = (u_1^a(x), u_2^a(x), \cdots, u_{|\mathcal{B}|}^a(x))$ and $u^b(x) = (u_1^b(x), u_2^b(x), \cdots, u_{|\mathcal{B}|}^b(x))$, such that $\rho_j^a = \int_{\mathcal{R}} \frac{\gamma(x)}{c_j(x)} u_j^a(x)dx$ and $\rho_j^b = \int_{\mathcal{R}} \frac{\gamma(x)}{c_j(x)} u_j^b(x)dx$ for $j \in \mathcal{B}$. Next, we consider a convex combination of ρ^a and ρ^b for $0 < \delta < 1$, denoted by ρ^c. For BS j, this combination is defined as

$$\begin{aligned}\rho_j^c &= \delta\rho_j^a + (1-\delta)\rho_j^b \\ &= \int \frac{\gamma(x)}{c_j(x)} [\delta u_j^a(x) + (1-\delta)u_j^b(x)]dx. \end{aligned} \tag{4.8}$$

Let $u^c(x)$ be the association function associated with ρ^c; then $u_j^c(x) = \delta u_j^a(x) + (1-\delta)u_j^b(x)$. Note that ρ^c fulfils all conditions to be in set $\tilde{\mathcal{F}}_1$. Thus, the set $\tilde{\mathcal{F}}_1$ is convex. ■

The problem **[P2.2]** with the relaxation condition is given by

$$\textbf{[P2.2]} \quad \underset{\rho}{\text{minimize}} \quad X(\rho) = \sum_{j \in \mathcal{B}} \left(D(\rho_j) + e^{\Theta(\rho_j)} \right)$$
$$\text{subject to:} \quad \rho \in \tilde{\mathcal{F}}_1.$$

Remark: Note that although we formulate the optimization problem [P2.2] using $\tilde{\mathcal{F}}_1$, the user association algorithm which we propose in this chapter determines the deterministic user association (belonging to $\mathcal{F}_1$). This is shown in Theorems 4.5.2 and 4.5.3, later in this section.

Next we describe the working of the proposed user association algorithm. The proposed user association algorithm is a distributed MT-BS association scheme. To guarantee the convergence of the scheme, we assume that traffic arrival and departure processes occur at a faster time scale as compared to that at which the BSs broadcast their coalition factors. Thus, after the BSs broadcast their coalition factors, the users are able to make their association decisions based on the broadcast indicators before the next set of BS coalition factors are broadcast. We also assume that the BSs are synchronized and the coalition factors are broadcast at the same time. We begin with describing the user side and the BS side algorithms for carrying out the proposed user association.

1) **User side algorithm**: The time between two successive BS coalition factor updates is defined as the time slot in our algorithm. At the start of k-th time-slot the BSs send their coalition factors to the users through a broadcast signal. The users at location x in turn choose the BS they associate with based on these coalition factors and the rate offered by the BSs at their location. We use superscript (k) to denote the value of a particular variable at the beginning of the k-th time slot. The coalition factor, $\phi_j^{(k)}$ broadcast by

BS j at the beginning of the k-th time slot is defined as

$$\begin{aligned}\phi_j^{(k)} &= \frac{\partial X^{(k)}(\rho)}{\partial \rho_j^{(k)}} \\ &= \frac{\partial \left(\sum_{j \in \mathcal{B}} \left(\frac{\rho_j^{(k)}}{1-\rho_j^{(k)}} + e^{\frac{L(j)}{E(j)}} \right) \right)}{\partial \rho_j^{(k)}} \\ &= \frac{\partial \left(\sum_{j \in \mathcal{B}} \left(\frac{\rho_j^{(k)}}{1-\rho_j^{(k)}} + e^{\frac{P_0 + \Delta P(j) \rho_j^{(k)}}{E(j)}} \right) \right)}{\partial \rho_j^{(k)}} \\ &= \frac{1}{(1-\rho_j^{(k)})^2} + \frac{\Delta P(j)}{E(j)} e^{\Theta^{(k)}(j)}. \end{aligned} \tag{4.9}$$

The MTs associate with a BS based on the following rule

$$w^{(k)}(x) = \arg\max_{j \in \mathcal{B}} \frac{c_j(x)}{\phi_j^{(k)}}, \tag{4.10}$$

where $w^{(k)}(x)$ is the index of the BS with largest value of $\frac{c_j(x)}{\phi^{(k)}(j)}$ and $c_j(x)$ is the rate offered by BS j at location x. The optimality of the proposed user association rule in terms of minimizing the objective function has been proved in the subsequent part of this section. The users update their association functions as

$$u_j^{(k)}(x) = \begin{cases} 1 & \text{if } j = w^{(k)}(x) \\ 0 & \text{otherwise} \end{cases}. \tag{4.11}$$

For an individual user, the computational complexity of the proposed user side algorithm is $O(|\mathcal{B}|)$.

2) **BS side algorithm:** The BSs measure their load levels at the end of the

Algorithm 6 User Association Algorithm

1: MTs: At the k-th iteration, MTs measure the average transmission rate $c_j(x)$ ($\forall j \in \mathcal{B}$) and receive the BS coalition factor broadcasted by these BSs. Then, the MTs select the BS $w^{(k)}(x)$ according to Equation (4.10).
2: BSs: At the end of the k-th iteration, each BS estimates its load and updates its traffic load $\rho_j^{(k+1)}$ to be used for evaluating the coalition factor to be broadcast for the next iteration.

k-th time slot which we denote by $T_j(\rho_j^{(k)})$ and it can be given as

$$T_j(\rho_j^{(k)}) = \min\left(\int_{\mathcal{R}} \frac{\gamma(x)}{c_j(x)} u_j^{(k)}(x)dx, 1-\epsilon\right). \tag{4.12}$$

After measuring this traffic load, the BS updates its traffic load to be used in evaluating the next coalition factor to be broadcast for time slot $k+1$ as [93]

$$\rho_j^{(k+1)} = \theta\rho_j^{(k)} + (1-\theta)T_j(\rho_j^{(k)}) \tag{4.13}$$

with $0 < \theta < 1$ being an averaging exponential factor. The pseudocode for the user association algorithm mentioned above is given in Algorithm 6.

Next, we present the proofs to show the optimality and convergence of the proposed user association algorithm.

Lemma 4.5.1. *The objective function* $X(\rho) = \sum_{j\in\mathcal{B}}\left(D(\rho_j) + e^{\Theta(\rho_j)}\right)$ *is convex in* ρ *when* ρ *is defined on* $\tilde{\mathcal{F}}_1$.

Proof. Please refer to Appendix C for the proof. ■

Lemma 4.5.2. *A unique optimal user association* $\rho^* \in \tilde{\mathcal{F}}_1$ *exists which minimizes* $X(\rho) = \sum_{j\in\mathcal{B}}\left(D(\rho_j) + e^{\Theta(\rho_j)}\right)$.

Proof. This follows from the fact that the objective function $X(\rho)$ is a convex function of ρ when $\rho \in \tilde{\mathcal{F}}_1$ (as shown in Lemma 4.5.1). ■

Lemma 4.5.3. *When $\rho^{(k)} \neq \rho^*$, then $T(\rho^{(k)})$ provides a descent direction for $X(\rho^{(k)})$ at $\rho^{(k)}$.*

Proof. Please refer to Appendix D for the proof. ■

In Theorems 4.5.2 and 4.5.3, we prove the convergence and optimality of the proposed user association scheme, respectively.

Theorem 4.5.2. *The traffic load ρ converges to the traffic load $\rho^* \in \mathcal{F}_1$.*

Proof. To prove this, we show that $\rho^{(k+1)} - \rho^{(k)}$ is also a descent direction of $X(\rho^{(k)})$. For this we consider the following expression

$$\begin{aligned} \rho_j^{(k+1)} - \rho_j^{(k)} &= \theta\rho_j^{(k)} + (1-\theta)T_j(\rho_j^{(k)}) - \rho_j^{(k)} \\ &= (1-\theta)(T(\rho_j^{(k)}) - \rho_j^{(k)}). \end{aligned} \tag{4.14}$$

Now, based on Lemma 3, we have already shown that $(T(\rho^{(k)}) - \rho^{(k)})$ is the descent direction of $X(\rho^{(k)})$, and additionally we have $(1-\theta) > 0$ as $0 < \theta < 1$. Thus even $\rho^{(k+1)} - \rho^{(k)}$ gives the descent direction of $X(\rho^{(k)})$. Further, as $X(\rho^{(k)})$ is a convex function we can easily state that $X(\rho^{(k)})$ converges to the user association vector ρ^*. Suppose $X(\rho^{(k)})$ converges to any point other than $X(\rho^*)$. Then $\rho^{(k+1)}$ again gives a descent direction so as to decrease $X(\rho^{(k)})$, which is contradiction to the assumption of convergence. Additionally, as $\rho^{(k)}$ is derived based on (4.10) and (4.11) where $u_j(x) \in \{0,1\}$, ρ^* is in the feasible set $\mathcal{F}_1$. ■

Theorem 4.5.3. *If the set $\mathcal{F}_1$ is non-empty and the traffic load ρ converges to ρ^*, the user association corresponding to ρ^* minimizes $X(\rho)$.*

Proof. Let $u^* = \{u_j^*(x) | u_j^*(x) \in \{0,1\}, \forall j \in \mathcal{B}, \forall x \in \mathcal{R}\}$ and $u = \{u_j(x) | u_j(x) \in \{0,1\}, \forall j \in \mathcal{B}, \forall x \in \mathcal{R}\}$ be the user association corresponding to ρ^* and ρ,

where ρ is some traffic load vector satisfying $\rho \in \mathcal{F}_1$. Let $\Delta\rho^*= \rho - \rho^*$. As X($\rho$) is a convex function over ρ, the theorem can be proved by showing $< \nabla X(\rho^*), \Delta\rho^* > \geq 0$. In the proof below, we substitute $\frac{\partial X(\rho^*)}{\partial \rho_j^*}$ as $\phi_j(\rho_j^*)$ for notational clarity (these expressions are identical as shown in the derivation leading to (4.9).

$$\begin{aligned} < \nabla X(\rho^*), \Delta\rho^* > &= \sum_{j\in\mathcal{B}} \phi_j(\rho_j^*)\,(\rho - \rho^*) \\ &= \sum_{j\in\mathcal{B}} \left(\int_{\mathcal{R}} \frac{\gamma(x)(u_j(x) - u_j^*(x))}{c_j(x)\phi_j^{-1}(\rho_j^*)} dx \right) \\ &= \int_{\mathcal{R}} \gamma(x) \sum_{j\in\mathcal{B}} \frac{(u_j(x) - u_j^*(x))}{c_j(x)\phi_j^{-1}(\rho_j^*)} dx. \end{aligned}$$

But as optimal user association is determined by the following rule

$$u_j^*(x) = \begin{cases} 1, & \text{if } j = \arg\max_{j\in\mathcal{B}} \frac{c_j(x)}{\phi_j(\rho_j^*)}, \\ 0, & \text{otherwise.} \end{cases},$$

we thus have,

$$\sum_{j\in\mathcal{B}} \frac{u_j^*(x)}{c_j(x)\phi_j^{-1}(\rho_j^*)} \leq \sum_{j\in\mathcal{B}} \frac{u_j(x)}{c_j(x)\phi_j^{-1}(\rho_j^*)}. \tag{4.15}$$

Hence, $< \nabla X(\rho^*), \Delta\rho^* > \geq 0$ which proves the theorem. ■

Algorithm 7 summarizes the sequence of the various operations inovolved in solving the problem [P1] using the GAURA Algorithm.

The overall worst case complexity of the proposed GAURA scheme for the centralized server is $O(Z|\mathcal{B}|^2)$ which results from the operations required to determine the power levels of the BSs during the different hours for the day. For the MTs, the complexity is $O(|\mathcal{B}|)$ whereas for the BSs it is $O(1)$ which come from the user-association algorithm.

Algorithm 7 Sequence of operations: GAURA

1: Perform Green energy allocation for the different hours during the day using the TEA algorithm.
2: **for** $t = 1 : 24$ **do**
3: **while** power control convergence **do**
4: **while** user association convergence **do**
5: Solve user association problem for the given hour using the green energy allocated for that hour and the predicted traffic.
6: **end while**
7: Solve power control problem for the underlying user-association determined in the inner while loop.
8: **end while**
9: **end for**

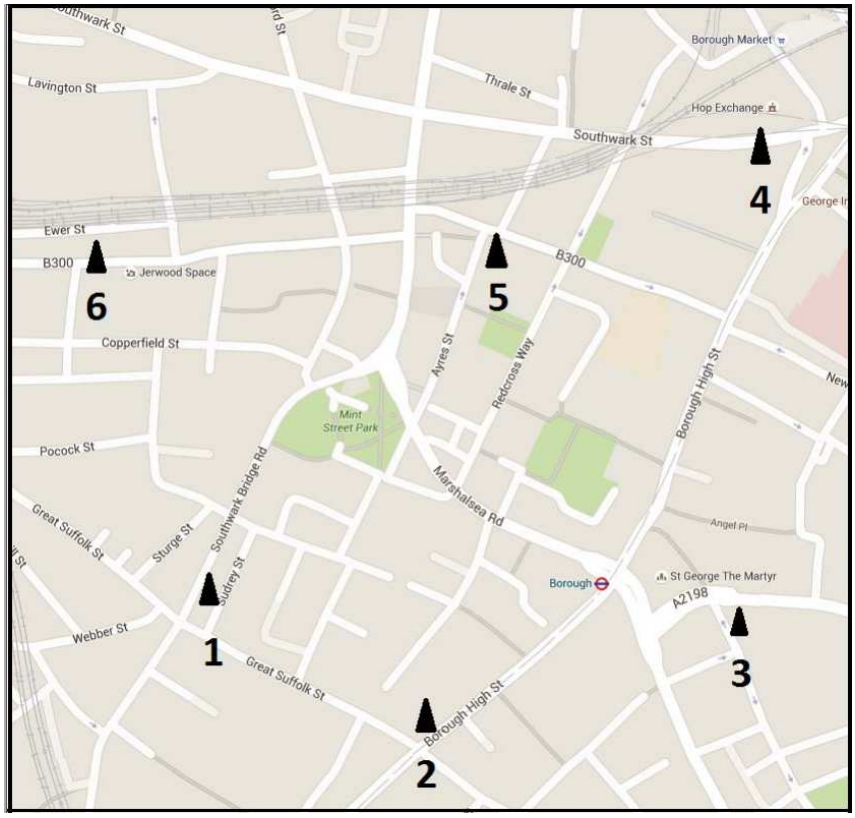

Figure 4.3: 3G BS deployment near Southwark (London).

4.6 Numerical results

To validate the performance of the proposed scheme, we consider a 3G BS deployment by network provider Vodafone near Southwark, London, UK in an area of 1 km^2 with 6 BSs as shown in Figure 4.3. We assume that 12 V,

205 Ah flooded lead acid batteries are used by the BSs. Each BS is assumed to be equipped with PV panel of 6 kW DC rating and 10 batteries. We consider a carrier frequency of 2.5 GHz and 10 MHz bandwidth with full frequency reuse. We take the noise power to be -174 dBm/Hz. We assume log normal shadowing with standard deviation 8 dB with the correlation distance for shadowing taken as 50 m [115]. The path loss, denoted by PL has been modeled as [114]

$$PL(dB) = 40(1 - 4 \times 10^{-3} h_{BS}) log_{10}(R) - 18 log_{10}(h_{BS}) + 21 log_{10}(f) + 80$$

where R is the distance between the BS and the MT, h_{BS} is the base station antenna height above rooftop and f is the carrier frequency in MHz. Based on the suggestions from the baseline test scenario mentioned in the IEEE 802.16 evaluation methodology document [115], we take h_{BS} as 15 metres and the carrier frequency is 2.5 GHz. Thus, the path loss is calculated as

$$PL(dB) = 130.19 + 37.6 \log(R). \tag{4.16}$$

A homogeneous Poisson point process is used to generate the file transfer requests. The rate of the Poisson process depends on the hour of the day, with the smallest number of file transfer requests in the morning (2-5 a.m.) with an average of 20 requests per unit area (km^2) and the largest number of requests in the evening (5-7 p.m.) with an average of 200 requests per unit area. To model temporal traffic dynamics, a new spatial profile of file transfer requests is generated after every 2 minutes. Each file transfer request is assumed to request 50 KB of data traffic to be served. The entire area (of 1 km^2) is divided into 1600 locations with each location representing a 25 m x 25 m area. The location based traffic load density

is calculated based on the traffic model. For performance analysis we consider solar insolation on 12^{th} January of typical meteorological year (TMY) data for London from the NREL database [17]. The total energy harvested on this day by a PV panel with 6 kW DC rating is 8.67 kW. P_0, P_{max} and Δ for the BSs are taken as 412.4 W, 40 W and 22.6 respectively [101]. B_{cr} is taken as the estimated energy required to power the BS to operate for at least 5 hours during the early morning hours and it has been taken as $0.4B_{cap}$ for the numerical simulations. ν, the limiting state of charge which decides B_c is taken as 0.3. B_{ini} has been randomly chosen for different BSs. ω, the granularity of the transmit power control has been taken as 5 W. We assume that a BS is turned off when its transmit power level is 0 W. The averaging factor for the BS side algorithm θ, has been taken as 0.95, and with this value the proposed user-association algorithm was observed to converge to the optimal solution within 20 iterations.

As a benchmark for comparison, we consider a Best-Effort scheme where all BSs operate with transmit power 20 W and a MT associates with the BS that has the strongest signal strength at the MT's location. We also consider ICE [91] and GALA [94] schemes with BSs operating at transmit power 20 W, and SWES [86] which is a BS on-off scheme with BSs operating at 40 W when they are switched on. The ICE, GALA and SWES schemes have been discussed in Section 4.2.

4.6.1 Green energy performance

Figure 4.4 shows the battery discharging-charging profiles for the various benchmarks and the proposed algorithm. For clarity, battery levels have been normalized with respect to the maximum battery capacity. It can be

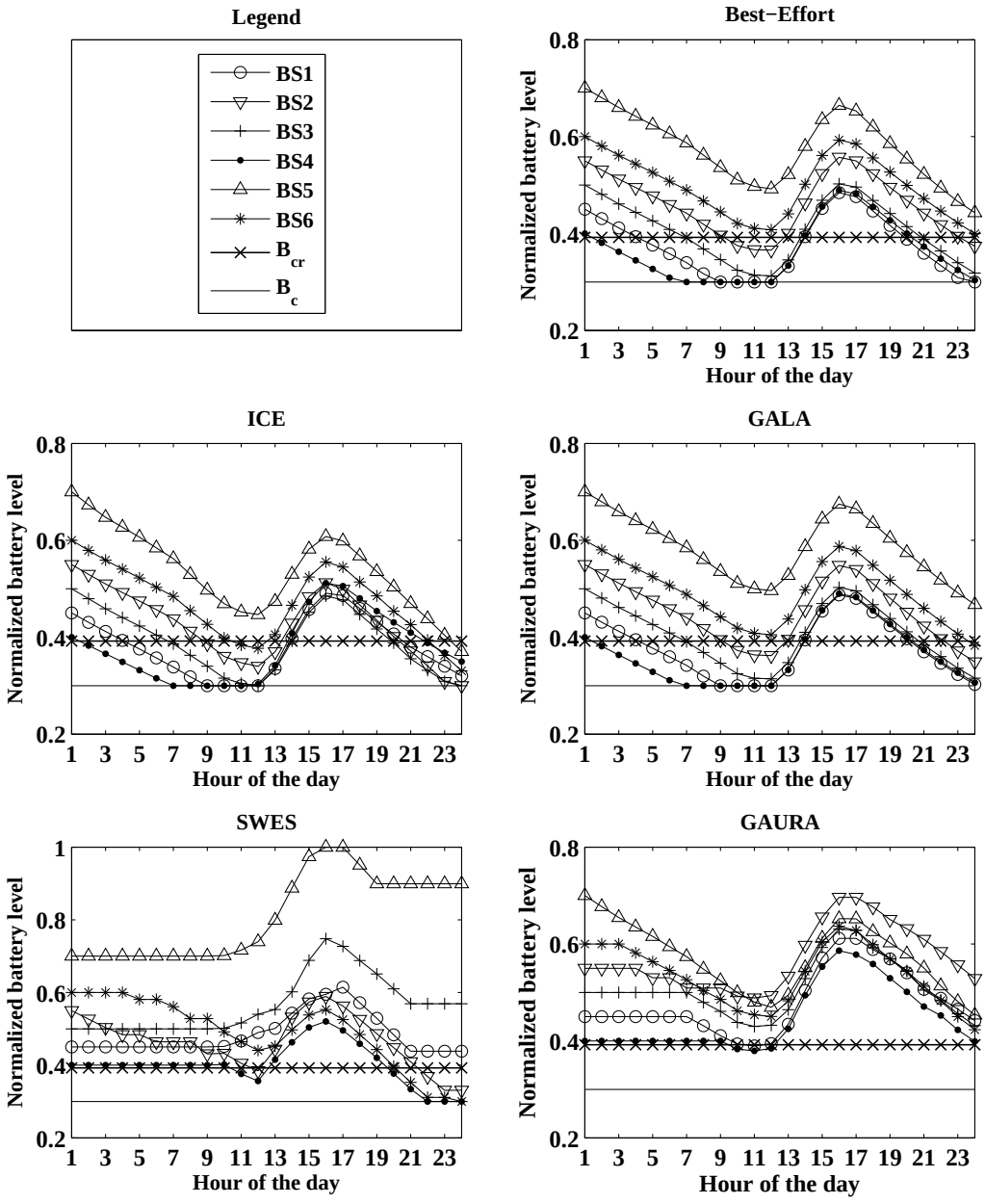

Figure 4.4: Battery discharging-charging profiles for the different algorithms

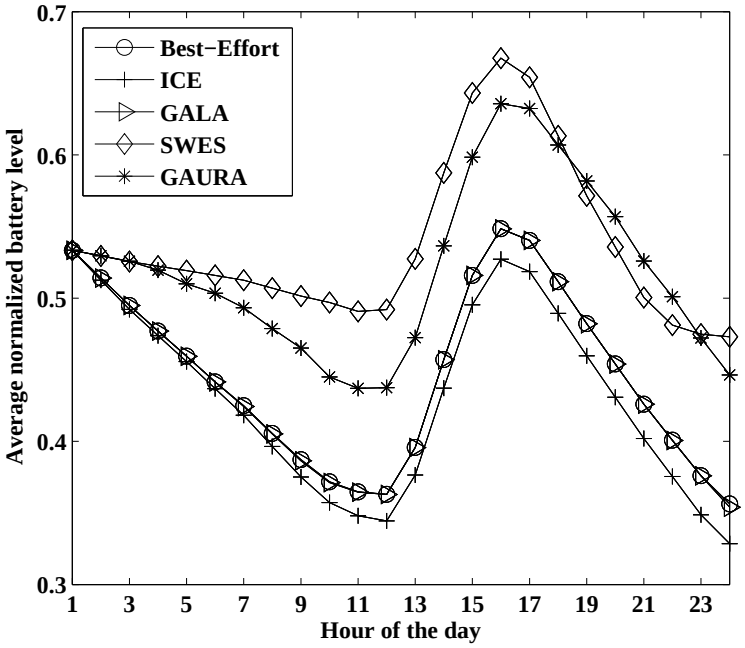

Figure 4.5: Average normalized battery charge for the different schemes.

seen that the Best-Effort scheme can lead to some of the BSs to run very low on energy at the end of the day. Additionally, one of the BS (BS 4) faces around 6 hours of energy outage during the day. The ICE scheme does better than the Best-Effort scheme by trying to equalize the available green energy. However even in the ICE scheme some of the BSs run low on battery levels at the end of the day and BS 4 still faces 6 hours of energy outage during the day. The performance of the GALA scheme in terms of the battery level profile for the BSs is similar to that of the Best-Effort scheme and BS 4 faces energy outage for around 6 hours during the day. Note that the Best-Effort, ICE and GALA schemes lead to some of the BSs ending up below the critical battery level (B_{cr}) at the end of the day which indicates that there would be energy outages in the early morning hours on the next day. The SWES scheme leads to an un-even discharge of battery levels (as BSs turn on/off so as to maximize the number of BSs to be switched off). Although with this scheme there is no energy outage for any

Table 4.1: Comparison of Averaged Metrics for Different Schemes

Scheme	$Var(B)$	Λ_{out}	$P_{avg}(W)$	B_{avg}	D_{avg}
Best-Effot	0.86	7.66	544	0.36	6.72
ICE	0.60	7.66	610	0.33	12.73
GALA	0.82	5.55	562	0.34	5.6
SWES	3	2.78	400	0.47	6.85
GAURA	0.43	0	475	0.44	4.96

BS during the day, some of the BSs run very low on energy and face energy outage at the end of the day. Note that the proposed GAURA scheme provides a greater capability to avoid uneven discharging. Additionally, it ensures that the battery level of none of the BSs goes below the critical level (B_{cr}) at the end of the day.

Figure 4.5 shows the average values of battery levels for the BSs for the various schemes, normalized with respect to the battery capacity. Note that the Best-Effort, ICE and GALA schemes can lead to very low values of average battery level at the end of the day. SWES achieves a higher average battery level since some of the BSs have higher battery levels. Additionally, as discussed earlier, due to un-even discharging some of the BSs can run very low on energy in the SWES scheme. The average values of battery levels for the proposed GAURA scheme is greater than the Best-Effort, ICE and GALA scheme but lower than that of the SWES scheme. However as discussed earlier, the GAURA scheme has a more even discharging profile for the various BSs. Table 4.1 summarizes some key parameters quantifying the battery level variations, energy outage probability and the delay performance of the BSs for the benchmarks and the proposed scheme. To quantify the even-ness of battery charge levels in the different BSs, we calculate the variance $Var(B)$ which denotes the sum of the variances of the

normalized battery levels of the BSs over the day. $Var(B)$ is calculated as

$$Var(B) = \sum_{t=1}^{24} \sum_{j=1}^{|\mathcal{B}|} \left(\frac{B_t(j) - \tilde{B}_t}{B_{cap}} \right)^2 \tag{4.17}$$

where $B_t(j)$ is the battery level of j-th BS at the end of the t-th hour and $\tilde{B}_t$ is the average value of battery levels of the different BSs at the end of t-th hour. Note that for the SWES scheme this parameter is the highest as battery charge profiles of different BSs are very un-even. For the proposed GAURA scheme it is the lowest, indicating comparatively more even discharging among the batteries. Λ_{out} denotes the energy outage probability and is calculated as

$$\Lambda_{out} = \frac{H_{out}}{24|\mathcal{B}|} \tag{4.18}$$

where H_{out} denotes the number of outage events in the network during the day (i.e. 24 hours of operation). Note that the energy outage probability for the proposed GAURA scheme is 0 whereas for all other schemes there are some energy outage events during the day. Further, we calculate the average BS power consumption and the average normalized battery level at the end of the day which are denoted as P_{avg} and B_{avg} respectively, and are given by

$$P_{avg} = \frac{1}{24\mathcal{B}} \sum_{t=1}^{24} \sum_{j=1}^{|\mathcal{B}|} L_t(j) \tag{4.19}$$

$$B_{avg} = \frac{1}{\mathcal{B}} \sum_{j=1}^{|\mathcal{B}|} \frac{B_{24}(j)}{B_{cap}}. \tag{4.20}$$

Note that the average BS power consumption for the Best-Effort, ICE and the GALA schemes are significantly higher than the SWES and GAURA scheme which lead to lower average normalized battery level at the end of the day (B_{avg}). Specifically, we note that the average battery level at the

end of the day for the GAURA scheme is 22% higher than that using the traditional Best-Effort scheme.

4.6.2 Delay performance

Figure 4.6 shows the delay performance for the schemes during the different hours of the day. It can be observed from the figure that GALA has better latency performance as compared to the Best-Effort scheme. However, as discussed earlier, GALA is unable to avoid energy outages in some of the BSs and from some of the BSs running very low on energy at the end of the day. The performance of the ICE and SWES schemes is worse than the performance of the Best-Effort scheme in terms of the delay performance. Note that as compared to the Best-Effort scheme, the benefit of more even discharging of batteries in the ICE scheme and the benefit of higher average battery levels in the SWES scheme are at the cost of increased delay. In contrast, the proposed GAURA scheme reduces the system latency while simultaneously ensuring that the battery levels do not become very low. The last column in Table 4.1 lists the average delay value, denoted by D_{avg}, for the different schemes. D_{avg} is calculated as

$$D_{avg} = \frac{1}{24|\mathcal{B}|} \sum_{t=1}^{24} \mathcal{D}_t. \tag{4.21}$$

Note that the proposed GAURA scheme gives the lowest average delay followed by GALA, Best-Effort and the SWES scheme, and the value is largest for the ICE scheme. The average delay for the GAURA scheme is 26% less than the traditionally used Best-Effort scheme.

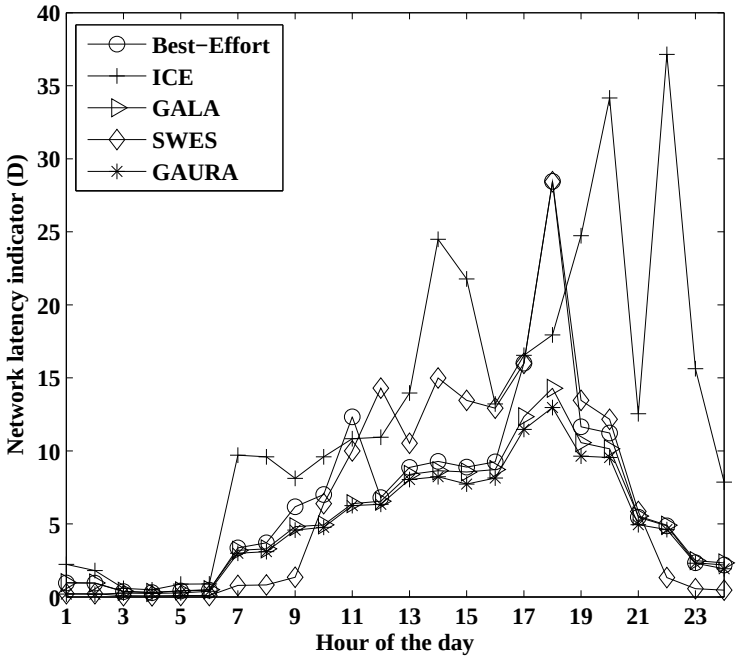

Figure 4.6: Delay performance for the different schemes.

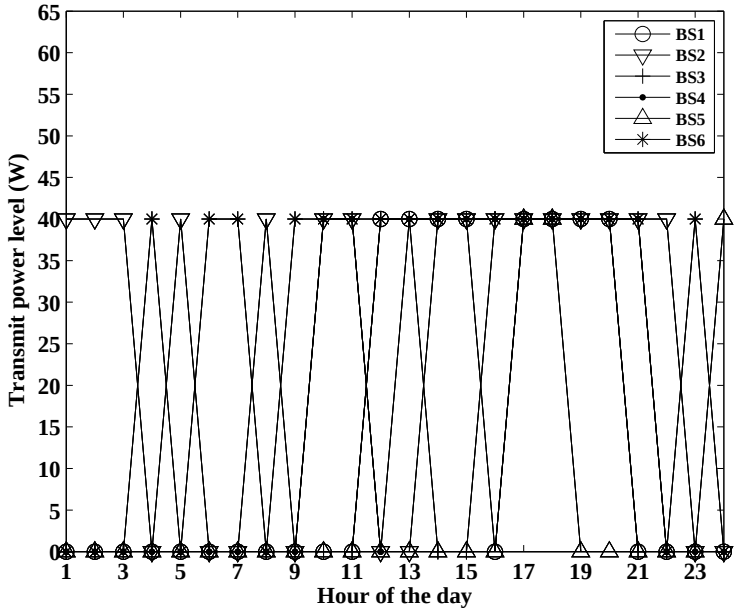

Figure 4.7: Transmit power levels for various BSs during the day (SWES).

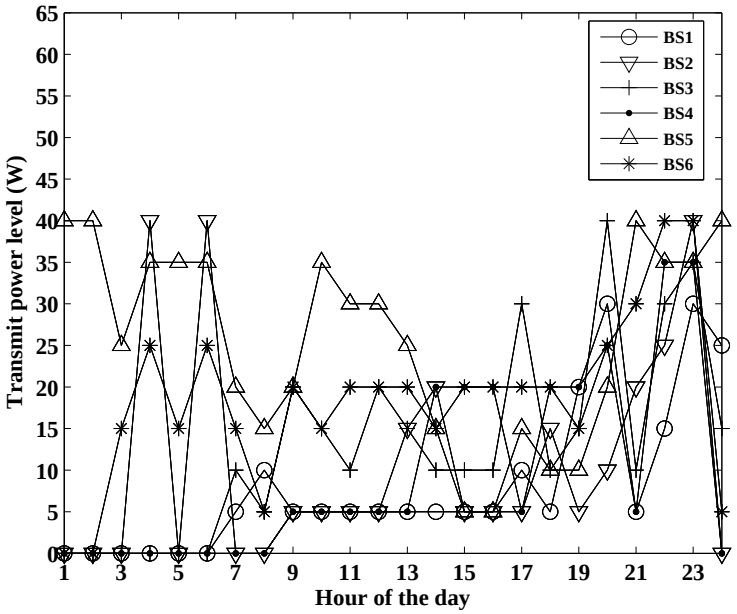

Figure 4.8: Transmit power levels for various BSs during the day (GAURA).

4.6.3 Transmit power levels

Figures 4.7 and 4.8 show the transmit power levels at which the BSs operate during the different hours of the day for the SWES and the proposed GAURA scheme, respectively. The BSs in Best-Effort, ICE and GALA schemes operate at a fixed transmit power level of 20 W. Note that although SWES can reduce the energy consumption during morning hours by completely switching off most of the BSs, the battery levels fall quickly during afternoon and evening hours on account of most of the BSs being switched on and operating at full transmit power. While GAURA also switches off most of the BSs during morning hours, it avoids a quick decrease in the battery levels during the afternoon and evening hours by adapting the transmit power levels of the BSs to lower values, and the adjustments are done in such a way that the system latency is improved. BSs with very low energy shut down during the early morning hours, and further even during other hours the BSs prefer to operate at lower power levels to save energy.

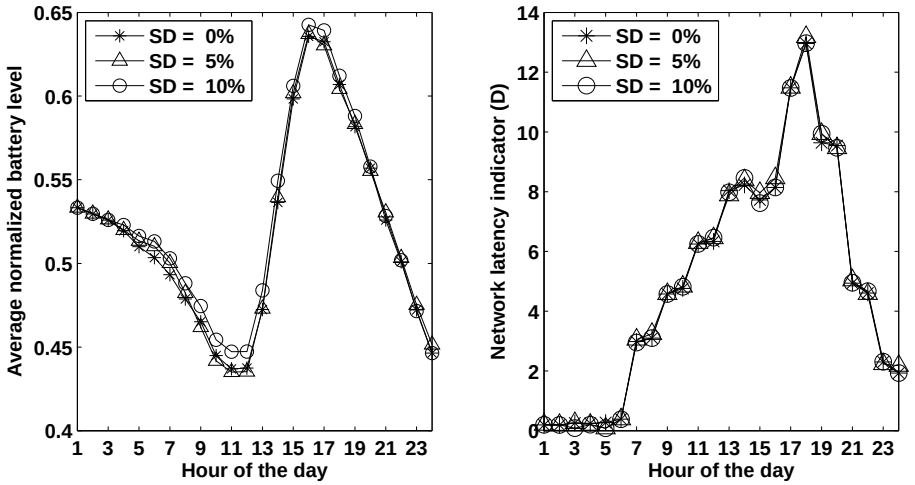

Figure 4.9: a. Average normalized battery level for GAURA with prediction error b. Delay performance for GAURA with prediction error.

Remark: Note that the proposed model assumes perfect knowledge of solar energy and network traffic by the central server. Additional simulations conducted by us show that the performance degradation is not significant even in the presence of 5-10% error in the predicted values of solar energy and network traffic. Figure 4.9 shows these results. The simulation results correspond to scenarios where the errors in the harvested energy and traffic load follow independent Gaussian distributions with zero mean and standard deviation (SD) of 5% and 10% of the actual value. Note that a SD of 0% represents no prediction error. As can be seen, the presence of errors does not have much of an impact.

4.7 Conclusion

This chapter proposed a framework for avoiding energy outages and improving the traffic latency for a network of off-grid solar powered BSs. We formulated the problem of minimizing the network latency given the constraints on the green energy availability at the BSs. We first proposed a

methodology for intelligently allocating the green energy available to the BSs over time. Next, with the given energy allocation, we addressed the problem of avoiding energy outages and improving the traffic latency using the proposed green energy and delay aware power control and user association algorithm. The proposed framework was evaluated using real BS deployment data and solar energy traces, and it outperforms existing benchmarks in terms of reducing energy outages while ensuring good delay performance. From our analysis, we noted that on a bad weather day, GALA, ICE and Best-Effort schemes can lead to energy outages in some of the BSs during the day and some of the BSs running very low on energy at the end of the day (indicating energy outages during the morning hours of the subsequent day). The GALA scheme, however, has better latency performance than the Best-Effort scheme. The ICE scheme has more even battery discharging profile for the BSs as compared to the Best-Effort scheme but at the cost of higher delay. The SWES scheme has an higher average battery level profile than the Best-Effort scheme, but it is at the cost of a higher delay. The proposed GAURA scheme has been shown to perform better than the existing schemes both in terms of avoiding energy outages and the delay performance.

Chapter 5

Delay Aware Resource Management for Grid Energy Savings in Green Cellular Base stations with Hybrid Power Supplies

5.1 Introduction

In the previous chapter we considered strategies for operating a network of off-grid solar powered BSs where the BSs are solely powered by solar energy. Locations that are very rich in solar resources can have base stations completely powered by solar energy. However, for locations with occasional bad weather periods, the size of harvesters and storage devices (e.g. PV (photo-voltaic) panels and batteries) required becomes very large

which leads to very high CAPEX (capital expenditure), thus discouraging operators from adopting such a solution [16]. In such scenarios and in scenarios where the BSs are already connected to the grid, using renewable energy in conjunction with grid energy is a more viable approach. Powering the BSs by solar energy can reduce the grid energy consumption. Intelligent management of the harvested solar energy by such BSs and cooperation among them can lead to further reduction in the grid energy consumption in the network. Note that while doing so, the operators also have to take into account the quality of service (QoS) offered to the users in terms of the network latency, and have to consider the trade-off between cost savings and the network latency. Existing literature on joint management of grid energy consumption and the network latency uses only user-association reconfiguration to achieve the same. Additionally, some works propose dynamic BS operation (i.e. BS on/off strategies) which is also a means of bringing about grid energy savings through network energy minimization. In contrast to these approaches, we propose the use of intelligent green energy allocation and the use of down-link power control and user-association reconfiguration to address the problem. The efficacy of the proposed methodology has been shown by simulations using real BS deployment and solar energy traces for London, UK and by comparison against existing benchmarks. We show that the proposed framework can lead to around 60% grid energy savings as well as better network latency performance than the traditionally used scheme [116].

In existing lietrature there exist some studies which consider BSs connected to the grid and consider dynamic electricity pricing and energy management in conetext of a smart grid environment such as [119]-[123] (for details of smart grids please refer to [124] and [125]). However, in this thesis for

simplicity of analysis we consider static electricity prices, i.e., the electricity price does not vary with time.

The rest of this chapter is organized as follows. Section 5.2 presents a brief overview of related works. Section 5.3 describes the system considered in the chapter. Section 5.4 presents the problem formulation. Section 5.5 presents the solution methodology. Section 5.6 presents the numerical results and Section 5.7 summarizes the chapter.

5.2 Literature review

One of the possible ways of bringing grid energy savings in a network of grid-connected solar-powered BSs is to reduce the energy consumption in the network [90],[126]. In related work, authors in [81] propose dynamic BS switching to minimize the network energy consumption. The energy savings in dynamic BS switching is brought by switching off some of the BSs during low traffic periods. The authors in [86] present a practical scheme (named SWES) for the implementation of dynamic BS switching for a network of BSs. The scheme is a greedy heuristic which seeks to determine the minimum number of BSs to be switched on in order to serve the given area with a desired quality of covereage. BS switching for renewable energy powered cellular networks is considered in [117]. The problem of grid energy minimization is formulated and the BS on/off strategy to solve the problem is derived through a two-stage dynamic programming algorithm. Some other works which consider BS on-off include [82], [118] and [126]. In [127] the authors consider the problem of resource allocation and admission control in an OFDMA network and propose an algorithm for dynamic power adaptation of femtocells to minimize the overall power consumption

of the network. The authors in [89] propose a scheme which uses the adaptation of BS transmit power levels and coverage area (based on the channel condtions and traffic load) to improve the energy efficiency performance of an OFDMA system. An energy-efficient scheme for resource allocation in OFDMA systems with hybrid energy harvesting BSs is proposed in [90]. The scheme uses a stochastic dynamic programming approach for power allocation to minimize the network energy consumption. The authors in [91] propose an algorithm for green energy aware load balancing. The approach is based on tuning the beacon power levels (and not the actual transmit power levels) of the various BSs. By doing so, users are discouraged from joining BSs running low on green energy. In [128], the authors propose a Lyapunov optimization approach for bringing grid energy savings in a network of BSs where some of the BSs are connected to the grid whereas some are not.

Note that all of the above studies primarily focus on minimizing the overall network energy consumption and most of them neglect the effect of doing so on the delay experienced by the users in the network. Some of the recent studies addressing network delay include [92] which proposes a distributed user association scheme using primal-dual formulation for traffic load balancing. Authors in [93] propose an α-optimal user association for the flow level cell load balancing with the objective of maximizing the throughput or minimizing the system delay. However the above-mentioned schemes ([92],[93]) do not account for the green energy availability at the BSs.

Methodologies which consider the green energy availability in addition to the delay performance of the system include [94, 95, 129] and [130]. These studies address the issue of bringing grid energy savings while managing the quality of service (in terms of the traffic latency) [131]. The authors in

[94],[129] propose the GALA scheme which accounts for the green energy availability at the BS while making user-association decisions. The authors formulate the problem of minimizing the sum of weighted latency ratios of the BSs where the weights are chosen to account for the green energy availability at the BSs. Authors in [95] consider BSs powered by hybrid supplies and formulate the problem of minimizing the weighted sum of the cost of average system latency and the cost of on-grid power consumption. The authors of [130] also consider BSs powered by hybrid supplies but formulate the problem of lexicographic minimization of the on-grid energy consumption so as to reduce both total and peak on-grid energy consumption. The framework proposed in [130] introduces a penalty function to account for the network latency. The approach in [94, 95, 129] and [130] to manage the available energy and network latency is by reconfiguring the BS-MT (mobile terminal) user-association. In contrast to such an approach, this chapter presents a methodology for energy and latency management based on BS downlink transmit power control in addition to user association reconfiguration, and demonstrates its performance gains over existing approaches. The use of intelligent temporal energy allocation has been shown to have a superior performance in terms of managing the green energy and delay jointly for an off-grid scenario in the previous chapter. In this chapter we use insights from the same and propose a temporal energy allocation scheme for BSs connected to grid.

5.3 System model

In this section we describe the traffic model considered in the chapter. We also describe the formulation of the BS load and the network latency.

5.3.1 Traffic model, BS load and Network latency

Let us consider a region $\mathcal{R}$ served by a set, $\mathcal{B}$, of BSs. We use $x \in \mathcal{R}$ to denote the user location. For simplicity we primarily focus only on downlink communication (i.e. BSs to mobile terminals (MTs)). We denote the downlink transmit power levels of the BSs by a vector P where the transmit power levels can take discrete values i.e. $P(j) \in \{0, \omega, 2\omega, \cdots, P_{max}\}$, where j is the index of the BS, ω is the granularity of power control and P_{max} is the maximum transmit power level allowed. File transfer requests are assumed to arrive following a Poisson point process with an arrival rate $\lambda(x)$ per unit area at location x, with average file size of $\frac{1}{\mu(x)}$ bytes. We define the traffic load density at location x as $\gamma(x) = \frac{\lambda(x)}{\mu(x)}$, where $\gamma(x)$ captures the spatial traffic variability. The rate offered at location x served by a BS j can be generally given using the Shannon-Heartley theorem [93] as

$$c_j(x) = BW_j \log_2(1 + SINR_j(x)) \tag{5.1}$$

where BW_j is the total bandwidth offered by the j-th BS and $SINR_j(x)$ is given by

$$SINR_j(x) = \frac{g_j(x)P(j)}{\sigma^2 + \sum_{m \in I_j} g_m(x)P(m)} \tag{5.2}$$

where $g_j(x)$ denotes the channel gain between the j-th BS and the user at location x which accounts for the path loss and the shadowing loss, σ^2 denotes the noise power level and I_j is the set of interfering BSs for BS j. This chapter assumes perfect information of the channel gain which may be estimated given the topological details of the terrain, and drive-through site surveys. We introduce a user association indicator function $u_j(x)$ which indicates if the user at location x is served by BS j. If that is true then this variable has the value 1, and 0 otherwise. The BS load ρ_j, which denotes

the fraction of time the BS j is busy serving its traffic requests can thus be given as [94]

$$\rho_j = \int_{\mathcal{R}} \frac{\gamma(x)}{c_j(x)} u_j(x) dx. \tag{5.3}$$

Definition 5.3.1. We denote the feasible set of the BS loads $\rho = (\rho_1, \cdots, \rho_{|\mathcal{B}|})$ by $\mathcal{F}_2$ which can be defined as

$$\mathcal{F}_2 = \Big\{ \rho \mid \rho_j = \int_{\mathcal{R}} \frac{\gamma(x)}{c_j(x)} u_j(x) dx, \ 0 \leq \rho_j \leq \rho_{th}, \ \forall j \in \mathcal{B}, \\ u_j(x) \in \{0,1\}, \sum_{j \in \mathcal{B}} u_j(x) = 1, \ \forall j \in \mathcal{B}, \ \forall x \in \mathcal{R} \Big\},$$

where ρ_{th} is a threshold on the permitted BS load to avoid congestion at a given BS.

Note that as traffic requests follow a Poisson processes, the sum of such requests at a given BS is also a Poisson process. Further, as the BS's service time follows a general distribution, its operation can be modeled as a M/G/1 processor sharing queue. The average number of flows at BS j can thus be given by $\frac{\rho_j}{1-\rho_j}$ [95]. According to Little's law, the delay experienced by a traffic flow is directly proportional to the average number of flows in the system [100]. Thus we take the total sum of the flows in the network as the network latency indicator, $\mathcal{D}(\rho)$, which is given by [95]

$$\mathcal{D}(\rho) = \sum_{j \in \mathcal{B}} \frac{\rho_j}{1 - \rho_j}. \tag{5.4}$$

5.3.2 BS power consumption

This chapter considers macro BSs where the power consumption for BS j, denoted by $L(j)$, can be modeled as [101]

$$L(j) = P_0 + \Delta P(j)\rho_j, \;\; 0 \leq \rho_j \leq 1, 0 \leq P(j) \leq P_{max} \tag{5.5}$$

where P_0 is the power consumption at no load (zero traffic) and Δ is the slope of the load dependent power consumption.

5.3.3 Solar energy resource and batteries

We consider solar irradiation data provided by National Renewable Energy Laboratory (NREL) for London, UK [17]. This data is fed to NREL's System Advisor Model (SAM), to obtain the hourly energy generated by a PV panel of a given rating. We assume that the BSs use lead acid batteries to store the excess energy harvested by the PV panels.

5.4 Problem formulation

This section describes the problem formulation. We begin by describing the mechanism for green energy allocation over time. This mechanism is an important pre-requisite before formulating the optimization problem which jointly manages the grid energy savings and the traffic latency. After describing the green energy allocation scheme, we formulate the optimization problem.

5.4.1 Green energy allocation

The green energy available to the BSs is in the form of energy stored in the batteries and the energy harvested during the day. This budget of green energy available to a BS needs to be intelligently allocated during the different hours of the day so as to optimize the use of the green energy, and in turn to minimize the grid energy usage. The green energy allocation for a given hour is done based on the energy available in the BS's battery at that time and the energy expected to be harvested in future hours during the day. Additionally, to avoid battery degradation, we dis-allow the battery from discharging below a certain charge level given by νB_{cap} where B_{cap} is the battery capacity. The green energy budget $\mathcal{M}_t$ at the beginning of a hour t is the green energy available for allocation from that hour to the last hour of the day (i.e. $t = 24$). Please note that we use the subscript t to denote the value of the variable during the t-th hour throughout this chapter. Considering the t-th hour of operation for the j-th BS, the green energy budget at the begining of hour t can be given as

$$\mathcal{M}_t(j) = B_{t-1}(j) - B_{sm}(j) + \sum_{h=t}^{24} \mathcal{H}_h(j) \tag{5.6}$$

where B_{t-1} denotes the battery level at the end of the previous hour, and $\mathcal{H}_t$ denotes the green energy harvested during the hour t. $\sum_{h=t}^{24} \mathcal{H}_h(j)$ denotes the sum of the green energy to be harvested during the given hour t and the coming hours of the day. The battery levels are dis-allowed to go below state of charge νB_{cap} at any point of time. Because the energy allocation is done based on the expected energy to be harvested during the day which is a random process, we add a margin of safety to reduce the likelihood that the battery level goes below νB_{cap}. Thus we take $B_{sm} = (1 + \beta)\nu B_{cap}$ where

Algorithm 8 The LPEA Algorithm

1: **for** $j = 1 : \mathcal{B}$ **do**
2: $\mathcal{M}_t(j) = B_{t-1}(j) - B_{sm}(j) + \sum_{h=t}^{24} \mathcal{H}_h(j)$;
3: $G_t(j) = \mathcal{M}_t(j) \frac{A_t(j)\rho_j^{(t)} + P_0}{A_t(j)\rho_j^{(t)} + C_t(j)}$;
4: **end for**

β is the safety margin. Based on the information of the energy budget available, we allocate green energy to the given hour in proportion to the traffic load in the given hour. The green energy allocated by the BS j for the hour t is denoted by G_t and is given by

$$\begin{aligned} G_t(j) &= \mathcal{M}_t(j) \frac{L_t(j)}{L_t(j) + \sum_{m=t+1}^{24} L_m(j)} \\ &= \mathcal{M}_t(j) \frac{P_0 + \Delta P_t(j)\rho_j^{(t)}}{P_0 + \Delta P_t(j)\rho_j^{(t)} + \sum_{m=t+1}^{24} L_m(j)} \end{aligned} \tag{5.7}$$

where $\rho_j^{(t)}$ denotes the load of BS j in the t-th hour. For sake of clarity we use the following notation

$$A_t(j) = \Delta P_t(j) \tag{5.8}$$

$$C_t(j) = P_0 + \sum_{m=t+1}^{24} L_m(j). \tag{5.9}$$

Thus the green energy allocated for the hour t is given by

$$G_t(j) = \mathcal{M}_t(j) \frac{A_t(j)\rho_j^{(t)} + P_0}{A_t(j)\rho_j^{(t)} + C_t(j)}. \tag{5.10}$$

The methodology for assigning the green energy described above has been summarized in Algorithm 8 as the load proportional energy allocation (LPEA) algorithm.

This chapter assumes that all energy allocation operations are done by a central server. The central server is assumed to have perfect information of the renewable energy that is harvested during the day which can be implemented in real life using weather forecasts. In existing literature there are many methodologies which predict the solar energy generation (e.g. [102], [103]). Integrating them with weather forecasts can give a more accurate prediction. The proposed algorithm needs only an hourly estimate of the solar energy generation, making the task even simpler. Also, for the initial green energy allocation (using the LPEA algorithm), any arbitrary load profile (like the one in [16] or [86]) can be used. Note that this energy allocation is just an initialization step and the green energy allocation is later iteratively updated after the downlink power control operations as discussed in Section 5.5.2.

The green energy allocated to the BS in a given hour, G_t, is used to power the BS. If it not sufficient, then additional energy is drawn from the grid. Thus the grid energy consumed by the network during hour t, denoted by $\mathcal{E}_t$, is given by

$$\mathcal{E}_t = \sum_{j \in \mathcal{B}} \max\left(0, L_t(j) - G_t(j)\right). \tag{5.11}$$

Claim 4.4.1. *Grid energy is drawn by BS j in the t-th hour only if the load value of that BS is greater than $\frac{\mathcal{M}_t(j) - C_t(j)}{A_t(j)}$.*

Proof. Considering BS j, the grid energy drawn by the BS can be written as

$$\mathcal{E}_t(j) = \max\left(0, L_t(j) - G_t(j)\right). \tag{5.12}$$

For energy to be drawn from the grid we need

$$L_t(j) - G_t(j) > 0. \tag{5.13}$$

Note that for clarity, we omit the subscript t in the later part of the proof. From (5.5) and (5.7), substituting the values of L and G we have

$$\begin{aligned} & P_0 + \Delta P(j)\rho_j - \mathcal{M}(j)\frac{A(j)\rho_j + P_0}{A(j)\rho_j + C(j)} > 0 \\ \Rightarrow\ & A(j)\rho_j + P_0 - \mathcal{M}(j)\frac{A(j)\rho_j + P_0}{A(j)\rho_j + C(j)} > 0 \\ \Rightarrow\ & (A(j)\rho_j + P_0)\left(1 - \frac{\mathcal{M}(j)}{A(j)\rho_j + C(j)}\right) > 0. \end{aligned} \tag{5.14}$$

Note that as ρ_j, $A(j)$ and P_0 are all positive, we have $(A(j)\rho_j + P_0) > 0$. Thus for the above inequality to be true we require the following

$$\begin{aligned} & 1 - \frac{\mathcal{M}(j)}{A(j)\rho_j + C(j)} > 0 \\ \Rightarrow\ & A(j)\rho_j + C(j) - \mathcal{M}(j) > 0 \\ \Rightarrow\ & \rho_j > \frac{\mathcal{M}(j) - C(j)}{A(j)}. \end{aligned} \tag{5.15}$$

This completes the proof of the lemma. ■

5.4.2 Problem formulation

We consider the following problem of minimizing the grid energy drawn and its trade-off with the network latency during the day which is formulated as problem [P3] and given by

$$\textbf{[P3]} \quad \underset{P_t,\ \rho^{(t)}}{\text{minimize}} \quad \sum_{t=1}^{24} \Big(\mathcal{D}_t(P_t, \rho^{(t)}) + \eta \mathcal{E}_t(P_t, \rho^{(t)}) \Big)$$
$$\text{subject to:} \quad \rho^{(t)} \in \mathcal{F}_2, \forall t$$

where η is a parameter which controls the trade-off between grid energy savings and the delay performance. Note that for $\eta = 0$, the problem reduces to minimizing the network latency, whereas for $\eta \to \infty$ the problem becomes minimizing the grid energy consumed without considering the delay performance. We propose to solve the above problem by using BS downlink transmission power control and user-association reconfiguration which involves suitably tuning the BS transmit power levels (P) and managing the BS loads (ρ). P_t and $\rho^{(t)}$ denote the BS power level vector and the load vector at time t.

Remark: Note that for a given hour the value of the network latency indicator ($\mathcal{D}_t$) generally lies in the range $\{0, 20\}$ whereas the grid energy consumption ($\mathcal{E}_t$) for a given hour generally lies in the range $\{0\text{kW}, 20\text{kW}\}$. Although the units of the two terms being added are different, where the first term ($\mathcal{D}_t$) is unit-less while the second term has kW as the unit, we consider the numerical values of these terms while evaluating the optimization problem [P3]. Additionally, note that in existing literature we do find some studies like [112] which consider a similar problem formulation where the weighted sum of the network latency indicator and the BS energy consumption (which have different units) is considered.

5.5 Solution methodology

This section presents the proposed methodology for addressing the problem [P3]. We address the problem using BS downlink power control and user association reconfiguration. The proposed framework for addressing the problem is named Green energy and Delay aware - Renewable Asset and resource Management (GD-RAM).

The problem [P3] is very challenging on account of the complexity arising from the coupling between BS power levels and the resulting user-association. Thus to make our analysis tractable, we make the assumption of time scale separation between the user association process and the period over which the power level control decisions are made. The user association process happens at a much faster time-scale than the time scale at which the green energy availability and the network traffic load vary. Studies have shown that the green energy availability and traffic pattern is nearly constant during a given hour of the day [86]. Further, as the time scale for determining the power levels of the BSs is of the order of that of traffic pattern and green energy availability variation (i.e. hours), it is much greater than that of the user-association process. Hence, with this assumption we decompose our problem into two sub-problems, in which the BS power control problem is solved at a slower time scale than the user association problem. The BS power level decisions are made on an hourly scale whereas the user-association scheme is periodically updated on a faster time scale. These sub-problems are given as follows:

1) **User association probelm:** For BSs operating with power levels specified by a vector P, the user association problem aims at load balancing (balancing the BS loads) so as to find the optimal BS load vector ρ that

Algorithm 9 Sequence of operations: GD-RAM

1: **for** $t = 1 : 24$ **do**
2: **while** power control convergence **do**
3: **while** user association convergence **do**
4: Perform Green energy allocation for given hour using the LPEA algorithm (Algorithm 8).
5: Solve user association problem for the given hour using the allocated green energy and the predicted traffic.
6: **end while**
7: Solve power control problem for the underlying user-association determined in the inner while loop.
8: **end while**
9: **end for**

minimizes the objective function. This problem is denoted as [P-UA] and can be expressed as

$$\textbf{[P-UA]} \quad \underset{\rho^{(t)} \in \mathcal{F}_2}{\text{minimize}} \quad \mathcal{D}_t(\rho^{(t)}, P_t) + \eta \mathcal{E}_t(\rho^{(t)}, P_t). \tag{5.16}$$

2) **BS power control problem:** The BSs try to adjust their power levels so as to minimize the objective function and the problem is denoted by [P-PC] which can be given as

$$\textbf{[P-PC]} \quad \underset{P_t \subset \tilde{\mathcal{P}}}{\text{minimize}} \quad \{\mathcal{Q}_t(P_t) = \mathcal{D}_t(P_t) + \eta \mathcal{E}_t(P_t)\}. \tag{5.17}$$

where $\tilde{\mathcal{P}}$ is the set of all possible power level vectors and $\mathcal{Q}_t(P_t)$ is defined as the solution to the user association problem in (5.16). Next, Section 5.5.1 describes the solution methodology for addressing the user association problem whereas Section 5.5.2 describes the solution methodology for addressing the BS power control problem. Algorithm 9 summarizes the sequence of operations inovolved in solving problem [P3].

Remark: Note that the problem [P-UA] does not have summation over time because user-association is a continuous process with the set of active users

changing with time. However the active users associate with the BSs according to the proposed user-association policy so as to minimize the objective function at a given time instant. Further the problem [P-PC] does not have summation because it is solved individually for every hour of the day, with user-association determined using the average traffic profile for that given hour.

5.5.1 Optimal user association policy

In this section we propose the user association policy which achieves the global optimal of value of the objective function (with BSs operating at a given set of power levels).

Since $u_j(x) \in \{0,1\}$, the set $\mathcal{F}_2$ is not convex. Thus, to formulate the problem [P-UA] as a convex optimization problem, we relax the constraint to $0 \leq u_j(x) \leq 1$. Here u_j can be interpreted as the probability that the user at location x associates with BS j. The relaxed set of BS loads, $\tilde{\mathcal{F}}_2$, can be given as

$$\tilde{\mathcal{F}}_2 = \Big\{\rho \mid \rho_j = \int_{\mathcal{R}} \frac{\gamma(x)}{c_j(x)} u_j(x)dx,\ 0 \leq \rho_j \leq \rho_{th},\ \forall j \in \mathcal{B},$$
$$0 \leq u_j(x) \leq 1, \sum_{j=1}^{|\mathcal{B}|} u_j(x) = 1,\ \forall j \in \mathcal{B},\ \forall x \in \mathcal{R}\Big\}.$$

Theorem 5.5.1 The feasible set $\tilde{\mathcal{F}}_2$ is convex.

Proof. The convexity of $\tilde{\mathcal{F}}_2$ can be proved following similar steps as in the proof of Theorem 4.5.1 in the previous chapter. ■

The problem [P-UA] with the relaxation condition is denoted as [P-UAR] and can be given as

$$\textbf{[P-UAR]} \quad \underset{\rho \in \tilde{\mathcal{F}}_2}{\text{minimize}} \quad \mathcal{U}(\rho) = \mathcal{D}(\rho) + \eta \mathcal{E}(\rho)$$

Remark: We drop the subscript t throughout this section as user association is an continuous process where the set of active users in the network keeps changing, but at all times they associate with the BSs according to the proposed user-association policy. Additionally, we drop P, as the time-scale of user-association problem is faster than that of the power control operations, and thus power levels of the BSs are assumed to be fixed during the user-association operations. Further for notational simplicity we denote the optimization function value in the problem [P-UAR] by $\mathcal{U}(\rho)$. Note that although we formulate the optimization problem [P-UAR] using $\tilde{\mathcal{F}}_2$, the user association algorithm which we propose in this chapter determines the deterministic user association (belonging to $\mathcal{F}_2$). This is shown in Theorems 5.5.2 and 5.5.3.

The working of the proposed user association algorithm is described as follows. The proposed user association algorithm operates in an iterative way. The BSs periodically measure their traffic loads and use it to determine an operational variable (called coalition factors in this section) and advertise it to the MTs. The mobile terminals choose which BS to associate with based on these coalition factors in order to minimize the objective function. The association between the MTs and the BSs is updated until convergence. To ensure convergence of the scheme, we assume that the traffic arrival and departure processes occur at a faster time scale as compared to that at which the BSs broadcast their coalition factors. This ensures that the users are able to make their association decisions for the broadcasted coalition factors before the next broadcast of coalition factors by the BSs. We assume BSs to be synchronized, thus broadcasting their coalition factors at the same

time. The proposed user-association scheme can be easily implemented in a distributed way where the BSs periodically broadcast their coalition factor that can be embedded in the the beacon signals of the BSs [112] and users can use them to choose which BSs to associate with as described above.

Next, we begin with describing the user side and the BS side algorithms for carrying out the proposed user association mechanism.

1) **User Side Algortihm:** We define the time between two successive BS-MT association updates as a time slot in our algorithm. At the start of k-th time slot, the BSs send their coalition factors to the users using a broadcast signal. The users at location x in turn choose the BSs they associate with based on the coalition factors. In this section, superscript k is used to denote the value of a particular variable at the beginning of the k-th time slot. The coalition factor broadcast by BS j is given as

$$\begin{aligned}\phi_j^{(k)} &= \frac{\partial \mathcal{U}^{(k)}(\rho)}{\partial \rho_j^{(k)}} \\ &= \frac{1}{(1-\rho_j^{(k)})^2} + \eta \zeta_j A(j) \left(1 - \mathcal{M}(j) \frac{C(j) - P_0}{(A(j)\rho^{(k)}(j) + C(j))^2}\right)\end{aligned} \tag{5.18}$$

where ζ_j is a variable which captures whether BS j is drawing power from the grid. If the BS is drawing power from the grid then this variable is 1, else it is set to zero. The MTs update their user association functions as

$$u_j^{(k)}(x) = \begin{cases} 1 & \text{if } j = \arg\max_{j \in \mathcal{B}} \frac{c_j(x)}{\phi_j^{(k)}} \\ 0 & \text{otherwise.} \end{cases} \tag{5.19}$$

Note that the association functions ($u_j(x)$) are indicator of which BS the MTs at location x associate with as discussed in Section 5.3.1. The com-

putational complexity of the user side algorithm for an individual user is $O(|\mathcal{B}|)$.

2) **BS side algorithm:** At the end of the k-th time slot, the BSs measure their load levels which we denote by $T_j(\rho_j^{(k)})$, and is given as

$$T_j(\rho_j^{(k)}) = \min\left(\int_{\mathcal{R}} \frac{\gamma(x)}{c_j(x)} u_j(x)dx, \rho_{th}\right). \tag{5.20}$$

After measuring $T_j(\rho_j^{(k)})$, the BS updates its traffic load which is used to evaluate the next coalition factor to be broadcast for time slot $k+1$ as [93]

$$\rho_j^{(k+1)} = \theta\rho_j^{(k)} + (1-\theta)T_j(\rho_j^{(k)}) \tag{5.21}$$

with $0 < \theta < 1$ being an averaging exponential factor.

Next, the proof of convergence and optimality and convergence of the proposed user association algorithm is presented. We begin with proving the objective function $\mathcal{U}$ to be convex in $\rho \in \tilde{\mathcal{F}}_2$ in Lemma 5.5.1. This leads to Lemma 5.5.2 which indicates that there is a unique optimal user association which minimizes the objective function.

Lemma 5.5.1 *The objective function $\mathcal{U}(\rho) = \mathcal{D}(\rho) + \eta\mathcal{E}(\rho)$ is convex in ρ when ρ is defined on $\tilde{\mathcal{F}}_2$.*

Proof. Please refer to Appendix E for the proof. ■

Remark: Note that as we consider the steady state analysis of the system, the proof above assumes that $\frac{\partial f(\rho_j)}{\partial \rho_g} = 0$, $j \neq g$ ([91], [93], [95]) where $f(\rho_j)$ is purely a function of ρ_j and does not depend on ρ_g ($g \neq j$).

Lemma 5.5.2 *A unique optimal user association $\rho^* \in \tilde{\mathcal{F}}_2$ exists which minimizes $\mathcal{U}(\rho) = \mathcal{D}(\rho) + \eta\mathcal{E}(\rho)$.*

Proof. It has been shown in Lemma 5.5.1 that the objective function $\mathcal{U}(\rho)$ is a convex function of $\rho \in \tilde{\mathcal{F}}_2$. Thus there exists a unique optimal $\rho = \rho^*$ which minimizes $\mathcal{U}(\rho)$. ■

Next we prove the convergence of the proposed user-association algorithm. We begin with proving that $T_j(\rho^{(k)})$ gives a descent direction for $\mathcal{U}(\rho^{(k)})$ at $\rho^{(k)}$ (shown in Lemma 5.5.3). Thus after some iterations the traffic load converges which is proved in Theorem 5.5.2. Further, in Theorem 5.5.3 we prove that the trafic load thus obtained minimizes the objective function $\mathcal{U}(\rho)$.

Lemma 5.5.3 *For $\rho^{(k)} \neq \rho^*$, $T(\rho^{(k)})$ gives a descent direction for $\mathcal{U}(\rho^{(k)})$ at $\rho^{(k)}$.*

Proof. Please refer to Appendix F for the proof. ■

Theorem 5.5.2 *The traffic load ρ converges to the traffic load $\rho^* \in \mathcal{F}_2$.*

Proof. The proof of this theorem is similar to the proof of Theorem 4.5.2 in Chapter 4 (with the only difference that here the objective function is $\mathcal{U}$ instead of X). ■

Theorem 5.5.3: *If the set $\mathcal{F}_2$ is non-empty and the traffic load ρ converges to ρ^*, the user association corresponding to ρ^* minimizes $\mathcal{U}(\rho)$.*

Proof. This can be easily proved following the proof of Theorem 4.5.3 in Chapter 4. ■

5.5.2 Base station transmission power control

We assume that the power control operations are decided by the central server before a day begins and that guides the power levels of the BSs dur-

ing the day. Further as the power level decisions are made on a time-scale of an hour, the power control operations just require the average traffic profile at a given location for each hour. We assume that the central server has this average traffic profile information which is used to evaluate the underlying user association for facilitating the power control decisions. There are a number of existing papers in literature which study, model and predict cellular network traffic like [107], [109] and [108] . The information/ideas from these models could be used in real time implementation of our work. Additionally, such information could be also predicted by the operators using the traffic pattern during past few weeks/months. Note that the above-mentioned assumptions have been considered in several contemporary works (e.g. [110], [111]). Next, we show an important observation about the downlink power control.

Proposition 5.5.1: *The objective function* $\mathcal{Q}_t(P_t) = \mathcal{D}_t(P_t) + \eta\mathcal{E}_t(P_t)$ *is a non-convex function of the BS power levels.*

To verify this proposition using simulations, we consider a network of BSs as shown in Figure 4.3. The simulation settings are as described in Section 5.6. We consider BSs operating at 3 p.m ($t = 15$) on January 1st with BSs 2, 4, 5 and 6 operating at transmit power level 20 W. Next, we vary the power levels of BSs 1 and 3 and study the effect of the same on the objective function. Figure 5.1 shows the objective function (for $\eta = 2$) and from the figure we can easily conclude that the objective function is a non-convex function of the BS power levels.

As shown above, the power level control problem to minimize the objective function is a non-convex optimization problem. Finding the optimal solution for such a problem requires a search over the entire state space and has a very high computational complexity. The order of such computations

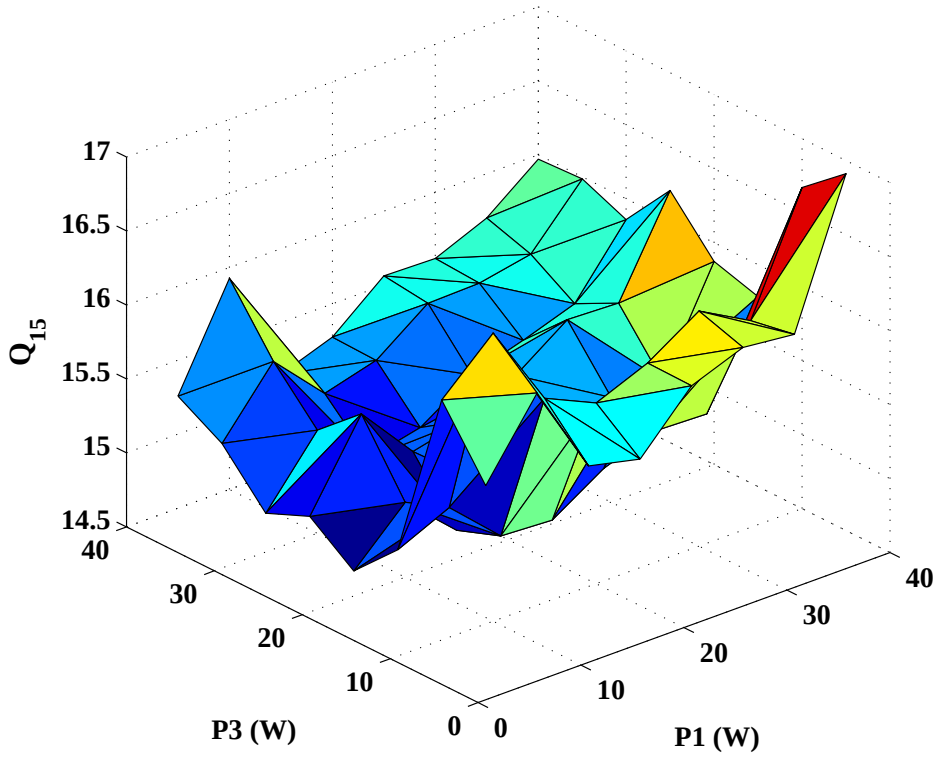

Figure 5.1: Objective function ($\mathcal{Q}_t$) value variation with power control operations on BS 1 and BS 3 ($\eta = 2$, t =15).

increases exponentially with the number of BSs ($\mathcal{B}$) and the hours under consideration (denoted by T) and is given by $O(Z^{|\mathcal{B}|T})$ where Z denotes the number of possible power levels the BSs can operate at. To make the power control approach feasible, we resort to developing a greedy heuristic for addressing the problem of power control and the proposed downlink transmit power control algorithm is presented in Algorithm 10.

The proposed algorithm is carried out sequentially for each hour of the day. The working of the downlink transmit power control algorithm can be explained as follows. For every hour, all the BSs start with a transmit power level of P_{max}. Next we check for which BS the decrement of power level brings the largest improvement in the objective function ($\mathcal{Q}$). For this purpose we introduce a vector $\mathcal{Q}'$ which stores the value of objective func-

Algorithm 10 Downlink Transmit Power Control Algorithm

1: Initialization
2: Set $P_t(j) = P_{max}$ for all $j \in \mathcal{B}$
3: Compute $\mathcal{Q}_t(P_t)$; Set $\delta\mathcal{Q} = 1$
4: **while** $\delta\mathcal{Q} > 0$ **do**
5: $\mathcal{Q}_{old}$= $\mathcal{Q}_t(P_t)$ ▷ Storing objective function value before power control operation
6: **for** $j = 1 : |\mathcal{B}|$ **do** ▷ Loop to check objective fn value with power control decrement
7: $P_{curr} = P_t$
8: $P_{curr}(j) = \max(0, P_t(j) - \omega)$ ▷ Reducing BS power level
9: $\mathcal{Q}'(j) = \mathcal{Q}_t(P_{curr})$
10: **if** $\max(\rho^{(t)}) > \rho_{th}$ **then** ▷ checking system constraint satisfaction
11: $con(j)$= 0
12: **else** $con(j)$= 1
13: **end if**
14: **end for**
15: a. z : index of BS having $con = 1$ for which power control leads to minimum objective function value ($\mathcal{Q}'$)
16: b. Set $\mathcal{Q}_{new}$ = $\mathcal{Q}'(z)$
17: $\delta\mathcal{Q} = \mathcal{Q}_{old} - \mathcal{Q}_{new}$
18: **if** $\delta\mathcal{Q} > 0$ **then**
19: $P_t(z) = \max(0, P_t(z) - \omega)$; ▷ BS power level update
20: **end if**
21: **end while**

tion after decrement of the power level (i.e $\mathcal{Q}'(1)$ would hold the objective function value when BS1 is powered down by ω). The BS with the largest reduction in the objective function while satisfying the system constraints (which is tracked in the algorithm by the variable *con*) is chosen for transmit power reduction (line 15). This is done until no further improvement in the objective function can be realized. Note that in a particular iteration, z is the index of the BS for which power control leads to the minimum objective function value while satisfying the system constraints (line 15). The value of the objective function corresponding to powering down this BS is denoted as Q_{new} (line 16). The objective function value before the powering down operation was stored in Q_{old} and if it is higher than Q_{new}, it means

that there is an improvement in the delay by the power control operation. Thus the BS whose powering down leads to least objective function value is powered down (line 19). The improvement in the delay component of the objective function in the power control operations is due to its interference management and load balancing effect. The reduction in the grid energy consumption is due to the transmit power level of a BS low on green energy going down, and further, some users being offloaded (which reduces ρ), thus decrementing the BS power consumption. The worst case computational complexity of this algorithm for T hours is $O(T(Z-1)|\mathcal{B}|^2)$. The explanation for this worst case computational complexity for this algorithm is same as that for the worst case computational complexity for the power control algorithm described in Section 4.5.2. Note that the load levels of the BSs change after every iteration of power control operations. Thus after this algorithm is carried out for all the hours of the day, we have different traffic load profiles for the different hours as compared to that used for initial energy allocation during the day (using Algorithm 8). Consequently, we repeat the energy allocation followed by another application of the downlink transmit power control algorithm for the day. After some iterations of doing this (typically 3-4 iterations) the solution for the downlink power levels converges. Note that the proposed power control approach does not guarantee an optimal solution but gives an local optimal solution. It follows the intution of greedy descent approach to minimize the objective function. At a given iteration, the BS for which the power level decrement leads to maximum delay reduction is chosen to be powered down. Thus the power levels for the next iteration gives a delay performance better than that at the previous iteration. Additionally as the number of power levels a BS can take are limited and lower-bounded by 0, the algorithm is guaranteed to converge.

5.6 Numerical results

For performance analysis of the proposed scheme, we consider a 3G BS deployment (shown in Figure 4.3 of Chapter 4) deployed by network provider Vodafone near Southwark, London, UK with 6 BSs providing coverage to an area of 1 km^2. We assume that the BSs use 12 V, 205 Ah flooded lead acid batteries. The BSs are assumed to be equipped with PV panel with DC rating 6 kW and 10 batteries. We consider that the BSs use 12 V, 205 Ah flooded lead acid batteries. The carrier frequency is 2.5 GHz and we assume 10 MHz bandwidth with full frequency reuse. Log normal shadowing with standard deviation 8 dB with the correlation distance for shadowing taken as 50m has been considered [115]. We model the path loss, PL, as [114]

$$PL(dB) = 40(1 - 4 \times 10^{-3} h_{BS}) log_{10}(R) - 18 log_{10}(h_{BS}) + 21 log_{10}(f) + 80$$

where R denotes the distance between the MT and the BS, h_{BS} is the base station antenna height above rooftop and f is the carrier frequency in MHz. We take h_{BS} as 15 metres and the carrier frequency is 2.5 GHz, based on the suggestions from the baseline test scenario mentioned in IEEE 802.16 evaluation methodology document [115]. Thus, the path loss is calculated as $PL(dB) = 130.19 + 37.6 \log(R)$. We take the noise power to be -174 dBm/Hz [115]. A homogeneous Poisson point process is used to generate the file transfer request. The rate of the Poisson process depends on the hour of the day, with the smallest number of file transfer requests during early morning hours (2-5 am) with an average of 20 requests per unit area (km^2) and the largest number of requests in the evening (5-7 pm) with an average of 200 requests per unit area. For weekends a lower traffic level with

minimum and maximum number of file transfer requests (per unit area) of 10 and 150 respectively, in the corresponding hours have been considered. For simplicity, we assume that each file transfer request requires 50 KB of data traffic to be served. To model temporal traffic dynamics, a new spatial profile of file transfer requests is generated after every 2 minutes. The entire area (of 1 km^2) is divided into 1600 locations with each location representing a 25 m x 25 m area. The location based traffic load density is calculated based on the traffic model. For simulations we consider solar energy data obtained from NREL [17] for the month of January of typical meteorological year (TMY) data for London. Figure 5.2 shows the solar energy harvested by the PV panels during the different days of this month by the BSs (with PV panels having DC rating 6 kW). Additionally we assume that 1^{st} January is Monday (i.e. weekday load profile). The values of P_0, P_{max} and Δ used for the results were 412.4 W, 40 W and 22.6 respectively [101]. The granularity of power control, ω, was 5 W and ρ_{th} used for the results was 0.85. The value of ν, the limiting state of charge was taken as 0.3, and the safety margin β was taken as 0.1. The initial battery levels were randomly chosen for the different BSs for 1^{st} January. We take the averaging factor for the BS side algorithm θ to be 0.95, and with this value the proposed user-association algorithm was observed to converge to the optimal solution within 20 iterations.

As a benchmark for comparison, we consider a Best-Effort scheme where all BSs operate with transmit power 20 W and the MTs associate with the BS with the strongest signal strength at that location. BSs use green energy as long as it is available and when it falls short energy is drawn from the grid. We also consider the GALA [94] scheme with BSs operating at transmit power 20 W, and the SWES [86] scheme which is a BS on-off scheme with

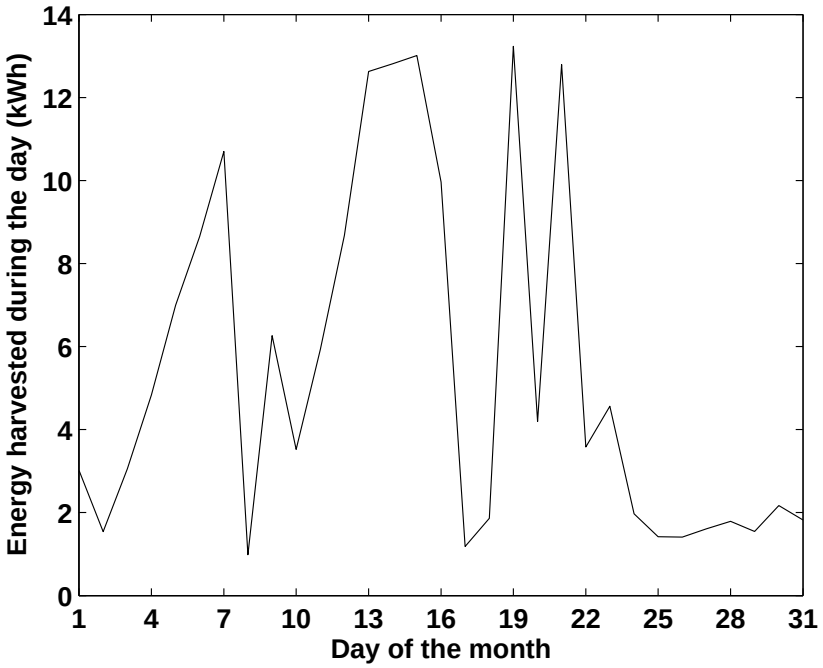

Figure 5.2: Solar energy harvested during the day by the BSs (PV panel rating: 6 kW).

BSs operating at 40 W when they are switched on. The GALA and the SWES scheme have been briefly described in Section 5.2.

5.6.1 Grid energy savings

Figure 5.3 shows the grid energy consumption for the different schemes for the month of January. It can be seen that the Best-Effort scheme leads to very high values of grid energy consumption. The GALA scheme shows significant grid energy savings as compared to the Best-Effort scheme. Note that the SWES scheme has lower grid energy consumption than the Best-Effort and the GALA scheme. This is because in this scheme some of the BSs switch off to reduce the overall network power consumption. The BSs which are switched off save energy and the energy harvested during this period is stored in the batteries to be used for future hours, thus reducing

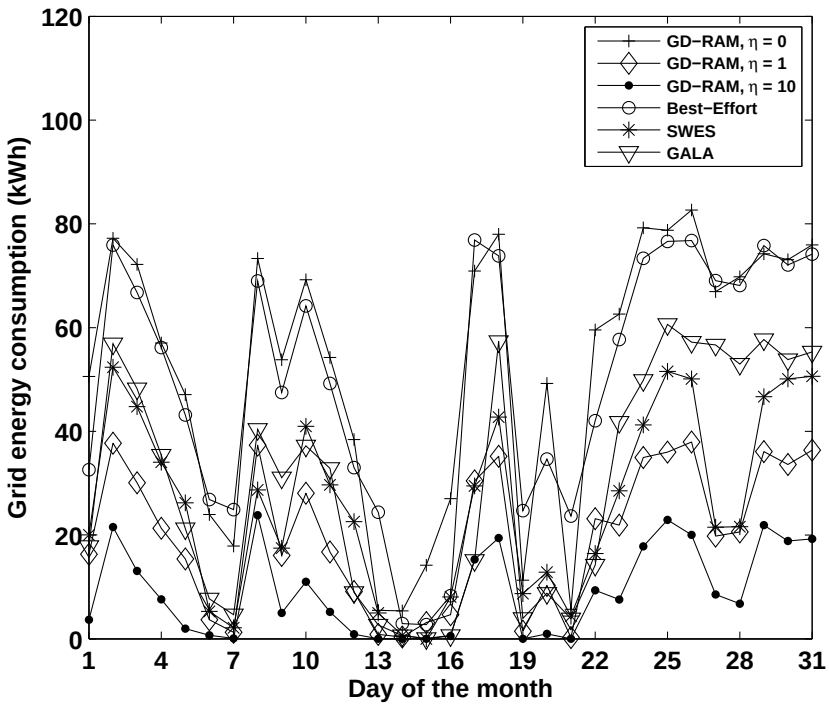

Figure 5.3: Grid power consumption for the different schemes.

the need to draw energy from the grid. The proposed GD-RAM scheme allows a wide range of control over the grid energy consumption. Note that with $\eta = 0$, the grid energy consumption is the highest which is comparable to the Best-Effort scheme. This is because for this case, the power control and user association operations are done solely considering the network delay. For $\eta = 1$, we observe that the grid energy consumed is smaller as compared to the other benchmark schemes. Further, for $\eta = 10$ the energy drawn from the grid is even smaller. Note that the grid energy savings in the SWES scheme and our scheme for $\eta = 10$ is at the expense of an increase in the network latency (Figure 5.4) which is discussed in the next subsection.

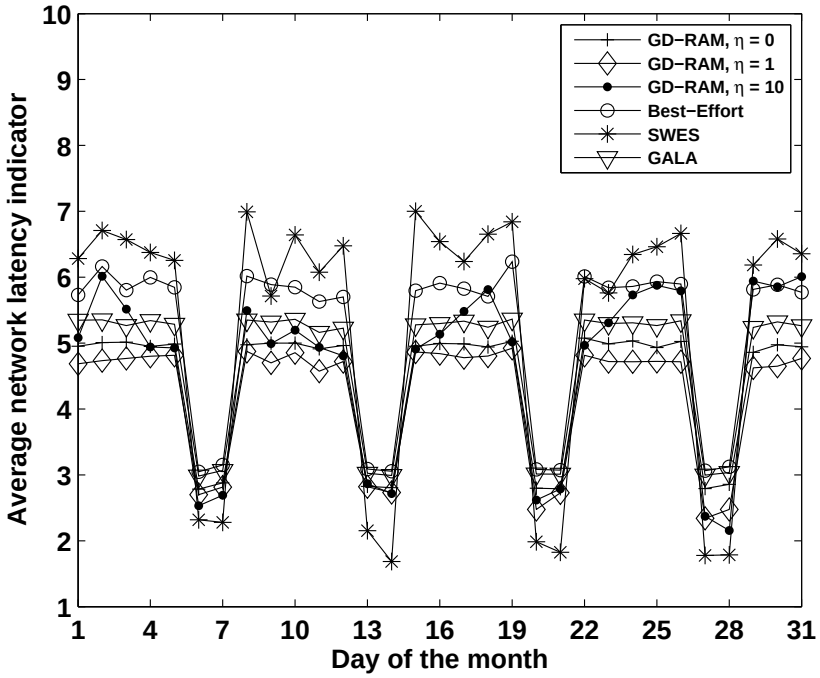

Figure 5.4: Average latency performance for the different schemes.

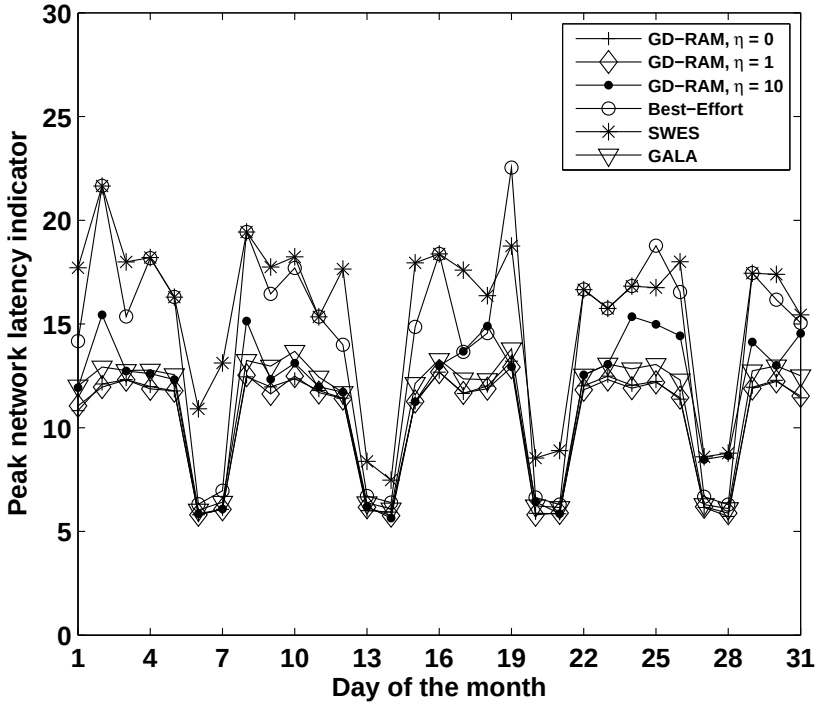

Figure 5.5: Peak network latency performance for the different schemes.

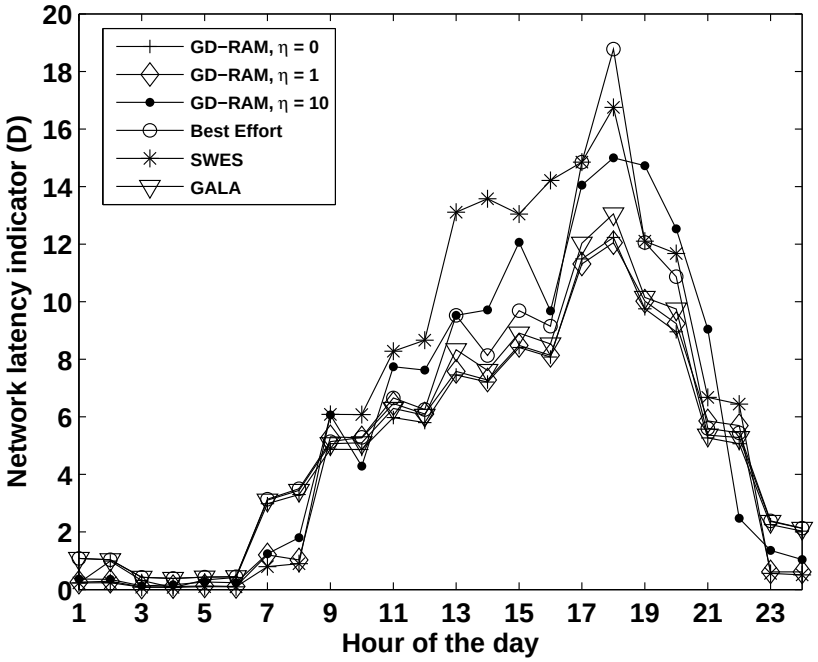

Figure 5.6: Hourly network latency for the different schemes (25^{th} January).

5.6.2 Delay performance

Figures 5.4 and 5.5 show the average network latency and the peak network latency for the benchmark schemes and for the proposed scheme for three different values of the trade-off factor η for the days under consideration. Note that the proposed algorithm shows delay performance better than the Best-Effort and the SWES scheme for all three η values. The network latency performance of the GALA scheme is better than the Best-Effort and the SWES scheme. Note that for most of the days, the average latency for $\eta = 1$ is smaller than that for $\eta = 0$. This is because of the non-convexity of the objective function with respect to power control operations. Note that for $\eta = 1$, the BS power levels reduce to lower values as compared to the case for $\eta = 0$, so as to bring grid energy savings. Our experiments show that at lower BS power levels, there is better interference management through the power control operations, thus also bringing down the network latency. However, for $\eta = 10$, on certain days which have very bad weather,

the proposed scheme trades the network latency performance for bringing about grid energy savings. For example, the values of the average delay and peak delay on 25^{th} January (which is a bad weather day) for $\eta = 10$ are significantly higher than that for $\eta = 0$ and $\eta = 1$. However on good weather days, like 12^{th} January, the delay performance for $\eta = 10$ is comparable to that for $\eta = 0$ and $\eta = 1$. Additionally, the results show that the network latency is lower on weekends as compared to the weekdays. This is because the traffic to be served on these days is lower than that on weekdays. Note that the SWES scheme leads to a lower average delay on weekends as compared to all other schemes. This is because the traffic to be served during weekends is smaller and therefore most of the BSs turn off, thus reducing the interference to the BSs that are turned on. This contributes to reducing the system delay for the SWES scheme on these days. However on weekdays, as the traffic to be served is higher, turning off BSs has the effect of increasing the network latency as can be seen from the results.

Figure 5.6 shows the hourly delay for 25^{th} January. The network latency is low for all the schemes during the early morning hours due to the low traffic during those hours. However, during the daytime, the SWES scheme and the proposed scheme for $\eta = 10$ lead to a higher delay than the Best-Effort scheme. The GALA scheme and our proposed scheme (for $\eta = 0$ and $\eta = 1$) have better delay performance than the other benchmarks. Figure 5.7 shows the transmit power levels of the BSs on 25^{th} January for the GDRAM scheme for three different η values. Note that the power levels for $\eta = 0$ are relatively higher than for the cases when $\eta = 1, 10$. This is because for $\eta = 0$ the power control operations are aimed solely on delay reduction. As $\eta = 1$ also accounts even for the grid energy consumption,

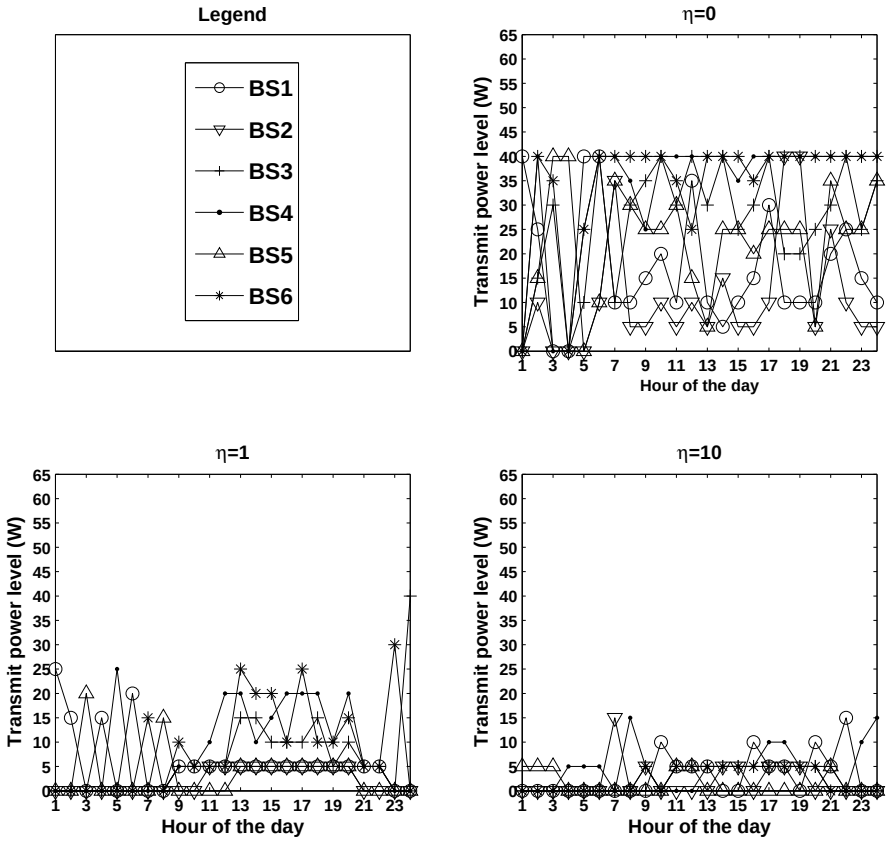

Figure 5.7: Transmit power levels for the GDRAM scheme for different η values (25^{th} January).

the power levels for this case are lower as compared to those with $\eta = 0$. For the case of $\eta = 10$, the power levels are still lower as compared to the case of $\eta = 1$.

5.6.3 Grid energy consumption and delay trade-off

Figures 5.8 and 5.9 show the grid energy consumption and delay trade-off for the proposed GD-RAM scheme for different trade-off parameter values and for the benchmark schemes (averaged for the month of January). Figure 5.8 considers the trade-off between the grid energy consumption and the average (over 31 days) of the hourly network latency whereas Figure

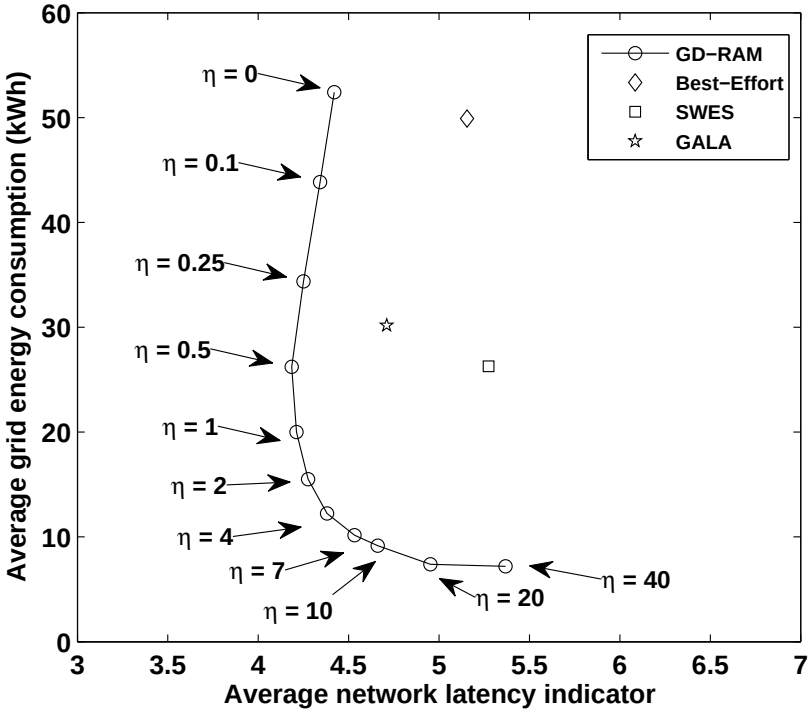

Figure 5.8: Tradeoff between grid energy savings and average network latency.

5.9 considers the trade-off between the grid energy consumption and the average (over 31 days) of the daily peak network latency. We can observe that for the proposed scheme, as we start increasing η from 0, the average grid energy consumption reduces sharply while there is no degradation in the latency. The reason for this phenomenon is the non-convexity of the objective function with respect to power control operations. Note that by increasing the η value from 0, the BS power levels reduce to much lower values so as to bring grid energy savings. However, the power level adjustments are made while accounting for the network latency in addition to accounting for the grid energy savings (as our objective function accounts for both the network latency and the grid energy). Figure 5.7 shows transmit power levels for three different η values ($\eta = 0, 1$ and 10). We can see that for $\eta = 1$, the transmit power levels for all the BSs is lower as compared to when $\eta = 0$. A reduction in the transmit power level of a BS implies that

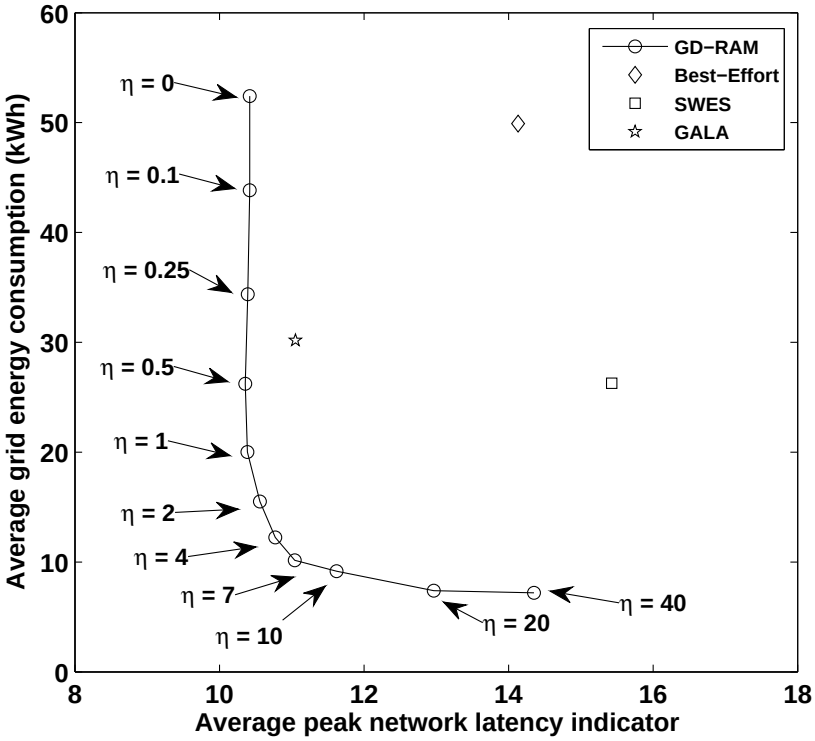

Figure 5.9: Tradeoff between grid energy savings and peak network latency.

the numerator in the SINR expression of the MTs served by it also reduces (Equation (5.2)). However, because the transmit power levels of the other BSs also reduce, the interference factor in the denominator of the SINR expression also reduces. Therefore, with the power levels decreasing with increasing η (and correspondingly the grid energy consumption decreasing) the SINR (and thus the rate offered by the BSs and in turn the network latency) does not necessarily degrade. Rather, slightly better latency performance is realized due to better interference management when BSs are operating at lower transmit power levels. However, for large values of η (say $\eta = 10$), as we can see from Figure 5.7, to save grid energy, the transmit power levels of the BSs are very low and additionally some of the BSs are switched off even during the peak traffic hours of the day (e.g. hour 16 (4 p.m.) to hour 20 (8 p.m.)). This increases the traffic that is handled

by the BSs which are switched on and degrades the network latency performance. Additionally, with the active BSs operating at such low transmit power levels, the impact of the noise power in degrading the SINR (and hence the rate and delay) is more prominent. These two factors contribute the degradation of network latency at higher η values. Therefore, for higher values of η (e.g. $\eta = 10$), when η is increased, the energy savings are less significant whereas the increase in the delay for the marginal savings in the grid energy is very high. For a η value of 1 we observe that there is around 60% grid energy savings as compared to the traditional Best-Effort scheme while ensuring a better network latency performance. For real life implementation of the proposed GD-RAM algorithm by telecom operators, the operator can estimate the grid energy consumed versus the average/peak network latency for certain values of η (like those considered in Figure 5.8) at the beginning of the day. Further, the operator can choose the η value based on the maximum tolerable average/peak network latency, which in turn decides how much grid energy would be consumed. For example, if the operator desires to avoid the average network latency indicator exceeding 4.5 (please see Figure 5.8), he/she can choose η to be 7, which in turn gives the grid energy consumption as 10 kWh.

5.7 Conclusion

In this chapter we considered a network of grid connected solar powered BSs. We proposed a methodology for reducing the grid energy consumption while ensuring a low traffic latency. The methodology also gives the operator the freedom to mange the trade-off between the grid energy savings and the traffic latency. The objective of reducing the grid energy con-

sumption while maintaining the traffic latency was achieved by intelligent temporal energy allocation, BS downlink transmit power control and user association. A real BS deployment scenario and real solar energy traces were used to test the performance of the proposed methodology and to show its superiority over existing benchmark schemes. We considered 3 benchmark schemes: Best-Effort, GALA and SWES. From the numerical results we observed that while the Best-Effort scheme leads to a higher grid energy consumption, SWES achieves significant grid energy savings, but at the expense of an increase in the network latency. The GALA scheme does better in terms of saving grid energy and the delay performance, however the proposed GD-RAM scheme has been shown to have superior performance than GALA. Compared to existing schemes, the proposed GD-RAM scheme provides control over trading energy for delay, and for a good choice of the trade-off factor (η), it can outperform all other benchmark schemes in terms of minimizing the grid energy required while maintaining lower traffic latency.

Chapter 6

Conclusion and future work

6.1 Conclusion

Cellular base stations powered by renewable energy like solar power have emerged as a promising solution to address the issues of reducing the carbon footprint of the telecom industry as well as that of the high operational cost associated with powering such BSs. This thesis has studied and proposed solutions for resource provisioning and dimensioning for such solar powered BSs and operational strategies for managing the various resources available to the BSs. We summarize the main contributions of the thesis as follows.

- In Chapter 2, we proposed a framework for optimally dimensioning resources (PV panels and batteries) for solar powered BSs. For such dimensioning in cellular networks, accurate characterization of solar energy is crucial to ensure the service requirements. Thus we proposed a multi-state Markov model to characterize the hourly harvested solar energy and the model was based on an approach that

combined daily correlations in weather conditions affecting the solar energy with fine-grained, hourly transitions in the solar energy levels. The proposed model was then used for dimensioning resources for solar powered BS. In the chapter, we also also presented insights on factors that affect the resource dimensioning.

- In Chapter 3, we addressed one of the key issues in dimensioning resources for solar powered BS. A fundamental step in dimensioning of resources for a BS is to evaluate the outage probability and battery lifetime associated with any given PV panel and battery size configuration. Thus in this chapter, we presented an analytic model to evaluate the outage probability and battery lifetime of a solar powered BS. The proposed model factored in the daily and hourly variations in the harvested solar energy and the traffic dependent BS load, and developed a discrete-time Markov process to model the battery level. We presented the methodology of evaluating the steady state probability for the different states in the model which were further used to evaluate the outage probability and battery lifetime associated with a given configuration of PV panel and battery size. Next, we used the proposed model to dimension resources for a solar powered BS. To show the accuracy of the proposed model, we compare the results obtained using the proposed model against that using real traces of solar energy and BS power consumption data.

- In Chapter 4, we targeted a network of stand-alone solar powered BSs. A major concern while operating such BSs is to avoid power outages in the BSs and to strategize cooperation among BSs to improve the network latency performance. Additionally, the solar energy harvested needs to be intelligently allocated over time to address the

aforementioned requirements. With these issues in mind, we proposed a strategy to intelligently allocate the harvested solar energy over time. We also proposed green energy and delay aware downlink power control and user association. Also, we showed the performance gains of the proposed strategy over the state-of-the-art existing strategies that are solely based on user association reconfiguration and BS on/off strategies.

- In Chapter 5, we investigated operational strategies for grid connected solar powered BSs. Solely powering BSs by solar energy may not be viable for certain locations due to several economical and geographical reasons. In such a scenario, BSs can be provisioned with certain PV panel and battery resources which can reduce the grid energy consumption thus bringing cost savings in terms of the operational expenditure. Such grid energy savings can be increased by intelligently allocating the solar energy harvested over time. However, while doing so care has to be taken in managing the network latency performance which is imperative for customer satisfaction. There is a trade-off between the network latency and the grid energy savings. Thus, in this chapter, we presented a framework which jointly manages the network and the grid energy savings. We used downlink power control and optimal user association strategy to solve the problem and showed the trade-off between the QoS and the grid energy savings for the proposed framework.

6.2 Future work

In this section, we discuss possible extensions and directions for future work which we consider worthy of further investigation by extending the results presented in this thesis.

- For the problem of resource provisioning and dimensioning in Chapter 2, we focussed on the case of an off-grid solar powered BS. It would be interesting and important to investigate the problem of resource provisioning and dimensioning for BSs those have grid connectivity. Another direction of investigation could also be to consider resource provisioning and dimensioning for BSs which might be using other renewable resources like wind energy in addition to solar energy.

- In Chapter 3, we proposed a model for estimating the energy outage probability and the battery lifetime associated with a particular PV-battery size configuration. However, the study was done for stand-alone solar powered BSs. An interesting direction of further investigation would be to address these problems for BSs powered by hybrid supplies (i.e. with other renewable resources like wind energy or unreliable grid supplies in addition to solar energy).

- In Chapter 4, we proposed a methodology for intelligent energy allocation, and green energy and delay aware power control and user association. The proposed methodology requires the centralized server to carry out the energy allocation and power control decisions. It would be an interesting direction of further investigation to develop a distributed approach where the BSs could cooperate with each other and perform the power control operations. A similar extension could

be done for such operations for the set-up considered in Chapter 5.

- In Chapter 4 and Chapter 5, we considered a network of macro BSs. The extension of the proposed methodologies to heterogeneous networks (i.e network having micro, femto and pico BSs in addition to macro BSs) could be investigated.
- In Chapter 4 and Chapter 5, we focussed only on downlink communication. Nevertheless, it would be interesting to develop operational strategies which consider not only the downlink traffic, but the uplink traffic as well.
- The proposed downlink power control is a non-convex optimization problem and we proposed a greedy heuristic to arrive to a local optimal solution. Although our proposed methodology has been shown to perform better than existing methodologies in terms of managing the green energy and network delay, methodologies using power control which perform better than the one proposed in this thesis and achieve results closer to the globally optimal solution could be explored.

Appendix A

Proof of proposition 3.4.1

We prove this proposition by using proof through contradiction. The intuition behind the proof is to show that no two different set of values of $\{\alpha, \beta, b\}$ can lead to the same value of U. Let U_1 be the state corresponding to $\{\alpha_1, \beta_1, b_1\}$. Thus,

$$U_1 = 2N(\alpha_1 - 1) + \beta_1 + 2(b_1 - 1). \tag{A.1}$$

Now, let us assume that there exists an another set $\{\alpha_2, \beta_2, b_2\}$ which also leads to the same state number U_1 where $\{\alpha_1, \beta_1, b_1\}$ and $\{\alpha_2, \beta_2, b_2\}$ satisfy one or more of the following constraints: $\alpha_1 \neq \alpha_2, \beta_1 \neq \beta_2, b_1 \neq b_2$ (i.e. the sets $\{\alpha_1, \beta_1, b_1\}$ and $\{\alpha_2, \beta_2, b_2\}$ are not identical). Next, we prove that it is not possible for two such set of values to exist (proof by contradiction). Based on the above assumption that the set $\{\alpha_2, \beta_2, b_2\}$ leads to state number U_1, we have

$$U_1 = 2N(\alpha_2 - 1) + \beta_2 + 2(b_2 - 1). \tag{A.2}$$

From, Equation (A.1) and Equation (A.2) we can conclude that

$$\begin{aligned} 2N(\alpha_1 - 1) + \beta_1 + 2(b_1 - 1) &= 2N(\alpha_2 - 1) + \beta_2 + 2(b_2 - 1) \\ \Rightarrow N(\alpha_1 - \alpha_2) + (b_1 - b_2) &= \frac{(\beta_2 - \beta_1)}{2} \end{aligned} \tag{A.3}$$

As the feasible set for β is $\beta \in \{1, 2\}$, the possible values which $\beta_2 - \beta_1$ can take are $\beta_2 - \beta_1 \in \{1, -1, 0\}$. Now let us consider the following two cases (which are denoted as C1 and C2 respectively):

C1: $\beta_2 - \beta_1$ is either 1 or -1

For this case, $\frac{\beta_2 - \beta_1}{2}$ in Equation (A.3) comes out to be a fractional value (i.e. 0.5 or - 0.5). Note that this is a contradiction as the LHS (left hand side) in Equation (A.3) cannot be a fractional value. This is because based on their feasible sets, α and b are discrete values where $\alpha \in \{1, 2, 3\}$ and $b \in \{1, 2, \cdots, N\}$. Additionally N is also a discrete value.

C2: $\beta_2 - \beta_1$ is 0.

For this case, the load type for both the sets is the same (as $\beta_2 = \beta_1$). Next, we prove that even the solar day type and battery level for this case need to be the same to ensure the state for the two sets to be identical. With $\beta_2 = \beta_1$, Equation (A.3) can be written as

$$\begin{aligned} N(\alpha_1 - \alpha_2) + (b_1 - b_2) &= 0 \\ \Rightarrow (\alpha_1 - \alpha_2) &= \frac{(b_2 - b_1)}{N} \end{aligned} \tag{A.4}$$

As the feasible set for b is $b \in \{1, 2, ...N\}$, the possible values which $b_2 - b_1$ can take is $b_2 - b_1 \in \{-(N-1), -(N-2), \cdots, -2, -1, 0, 1, 2 \cdots, N-2, N-1\}$. Now let us consider the following two cases (which are denoted as C2.1 and C2.2 respectively)

C2.1: $b_2 - b_1$ is non-zero (i.e. $b_2 - b_1 \in \{-(N-1), -(N-2), \cdots, -2, -1, 1, 2, \cdots, N-2, N-1\}$)

For this case, $\frac{b_2 - b_1}{N}$ is a fractional value. Note that this is a contradiction as the LHS in Equation (A.4) cannot be a fractional value because based on the feasible set of α, $\alpha_1 - \alpha_2$ must be a discrete value.

C2.2: $b_2 - b_1$ is zero.

For this case, we have $b_2 = b_1$ and thus the battery level for both the states is the same. Substituting this in Equation (A.4) we get $\alpha_1 = \alpha_2$. Thus we have $\beta_1 = \beta_2, b_1 = b_2$ and $\alpha_1 = \alpha_2$, thus contradicting our initial assumption that the sets $\{\alpha_1, \beta_1, b_1\}$ and $\{\alpha_2, \beta_2, b_2\}$ are not identical. This completes the proof of the proposition.

Appendix B

Steady state probability analysis of critical states: Case 4-8

Following is the steady state probability analysis for the critical states for cases 4-8 mentioned in the Section 3.5.1.

- **Case 4:** k_2 **+ve,** $k_2' <$ **-1**

  To find the steady state probability of the critical states for this case we consider boundaries A-L in Figure B.1.

  First, we consider balance equations for boundaries B and E around states $2N + 2N_{sh} - 1$ and $2N + 2N_{sh}$ which can be written as

$$\pi_{2N_{sh}+2N-1} = p_{32}q_{21}P_3Q_2 \quad \text{(B.1)}$$

$$\pi_{2N_{sh}+2N} = p_{32}q_{22}P_3Q_2. \quad \text{(B.2)}$$

  Next we consider balance equations for boundaries H and K around

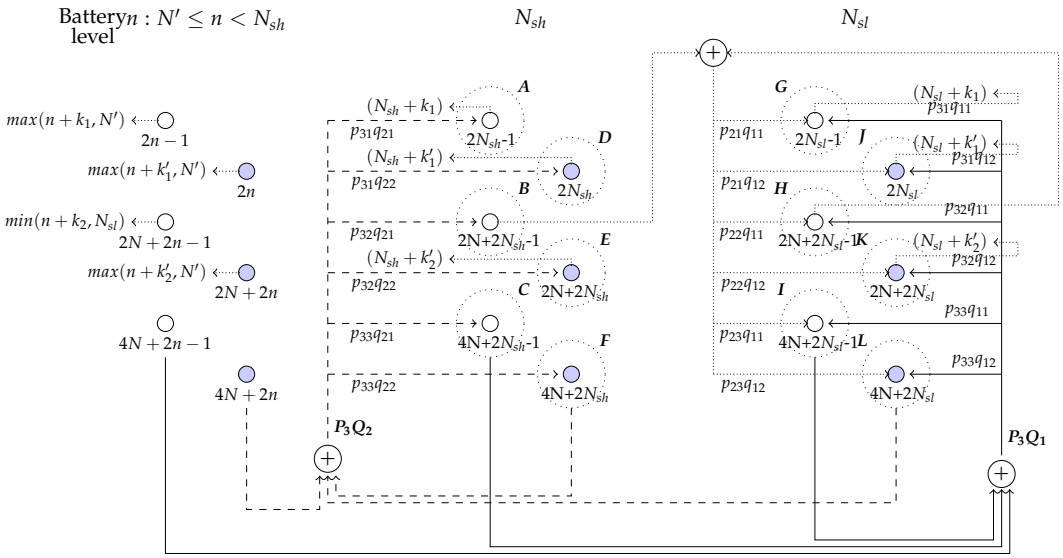

Figure B.1: State diagram for case 4.

states $2N + 2N_{sl} - 1$ and $2N + 2N_{sl}$ which can be written as

$$\pi_{2N_{sl}+2N-1} = p_{32}q_{11}P_3Q_1 + p_{22}q_{11}(\pi_{2N_{sh}+2N-1} + \pi_{2N_{sl}+2N-1})$$

$$\Rightarrow \pi_{2N_{sl}+2N-1} = \frac{p_{32}q_{11}P_3Q_1 + p_{22}q_{11}\pi_{2N_{sh}+2N-1}}{1 - p_{22}q_{11}} \tag{B.3}$$

$$\pi_{2N_{sl}+2N} = p_{32}q_{12}P_3Q_1 + (\pi_{2N_{sl}+2N-1} + \pi_{2N_{sh}+2N-1})p_{22}q_{12}. \tag{B.4}$$

Using the steady state probabilities above, the steady state probability of the other critical states can be obtained as

$$\begin{aligned}
\pi_{2N_{sh}-1} &= p_{31}q_{21}P_3Q_2 \\
\pi_{2N_{sh}} &= p_{31}q_{22}P_3Q_2 \\
\pi_{2N_{sl}-1} &= p_{31}q_{11}P_3Q_1 + (\pi_{2N_{sh}+2N-1} + \pi_{2N_{sl}+2N-1})p_{21}q_{11} \\
\pi_{2N_{sl}} &= p_{31}q_{12}P_3Q_1 + (\pi_{2N_{sh}+2N-1} + \pi_{2N_{sl}+2N-1})p_{21}q_{12}
\end{aligned} \tag{B.5}$$

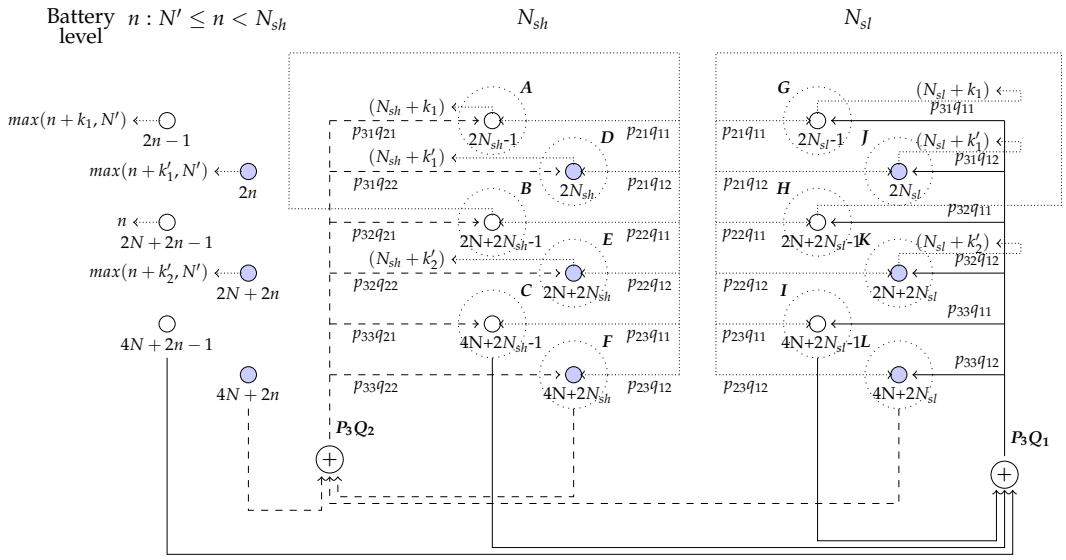

Figure B.2: State diagram for case 5.

$$\pi_{2N_{sh}+4N-1} = p_{33}q_{21}P_3Q_2$$

$$\pi_{2N_{sh}+4N} = p_{33}q_{22}P_3Q_2$$

$$\pi_{2N_{sl}+4N-1} = p_{33}q_{11}P_3Q_1 + (\pi_{2N_{sh}+2N-1} + \pi_{2N_{sl}+2N-1})p_{23}q_{11}$$

$$\pi_{2N_{sl}+4N} = p_{33}q_{12}P_3Q_1 + (\pi_{2N_{sh}+2N-1} + \pi_{2N_{sl}+2N-1})p_{23}q_{12}.$$

- **Case 5:** $k_2 = \mathbf{0}$ **,** $k_2' <$ **-1**

  To find the steady state probability of the critical states for this case we consider the boundaries shown by dotted circles in Figure B.2.

  The balance equations for boundaries B abnd H around states $2N_{sh} + 2N - 1$ and $2N_{sl} + 2N - 1$ can be written as

$$\pi_{2N_{sh}+2N-1} = p_{32}q_{21}P_3Q_2/(1 - q_{11}p_{22}) \tag{B.6}$$

$$\pi_{2N_{sl}+2N-1} = (p_{32}q_{11}P_3Q_1)/(1 - p_{22}q_{11}) \tag{B.7}$$

  Using steady state probabilities above, we can find the steady state

probability of the other critical states as

$$\pi_{2N_{sh}+2N} = p_{32}q_{22}P_3Q_2 + p_{22}q_{12}\pi_{2N_{sh}+2N-1}$$

$$\pi_{2N_{sl}+2N} = p_{32}q_{12}P_3Q_1 + p_{22}q_{12}\pi_{2N_{sl}+2N-1}$$

$$\pi_{2N_{sh}-1} = p_{31}P_3Q_2q_{21} + p_{21}q_{11}\pi_{2N_{sh}+2N-1}$$

$$\pi_{2N_{sh}} = p_{31}q_{22}P_3Q_2 + p_{21}q_{12}\pi_{2N_{sh}+2N-1}$$

$$\pi_{2N_{sl}-1} = p_{31}q_{11}P_3Q_1 + p_{21}q_{11}\pi_{2N_{sl}+2N-1}$$

$$\pi_{2N_{sl}} = p_{31}q_{12}P_3Q_1 + p_{21}q_{12}\pi_{2N_{sl}+2N-1}$$

$$\pi_{2N_{sh}+4N-1} = p_{33}q_{21}P_3Q_2 + p_{23}q_{11}\pi_{2N_{sh}+2N-1}$$

$$\pi_{2N_{sh}+4N} = p_{33}q_{22}P_3Q_2 + p_{23}q_{12}\pi_{2N_{sh}+2N-1}$$

$$\pi_{2N_{sl}+4N-1} = p_{33}q_{11}P_3Q_1 + p_{23}q_{11}\pi_{2N_{sl}+2N-1}$$

$$\pi_{2N_{sl}+4N} = p_{33}q_{12}P_3Q_1 + p_{23}q_{12}\pi_{2N_{sl}+2N-1}$$

- **Case 6:** $k_2 = \mathbf{0}$ **,** $k_2' = \mathbf{-1}$

  To find the steady state probability of the critical states for this case we consider the boundaries shown by dotted circles in Figure B.3.

  The balance equations for boundaries K and H around states $2N + 2N_{sl}$ and $2N + 2N_{sl} - 1$ can be written as

$$\pi_{2N_{sl}+2N} = p_{32}q_{12}P_3Q_1 + p_{22}q_{12}\pi_{2N_{sl}+2N-1} \tag{B.8}$$

$$\pi_{2N_{sl}+2N-1} = p_{32}q_{11}P_3Q_1 + p_{22}q_{11}\pi_{2N_{sl}+2N-1}$$

$$\Rightarrow \pi_{2N_{sl}+2N-1} = (p_{32}q_{11}P_3Q_1)/(1 - p_{22}q_{11}). \tag{B.9}$$

  From the previous two equations we can conclude that

$$\frac{\pi_{2N_{sl}+2N}}{\pi_{2N_{sl}+2N-1}} = \frac{q_{12}}{q_{11}}. \tag{B.10}$$

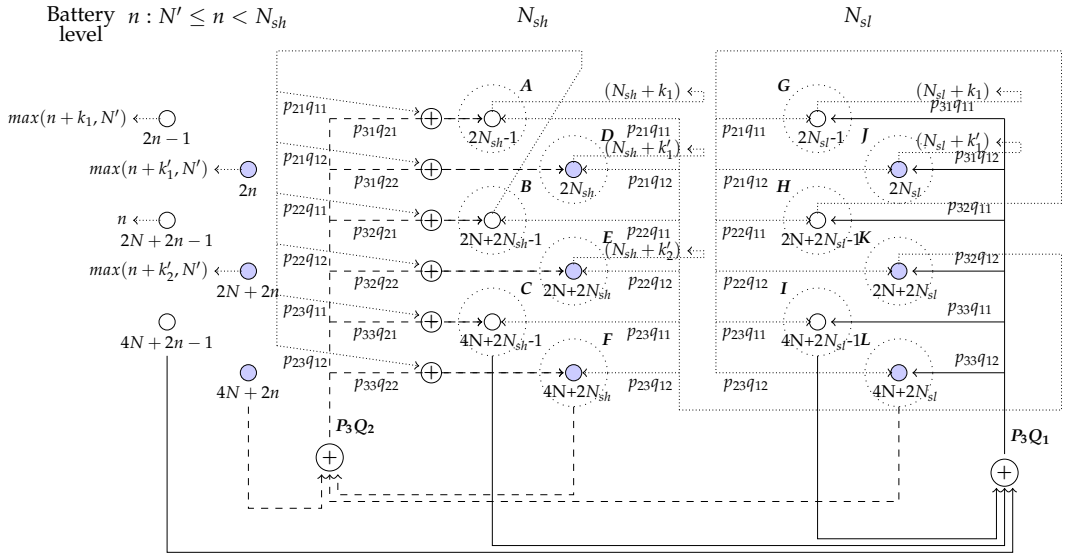

Figure B.3: State diagram for case 6.

Using the above relation and steady state probability of state $\pi_{2N_{sl}+2N-1}$, the steady state probability of state $\pi_{2N_{sl}+2N}$ can be given as

$$\pi_{2N_{sl}+2N} = \frac{p_{32}q_{12}P_3Q_1}{1 - p_{22}q_{11}} \tag{B.11}$$

Next we consider balance equations around boundaries B and E around the states $2N_{sh} + 2N - 1$ and $2N_{sh} + 2N$ which can be written as

$$\pi_{2N_{sh}+2N-1} = p_{32}q_{21}P_3Q_2 + p_{22}q_{21}\pi_{2N_{sl}+2N} + p_{22}q_{11}\pi_{2N_{sh}+2N-1}$$

$$\Rightarrow \pi_{2N_{sh}+2N-1} = \frac{p_{32}q_{21}P_3Q_2 + p_{22}q_{21}\pi_{2N_{sl}+2N}}{1 - p_{22}q_{11}} \tag{B.12}$$

$$\pi_{2N_{sh}+2N} = p_{32}q_{22}P_3Q_2 + p_{22}q_{22}\pi_{2N_{sl}+2N} + p_{22}q_{12}\pi_{2N_{sh}+2N-1}. \tag{B.13}$$

Using the steady state probabilities above, the steady state probability

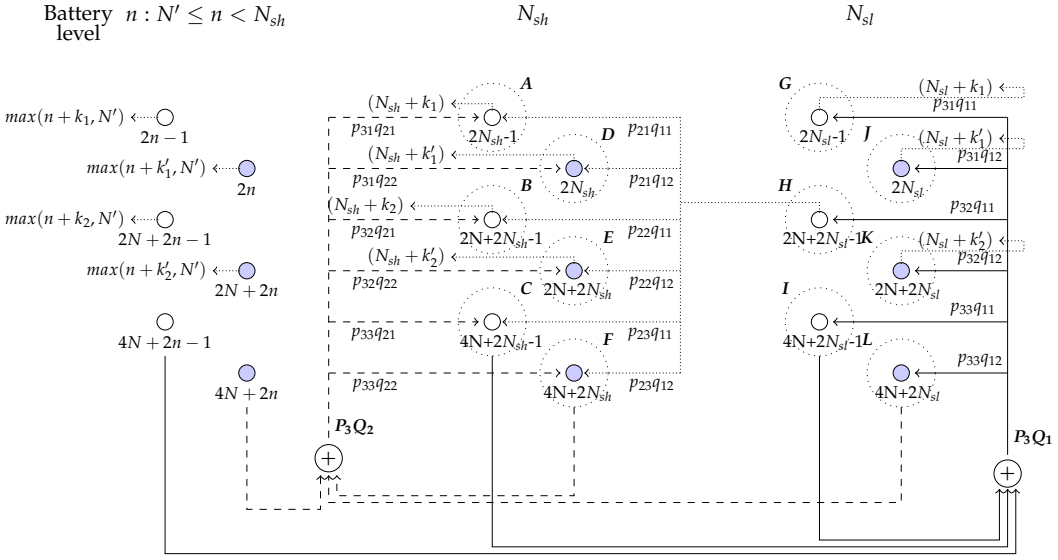

Figure B.4: State diagram for case 7.

of the other critical states can be obtained as

$$\pi_{2N_{sh}-1} = p_{31}P_3Q_2q_{21} + p_{21}q_{11}\pi_{2N_{sh}+2N-1} + p_{21}q_{21}\pi_{2N_{sl}+2N}$$

$$\pi_{2N_{sh}} = p_{31}q_{22}P_3Q_2 + p_{21}q_{11}\pi_{2N_{sh}+2N-1} + p_{21}q_{22}\pi_{2N_{sl}+2N}$$

$$\pi_{2N_{sl}-1} = p_{31}q_{11}P_3Q_1 + p_{21}q_{11}\pi_{2N_{sl}+2N-1}$$

$$\pi_{2N_{sl}} = p_{31}q_{12}P_3Q_1 + p_{21}q_{12}\pi_{2N_{sl}+2N-1}$$

$$\pi_{2N_{sh}+4N-1} = p_{33}q_{21}P_3Q_2 + p_{23}q_{11}\pi_{2N_{sh}+2N-1} + p_{23}q_{21}\pi_{2N_{sl}+2N}$$

$$\pi_{2N_{sh}+4N} = p_{33}q_{22}P_3Q_2 + p_{23}q_{11}\pi_{2N_{sh}+2N-1} + p_{23}q_{22}\pi_{2N_{sl}+2N}$$

$$\pi_{2N_{sl}+4N-1} = p_{33}q_{11}P_3Q_1 + p_{23}q_{11}\pi_{2N_{sl}+2N-1}$$

$$\pi_{2N_{sl}+4N} = p_{33}q_{12}P_3Q_1 + p_{23}q_{12}\pi_{2N_{sl}+2N-1}.$$

- **Case 7:** $k_2 =$ **-1,** $k_2' <$ **-1**

  To find the steady state probability of the critical states for this case we consider the boundaries shown by dotted circles in Figure B.4.

  The balance equations around boundaries K and H around states

$2N + 2N_{sl}$ and $2N + 2N_{sl} - 1$ can be written as

$$\pi_{2N_{sl}+2N} = p_{32}q_{12}P_3Q_1 \tag{B.14}$$

$$\pi_{2N_{sl}+2N-1} = p_{32}q_{11}P_3Q_1 \tag{B.15}$$

Using the steady state probabilities above, the steady state probability of the other critical states can be obtained as

$$\pi_{2N_{sh}+2N-1} = p_{32}q_{21}P_3Q_2 + p_{22}q_{11}\pi_{2N_{sl}+2N-1}$$

$$\pi_{2N_{sh}+2N} = p_{32}q_{22}P_3Q_2 + p_{22}q_{12}\pi_{2N_{sl}+2N-1}$$

$$\pi_{2N_{sh}-1} = p_{31}P_3Q_2q_{21} + p_{21}q_{11}\pi_{2N_{sh}+2N-1}$$

$$\pi_{2N_{sh}} = p_{31}q_{22}P_3Q_2 + p_{21}q_{12}\pi_{2N_{sh}+2N-1}$$

$$\pi_{2N_{sl}-1} = p_{31}q_{11}P_3Q_1$$

$$\pi_{2N_{sl}} = p_{31}q_{12}P_3Q_1$$

$$\pi_{2N_{sh}+4N-1} = p_{33}q_{21}P_3Q_2 + p_{23}q_{11}\pi_{2N_{sh}+2N-1}$$

$$\pi_{2N_{sh}+4N} = p_{33}q_{22}P_3Q_2 + p_{23}q_{12}\pi_{2N_{sh}+2N-1}$$

$$\pi_{2N_{sl}+4N-1} = p_{33}q_{11}P_3Q_1$$

$$\pi_{2N_{sl}+4N} = p_{33}q_{12}P_3Q_1.$$

- **Case 8 :** k_2 **+ve,** k_2' **= -1**

  To find the steady state probability of the critical states for this case we consider the boundaries shown by dotted circles in Figure B.5.

  The balance equations for boundaries K and H around states $2N +$

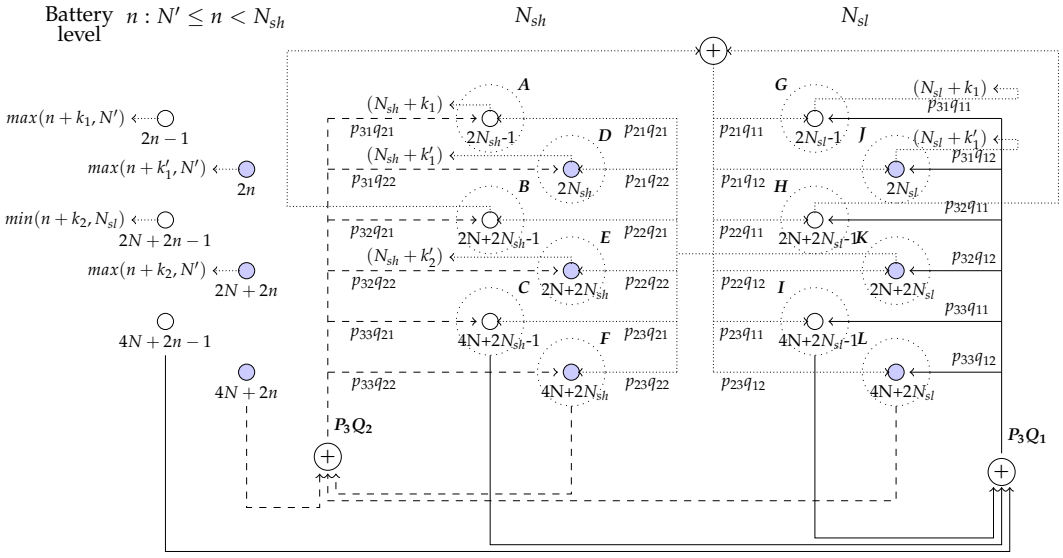

Figure B.5: State diagram for case 8.

$2N_{sl}$ and $2N + 2N_{sl} - 1$ can be written as

$$\pi_{2N_{sl}+2N} = p_{32}q_{12}P_3Q_1 + (\pi_{2N_{sh}+2N-1} + \pi_{2N_{sl}+2N-1})p_{22}q_{12} \quad \text{(B.16)}$$

$$\pi_{2N_{sl}+2N-1} = p_{32}q_{11}P_3Q_1 + (\pi_{2N_{sh}+2N-1} + \pi_{2N_{sl}+2N-1})p_{22}q_{11}. \quad \text{(B.17)}$$

From the previous two equations we can conclude that

$$\frac{\pi_{2N_{sl}+2N}}{\pi_{2N_{sl}+2N-1}} = \frac{q_{12}}{q_{11}} \quad \text{(B.18)}$$

Next we consider balance equations for boundaries E and B around states $2N + 2N_{sh}$ and $2N + 2N_{sh} - 1$ which can be written as

$$\pi_{2N_{sh}+2N-1} = p_{32}q_{21}P_3Q_2 + p_{22}q_{21}\pi_{2N_{sl}+2N} \quad \text{(B.19)}$$

$$\pi_{2N_{sh}+2N} = p_{32}q_{22}P_3Q_2 + p_{22}q_{22}\pi_{2N_{sl}+2N}. \quad \text{(B.20)}$$

From the previous two equations we can conclude that

$$\frac{\pi_{2N_{sh}+2N}}{\pi_{2N_{sh}+2N-1}} = \frac{q_{22}}{q_{21}}. \quad \text{(B.21)}$$

Using Equations (B.16)-(B.21), we can solve for the steady state value of $\pi_{2N_{sh}+2N-1}$ which can be written as

$$\pi_{2N_{sh}+2N-1} = \frac{-(p_{32}q_{12}P_3Q_1p_{22}q_{21} + p_{32}q_{21}P_3Q_2 - p_{32}P_3Q_2q_{21}p_{22}q_{11}}{(p_{22}^2q_{12}q_{21}p_{22}q_{11} - 1 + p_{22}q_{11} + p_{22}^2q_{12}q_{21} - p_{22}^3q_{12}q_{21}q_{11})}. \tag{B.22}$$

Note that the steady state probability of $\pi_{2N_{sh}+2N-1}$ (evaluated in Equation B.22) can be used to obtain the steady state probability of states $\pi_{2N_{sh}+2N}$, $\pi_{2N_{sl}+2N-1}$ and $\pi_{2N_{sl}+2N}$ using the equations and relationship in Equation (B.16)-(B.21). The steady state probability of the remaining critical states can be obtained as

$$\pi_{2N_{sh}-1} = p_{31}q_{21}P_3Q_2 + p_{21}q_{21}\pi_{2N_{sl}+2N}$$

$$\pi_{2N_{sh}} = p_{31}q_{22}P_3Q_2 + p_{21}q_{22}\pi_{2N_{sl}+2N}$$

$$\pi_{2N_{sl}-1} = p_{31}q_{11}P_3Q_1 + (\pi_{2N_{sh}+2N-1} + \pi_{2N_{sl}+2N-1})p_{21}q_{11}$$

$$\pi_{2N_{sl}} = p_{31}q_{12}P_3Q_1 + (\pi_{2N_{sh}+2N-1} + \pi_{2N_{sl}+2N-1})p_{21}q_{12}$$

$$\pi_{2N_{sh}+4N-1} = p_{33}q_{21}P_3Q_2 + p_{23}q_{21}\pi_{2N_{sl}+2N}$$

$$\pi_{2N_{sh}+4N} = p_{33}q_{22}P_3Q_2 + p_{23}q_{22}\pi_{2N_{sl}+2N}$$

$$\pi_{2N_{sl}+4N-1} = p_{33}q_{11}P_3Q_1 + (\pi_{2N_{sh}+2N-1} + \pi_{2N_{sl}+2N-1})p_{23}q_{11}$$

$$\pi_{2N_{sl}+4N} = p_{33}q_{12}P_3Q_1 + (\pi_{2N_{sh}+2N-1} + \pi_{2N_{sl}+2N-1})p_{23}q_{12}.$$

Appendix C

Proof of Lemma 4.5.1

To prove this we show that $\nabla^2 X(\rho) > 0$. This can be shown as follows. We consider the value of our objective function as

$$\begin{aligned} X(\rho) &= \sum_{j \in \mathcal{B}} \left(D(\rho_j) + e^{\Theta(\rho_j)} \right) \\ &= \sum_{j \in \mathcal{B}} \left(\frac{\rho_j}{1-\rho_j} + e^{\frac{L(j)}{E(j)}} \right) \\ &= \sum_{j \in \mathcal{B}} \left(\frac{\rho_j}{1-\rho_j} + e^{\frac{P_0 + \Delta P(j)\rho_j}{E(j)}} \right). \end{aligned} \tag{C.1}$$

The first and second order derivatives of the objective function with respect to ρ are given by

$$\begin{aligned} \nabla X(\rho) &= \sum_{j \in \mathcal{B}} \left(\frac{1}{(1-\rho_j)^2} + \frac{\Delta P(j)}{E(j)} e^{\frac{P_0 + \Delta P(j)\rho_j}{E(j)}} \right) \\ &= \sum_{j \in \mathcal{B}} \left(\frac{1}{(1-\rho_j)^2} + \frac{\Delta P(j)}{E(j)} e^{\Theta(\rho_j)} \right) \end{aligned} \tag{C.2}$$

$$\tag{C.3}$$

$$\nabla^2 X(\rho) = \sum_{j \in \mathcal{B}} \left(\frac{2}{(1-\rho_j)^3} + \left(\frac{\Delta P(j)}{E(j)} \right)^2 e^{\frac{P_0 + \Delta P(j)\rho_j}{E(j)}} \right). \tag{C.4}$$

Note that the term $\nabla^2 X(\rho)$ above is always positive as it is sum of terms which are all non-negative and the term $\frac{2}{(1-\rho_j)^3}$ is positive for all the BSs. This proves that the objective function $X(\rho)$ is convex with respect to ρ.

Remark: The proof above is based on the fact that we are considering steady state analysis of the system and thus we can assume the following [91], [93], [95]:

$$\frac{\partial f(\rho_j)}{\partial \rho_g} = 0 \ , \ j \neq g \tag{C.5}$$

where $f(\rho_j)$ is purely a function of ρ_j and does not depend on ρ_g ($g \neq j$).

Appendix D

Proof of Lemma 4.5.3

As the function $X(\rho)$ is a convex function of ρ when ρ is defined on $\tilde{\mathcal{F}}_1$, this lemma can be easily proved by showing $< \triangledown X(\rho^{(k)}), T(\rho^{(k)})) - \rho^{(k)} > \leq 0$ (where $< a, b >$ denotes the inner product of vectors a and b) [113]. Let $u_j(x)$ and $u_j^T(x)$ be user association indicators which result in BS traffic $\rho_j^{(k)}$ and $T_j(\rho_j^{(k)})$, respectively. Then the inner product is given by

$$
\begin{aligned}
&< \triangledown X(\rho^{(k)}), T(\rho^{(k)}) - \rho^{(k)} > \\
&\quad = \sum_{j\in\mathcal{B}} \left(\frac{1}{(1-\rho_j^{(k)})^2} + \frac{\Delta P(j)}{E(j)} e^{\Theta^{(k)}(\rho_j)} \right) \left(T_j(\rho^{(k)}) - \rho_j^{(k)} \right) \\
&\quad = \sum_{j\in\mathcal{B}} \left(\frac{1}{(1-\rho_j^{(k)})^2} + \frac{\Delta P(j)}{E(j)} e^{\Theta^{(k)}(\rho_j)} \right) \left(\int_{\mathcal{R}} \frac{\gamma(x)(u_j^T(x) - u_j(x))}{c_j(x)} dx \right) \\
&\quad = \int_{\mathcal{R}} \gamma(x) \sum_{j\in\mathcal{B}} \frac{\left(\frac{1}{(1-\rho_j^{(k)})^2} + \frac{\Delta P(j)}{E(j)} e^{\Theta^{(k)}(\rho_j)} \right) (u_j^T(x) - u_j(x))}{c_j(x)} dx.
\end{aligned}
$$

Note that

$$\sum_{j\in\mathcal{B}} \frac{\left(\frac{1}{(1-\rho_j^{(k)})^2} + \frac{\Delta P(j)}{E(j)} e^{\Theta^{(k)}(\rho_j)}\right)(u_j^T(x) - u_j(x))}{c_j(x)} \leq 0$$

holds because $u_j^T(x)$ from (4.10) and (4.11) maximizes the value of $\frac{c_j(x)}{\left(\frac{1}{(1-\rho_j^{(k)})^2} + \frac{\Delta P(j)}{E(j)} e^{\Theta^{(k)}(\rho_j)}\right)}$. Thus as a result we can claim that $< \nabla X(\rho^{(k)}), T(\rho^{(k)}) - \rho^{(k)} > \leq 0$ which proves the lemma.

Appendix E

Proof of Lemma 5.5.1

This can be proven by showing that $\nabla^2 \mathcal{U}_i(\rho) > 0$. The objective function can written in terms of ρ as

$$\begin{aligned}\mathcal{U}(\rho) &= \mathcal{D}(\rho) + \eta \mathcal{E}(\rho) \\ &= \sum_{j \in \mathcal{B}} \left(\frac{\rho_j}{1-\rho_j} + \eta \zeta_j \left(L(j) - G(j) \right) \right) \\ &= \sum_{j \in \mathcal{B}} \left(\frac{\rho_j}{1-\rho_j} \right) + \sum_{j \in \mathcal{B}} \left(\eta \zeta_j \left(A(j)\rho_j + P_0 - \mathcal{M}(j) \frac{A(j)\rho_j + P_0}{A(j)\rho_j + C(j)} \right) \right).\end{aligned} \tag{E.1}$$

We evaluate the first and second order derivatives of the objective function with respect to ρ which are given as

$$\nabla \mathcal{U}(\rho) = \sum_{j \in \mathcal{B}} \left(\frac{1}{(1-\rho_j)^2} + \eta \zeta_j A(j) \left(1 - \mathcal{M}(j) \frac{C(j) - P_0}{(A(j)\rho_j + C(j))^2} \right) \right) \tag{E.2}$$

$$\nabla^2 \mathcal{U}(\rho) = \sum_{j \in \mathcal{B}} \left(\frac{2}{(1-\rho_j)^3} + 2\eta \zeta_j A(j)^2 \mathcal{M}(j) \frac{C(j) - P_0}{(A(j)\rho_j + C(j))^3} \right). \tag{E.3}$$

Note that all the addition terms in the function above are non-negative, and

$\frac{2}{(1-\rho_j)^3}$ is always positive for all the BSs. Thus, the above term is always positive which proves that the function is convex. Also for the case when grid energy is not drawn, the component in the objective function for a particular BS just consists of the first term which is always positive. Thus even for the case when energy is not drawn from the grid, the objective function is convex in ρ.

Appendix F

Proof of Lemma 5.5.3

$\mathcal{U}(\rho)$ is a convex function of $\rho \in \tilde{\mathcal{F}}_2$. Thus the fact that $T(\rho^{(k)})$ gives a descent direction to $\mathcal{U}(\rho^{(k)})$ at $\rho^{(k)}$ can be easily proved by showing $< \nabla\mathcal{U}(\rho^{(k)}, T(\rho^{(k)})) - \rho^{(k)} > \leq 0$ (where $< a, b >$ denotes the inner product of vectors a and b) [113]. Let $u_j(x)$ and $u_j^T(x)$ be user association indicators which result in BS traffic $\rho_j^{(k)}$ and $T_j(\rho_j^{(k)})$, respectively. Then the inner product can be written as

$$
\begin{aligned}
&< \nabla\mathcal{U}(\rho^{(k)}), T(\rho^{(k)}) - \rho^{(k)} > \\
&\quad = \sum_{j\in\mathcal{B}} \left(\frac{1}{(1-\rho_j^{(k)})^2} + \eta\zeta_j A(j) \left(1 - \mathcal{M}(j) \frac{C(j) - P_0}{(A(j)\rho_j^{(k)} + C(j))^2} \right) \right) \left(T_j(\rho_j^{(k)}) - \rho_j^{(k)} \right) \\
&\quad = \sum_{j\in\mathcal{B}} \left(\frac{1}{(1-\rho_j^{(k)})^2} + \eta\zeta_j A(j) \left(1 - \mathcal{M}(j) \frac{C(j) - P_0}{(A(j)\rho_j^{(k)} + C(j))^2} \right) \right) \\
&\qquad\qquad \times \left(\int_{\mathcal{R}} \frac{\gamma(x)(u_j^T(x) - u_j(x))}{c_j(x)} dx \right) \\
&\quad = \int_{\mathcal{R}} \gamma(x) \sum_{j\in\mathcal{B}} \left(\frac{\left(\frac{1}{(1-\rho_j^{(k)})^2} + \eta\zeta_j A(j) \left(1 - \mathcal{M}(j) \frac{C(j) - P_0}{(A(j)\rho_j^{(k)} + C(j))^2} \right) \right)}{c_j(x)} (u_j^T(x) - u_j(x)) \right) dx.
\end{aligned}
$$

Note that

$$\sum_{j\in\mathcal{B}} \frac{\left(\frac{1}{(1-\rho_j^{(k)})^2}+\eta\zeta_j A(j)\left(1-\mathcal{M}(j)\frac{C(j)-P_0}{(A(j)\rho_j^{(k)}+C(j))^2}\right)\right)(u_j^T(x)-u_j(x))}{c_j(x)} \leq 0$$

holds because u_j^T evaluated based on (5.19) maximizes the value of $\frac{c_j(x)}{\left(\frac{1}{(1-\rho_j^{(k)})^2}+\eta\zeta_j A(j)\left(1-\mathcal{M}(j)\frac{C(j)-P_0}{(A(j)\rho_j^{(k)}+C(j))^2}\right)\right)}$. Thus we have $<\nabla\mathcal{U}(\rho^{(k)}), T(\rho^{(k)})-\rho^{(k)}>\leq 0$.

Bibliography

[1] Z. Hasan, H. Boostanimehr, and V. K. Bhargava, "Green cellular networks: A survey, some research issues and challenges," *IEEE Communications Surveys and Tutorials,* vol. 13, no. 4, pp. 524-540, Nov. 2011.

[2] H. Bogucka and O. Holland, "Multi-Layer Approach to Future Green Mobile Communications," *IEEE Intelligent Transportation Systems Magazine,* vol. 5, no. 4, pp. 28-37, 2013.

[3] M. Marsan, G. Bucalo, A. Di Caro, M. Meo and Y. Zhang, "Towards Zero Grid Electricity Networking: Powering BSs with Renewable Energy Sources," *Proc. IEEE Communications Workshops (ICC)*, pp. 596-601, Budapest, Hungary, June 2013.

[4] http://www.gsma.com/, Last accessed: Mar. 10, 2015.

[5] A. Jhunjhunwala et. al., "Powering Cellular Base Stations: A Quantitative Analysis of Energy Options", Technical Report, Indian Institute of Technology, Madras, 2012.

[6] http://www.gsma.com/mobilefordevelopment/wp-content/uploads/2013/07/Key-Messages-from-DR-Earthquake-Workshop.pdf, Last accessed: Mar. 10, 2015.

[7] http://www.nokia-siemens.com/flexiBS, Last accessed: Jan. 15, 2015.

[8] http://www.carritech.com/used-telecoms-products/access/nokia-bts-base-stations/, Last accessed: Mar. 10, 2015.

[9] http://www.vnl.in/solutions/, Last accessed: Dec. 18, 2015.

[10] X. Yunlong "Photovoltaic technologies: The sun is rising", Huawei Communicate, issue: 63, Dec 2011.

[11] D. Lopez et. al. "Grid-Connected Renewable Electricity Storage: Batteries vs. Hydrogen," *Advances in Mechanical and Electronic Engineering,* vol. 178, pp. 221-225, 2013.

[12] D. Marquet et. al. "The first thousand optimized solar BTS stations of Orange group, A very positive experience full of learning," *Proc. IEEE INTELEC,* pp. 1-9, Amsterdam, Oct. 2011.

[13] ip.access Case Study, *Small Cells Connect Developing World,* 2013.

[14] Altobridge, "Altobridge lite-site: Satellite Backhauled, Solar Powered, 2G/3G Solution for Remote Communities," datasheet, June 2012.

[15] Intelligent Energy, "Green Solutions for Telecom Towers: Part II, Solar Photovoltaic Applications," white paper, July, 2013.

[16] V. Chamola and B. Sikdar, " Resource Provisioning and Dimensioning for Solar Powered Base stations", *Proc. IEEE GLOBECOM,* Austin, USA, Dec 2014.

[17] http://www.nrel.gov, Last accessed: Mar. 10, 2015.

[18] H. ElSawy, E. Hossain and D. I. Kim, "HetNets with cognitive small cells: User offloading and Distributed channel allocation techniques", *IEEE Communications Magazine,* vol. 51, no. 6, pp. 28-36, June 2013.

[19] Y. Mao et al. "Energy Harvesting Small Cell Networks: Feasibility, Deployment and Operation," *IEEE Communications Magazine,* vol. 53, no. 6, pp. 94-101, Jun. 2015.

[20] T. Han and N. Ansari, "ICE: Intelligent Cell BrEathing to Optimize the Utilization of Green Energy," *IEEE Communications Letters,* vol. 16, no. 6, pp. 866-869, June 2012.

[21] R. Weissbach and J. King, "Estimating Energy Costs Using a Markov Model for a Midwest Off-Grid Residence." *Proc. IEEE GTC,* 2013.

[22] T. Han and N. Ansari, "Powering mobile networks with green energy," *IEEE Wireless Communications magazine*, vol. 21, no. 1, pp. 90-96, Feb. 2014.

[23] E. Oh, K. Son and B. Krishnamachari, "Dynamic base station switching-on/off strategies for green cellular networks," *IEEE Transactions on Wireless Communications,* vol 12, no. 5, pp. 2126-2136, May 2013.

[24] J. Xu, L. Duan and R. Zhang, "Cost-aware green cellular networks with energy and communication cooperation," *IEEE Communications Magazine,* vol. 53, no. 5. pp. 257-263, 2015.

[25] B. Lindemark and G. Oberg, "Solar Power for Radio Base Station (RBS) Sites Applications Including System Dimensioning, Cell Planning and Operation," *Proc. IEEE INTELEC,* Edinburgh, UK, 2001.

[26] G. Piro, M. Miozzo, G. Forte, N. Baldo, L. A. Grieco, G Boggia and P. Dini, "Hetnets powered by renewable energy sources: sustainable next-generation cellular networks," *Proc. IEEE Internet Computing,* 2013.

[27] E. Ofry and A. Braunstein, "The loss of power supply probability as a technique for designing stand-alone solar electrical (photovoltaic) systems," *IEEE Trans. Power App. Syst.*, vol. 1, no. 5, pp. 1171-1175, 1983.

[28] M. Bhuiyan and M. Asgar, "Sizing of a stand-alone photovoltaic power system at Dhaka", *Renewable Energy*, vol. 28, no. 6, pp. 929-938, 2003.

[29] C. Venu, Y. Riffonneau, S. Bacha, and Y. Baghzouz, "Battery storage system sizing in distribution feeders with distributed photovoltaic systems", *Proc. IEEE PowerTech,* Bucharest, Romania, 2009.

[30] N. Faruk et al., "Powering Cell Sites for Mobile Cellular Systems using Solar Power," *International Journal of Engineering and Technology,* vol. 2, no. 5, pp. 732-741, 2012.

[31] D. Marquet, O. Foucault and M. Aubree, "Sollan-Dimsol R& D Project, Solar and Renewable Energy in France Telecom," *Proc. IEEE INTELEC,* Providence, RI, September 2006.

[32] D. Marquet, M. Aubree and S. Le. Masson, "The first thousand optimized solar BTS stations of Orange group, A very positive experience full of learning," *Proc. IEEE INTELEC,* Amsterdam, Netherlands, 2011.

[33] V. Chamola and B. Sikdar, "Solar Powered Base Stations: Current Scenario, Issues and proposed Solutions,," *IEEE Communications magazine*, vol. 54, no. 5, pp. 108-114, May 2016.

[34] A. Jhunjhunwala et al., "Powering Cellular Base Stations: A Quantitative Analysis of Energy Options", Technical Report, Indian Institute of Technology, Madras, 2012.

[35] P. Nema, R. Nema and S. Rangnekar, "PV-solar/wind hybrid energy system for GSM/CDMA type mobile telephony base station", *International Journal of Energy and Environment,* vol. 1, no. 2, pp. 359-366, 2010.

[36] E. Negro "On PV simulation tools and sizing techniques: a comparative analysis towards a reference procedure," 13th European Photovoltaic Solar Energy Conference, Nice, France, pp. 687 - 691, October, 1995.

[37] http://www.homerenergy.com/software.html, Last accessed: Mar. 10, 2015.

[38] W. Zhou, et al. "Current status of research on optimum sizing of stand-alone hybrid solar–wind power generation systems," *Applied Energy,* vol. 87, no. 2, pp. 380 - 389, February 2010.

[39] V. Chamola and B. Sikdar, "Dimensioning Stand-Alone Cellular Base Station using Series-of-Worst-Months Meteorological Data," *Proc. IEEE ICCS*, Macau, Hong Kong, Nov. 2014.

[40] Knight, K. M., S. A. Klein and J. A. Duffie, "A methodology for the synthesis of hourly weather data," *Solar Energy*, vol. 46, iss. 2, pp. 109-120, 1991.

[41] A. Maafi and A. Adane, "Analysis of the performances of the first-order two-state Markov model using solar radiation properties," *Renewable Energy,* vol. 13, no. 2, pp. 175-193, 1998.

[42] Festa, R., S. Jain and C. F. Ratto, "Stochastic modelling of daily global irradiation," *Renewable energy*, vol. 2, iss. 1, pp. 23-34, 1992.

[43] Hokoi, S., M. Matsumoto and M. Kagawa, "Stochastic models of solar radiation and outdoor temperature," *ASHRAE Transactions (American Society of Heating, Refrigerating and Air-Conditioning Engineers)*, USA, 1990.

[44] L. L. Mora-Lopez and M. Sidrach-de-Cardona, "Multiplicative ARMA models to generate hourly series of global irradiation," *Solar Energy*, vol. 63, iss. 5, pp. 283-291, 1998.

[45] Dorvlo, SS. Atsu , A. J. Joseph and A. Al-Lawati, "Solar radiation estimation using artificial neural networks," *Applied Energy*, vol. 71, iss. 4, pp. 307-319, 2002.

[46] S. Rehman and M. Mohandes, "Artificial neural network estimation of global solar radiation using air temperature and relative humidity," *Energy Policy*, vol. 36, iss. 2, pp. 571-576, 2008.

[47] P. Philippe et al. , "Stochastic study of hourly total solar radiation in Corsica using a Markov model," *International journal of climatology* , vol. 20, iss. 14, pp. 1843-1860, 2000.

[48] L. Kamal and Y. Z. Jafri , "Stochastic modeling and generation of synthetic sequences of hourly global solar irradiation at Quetta, Pakistan," *Renewable energy,* vol. 18 iss. 4, pp. 565-572, 1999.

[49] G. Auer, et al., "Cellular energy efficiency evaluation framework," *Proc. IEEE VTC (Spring),* 2011.

[50] D. Willkomm, et. al., "Primary users in cellular networks: A large-scale measurement study," *Proc. IEEE DySPAN,* 2008.

[51] Y. Zhang and A. Arvidsson, "Understanding the characteristics of cellular data traffic," *ACM SIGCOMM Computer Communication Review,*

vol. 42, no. 4, pp. 461-466, September 2012.

[52] M. Shafiq, L. Ji, A. Liu and J. Wang "Characterizing and modeling internet traffic dynamics of cellular devices," *Proc. ACM SIGMETRICS* June 2011.

[53] Nan E, X. Chu, W. Guo and J. Zhang "User data traffic analysis for 3G cellular networks.," *Proc. IEEE CHINACOM*, Guilin, China, 2013.

[54] H. Smertnik et. al., *Green Power for Mobile Bi-annual Report,* GSM Association, August 2014.

[55] H. Mutlu, M. Alanyali and D. Starobinski, "Spot pricing of secondary spectrum usage in wireless cellular networks," *Proc. IEEE INFOCOM,* 2008.

[56] P. De Melo, et al., "Surprising patterns for the call duration distribution of mobile phone users," *Machine learning and knowledge discovery in databases,* pp. 354-369, Springer, 2010.

[57] `http://www.nrel.gov/rredc/solar_data.html`, Last accessed: Mar. 10, 2016.

[58] `https://sam.nrel.gov/`, Last accessed: Mar. 10, 2016.

[59] `http://www.nrel.gov/rredc/pvwatts/changing_parameters.html#dc2ac`, Mar. 10, 2016.

[60] Dufo-Lopez et al., "Comparison of different lead acid battery lifetime prediction models for use in simulation of stand-alone photovoltaic systems," *Applied Energy,* vol. 115, pp. 242-253, 2014.

[61] `http://www.usbattery.com/usb_images/cycle_life.xls.pdf`, Last accessed: Mar. 10, 2016.

[62] N. Kakimoto, S. Matsumura, K. Kobayashi and M. Shoji, "Two-State Markov Model of Solar Radiation and Consideration on Storage Size," *IEEE Transactions on Sustainable Energy,* vol. 5, no. 1, pp. 171-181, 2014.

[63] V. Chamola and B. Sikdar, " A Multi-State Markov Model for Dimensioning Solar Powered Cellular Base Stations," *IEEE Transactions on Sustainable Energy,* vol. 6, no. 4, pp. 1650-1652, 2015.

[64] M. Meo, Y. Zhang, R. Gerboni and M. A. Marsan "Dimensioning the power supply of a LTE macro BS connected to a PV panel and the power grid," *Proc. IEEE ICC*, London, UK, Jun. 2015.

[65] Cisco, "Cisco Visual Networking Index: Global Mobile Data Traffic Forecast Update : 2015–2020 , Feb. 2016," `http://www.cisco.com/`.

[66] `http://www.thesolarbiz.com/Trojan-J185P-AC-12V-Battery-205-AH#gsc.tab=0`, Last accessed: Mar. 10, 2016.

[67] `http://imprima.id/gallery/pv-system-for-telecommunication-2-2/`, Last accessed: Mar. 10, 2016.

[68] J. L. B. Agustin and D. Lopez " Simulation and optimization of standalone hybrid renewable energy systems," *Renewable and Sustainable Energy Reviews*, vol. 13, no. 8, pp. 2111-2118, 2009.

[69] I. Abouzahr and R. Ramakumar, "Loss of power supply probability of stand-alone photovoltaic systems: A closed form solution approach," *IEEE Trans. Energy Convers.*, vol. 6, no. 1, pp. 1-11, 1991.

[70] G. B. Shrestha and L. Goel, "A study on optimal sizing of stand-alone photovoltaic stations," *IEEE Trans. Energy Convers.*, vol. 13, no. 4, pp. 373-378, 1998.

[71] J. Song et al., "Development of a Markov-chain-based energy storage model for power supply availability assessment of photovoltaic generation plants", *IEEE Transactions on Sustainable Energy,* vol. 4, no. 2, pp. 491-500, 2013.

[72] H. Maghraby, M. Shwehdi, and G. Al-Bassam, "Probabilistic assessment of photovoltaic (PV) generation systems", *IEEE Transactions on Power Systems,* vol.17, no.1, pp. 205-208, 2002.

[73] V. Chamola and B. Sikdar, "Outage Estimation for Solar Powered Cellular Base Stations," *Proc. IEEE ICC*, London, UK, June 2015.

[74] V. Chamola and B. Sikdar, "Power Outage Estimation and Resource Dimensioning for Solar Powered Cellular Base Stations *IEEE Transactions on Communications,* Preprint online, pp. 1-12, July 2016 (DOI: 10.1109/TCOMM.2016.2587285)

[75] A. Maafi and A. Adane, "Analysis of the performances of the first-order two-state Markov model using solar radiation properties," *Renewable Energy,* vol. 13, no. 2, pp. 175-193, 1998.

[76] V. Chamola and B. Sikdar, "Synthetic Generation of Hourly Solar Irradiance Using a Multi-State Markov Model," *Proc. IEEE/IEIE ICEIC*, Singapore, Jan 2014.

[77] A. M. Aris and B. Shabani "Sustainable power supply solutions for off-grid base stations," *Energies,* vol. 8, iss.10, pp. 1034-1041, Sept 2015.

[78] D. Ike, A. U. Adoghe, A. Abdulkareem "Analysis of telecom base stations powered by solar energy," *International Journal of Scientific & Technology Research,* vol. 3, iss. 4, pp. 369-374, 2014.

[79] M. H. Alsharif, R. Nordin, M. Ismail "Energy optimisation of hybrid off-grid system for remote telecommunication base station deployment in Malaysia," *EURASIP Journal on Wireless Communications and Networking*, vol. 1, iss. 1, pp. 1-5, Dec. 2015.

[80] H. S. Dhillon, Y. Li, P. Nuggehalli, Z. Pi and J. G. Andrews, , " Fundamentals of heterogeneous cellular networks with energy harvesting" *IEEE Transactions on Wireless Communications*, vol. 13, iss. 5, pp. 2782–2797, 2014.

[81] M. A. Marsan, L. Chiaraviglio, D. Ciullo, and M. Meo, "Optimal energy savings in cellular access networks", *Proc. IEEE Greencomm*, Dresden, Germany, Jun. 2009.

[82] J. Gong, J. S. Thompson, S. Zhou and Z. Niu, " Base station sleeping and resource allocation in renewable energy powered cellular networks," *IEEE Transactions on Communications*, vol. 62, iss. 11, pp. 3801–3813, 2014.

[83] E. Oh and B. Krishnamachari, "Energy savings through dynamic base station switching in cellular wireless access networks", *Proc. IEEE GLOBECOM*, Miami, FL, Dec. 2010

[84] E. Oh, B. Krishnamachari, X. Liu, and Z. Niu, "Towards dynamic energy-efficient operation of cellular network infrastructure," *IEEE Communications Magazine*, vol. 49, no. 6, pp. 56-61, Jun. 2011.

[85] L. Bao, "QoS-aware BS switching and cell zooming design for OFDMA green cellular networks," *Proc. IEEE GLOBECOM*, Anaheim, CA, 2012.

[86] E. Oh, K. Son and B. Krishnamachari, "Dynamic base station switching-on/off strategies for green cellular networks," *IEEE Transactions on Wireless Communications*, vol 12, no. 5, pp. 2126-2136, 2013.

[87] Z. Niu, Y. Wu, J. Gong, and Z. Yang, "Cell zooming for cost-efficient green cellular networks," *IEEE Communications Magazine*, vol. 48, no. 11, pp. 74-79, Nov. 2010.

[88] Y. L. Chung, "Rate-and-power control based energy-saving transmissions in OFDMA-based multicarrier base stations," *IEEE Systems Journal*, iss. 9 , ver. 2, pp. 578-584 , 2013.

[89] S. Luo, Z. Rui and T. J. Lim, "Optimal Power and Range Adaptation for Green Broadcasting," *IEEE Systems Journal*, vol. 2, no. 9 , pp. 4592–4603, Sept. 2013.

[90] D. Ng, E. Lo and R. Schober, "Energy-efficient resource allocation in OFDMA systems with hybrid energy harvesting base station," *IEEE Transactions on Wireless Communications,* vol. 12, no. 7, pp. 3412-3427, 2013.

[91] T. Han and N. Ansari, "ICE: Intelligent Cell BrEathing to Optimize the Utilization of Green Energy," *IEEE Communications Letters,* vol. 16, no. 6, pp. 866-869, June 2012.

[92] Q. Ye, B. Rong, Y. Chen, M. Al-Shalash, C. Caramanis and J. Andrews, "User association for load balancing in heterogeneous cellular networks," *IEEE Trans. Wireless Commun.*, vol. 12, no. 6, pp. 2706–2716, Jun. 2013.

[93] H. Kim, D. G. Veciana G, X. Yang and M. Venkatachalam, "Distributed-optimal user association and cell load balancing in wireless networks.," *IEEE/ACM Transactions on Networking*, pp. 177-90, Feb. 2012.

[94] T. Han et. al., "Green-energy aware and latency aware user associations in heterogeneous cellular networks," *Proc. IEEE GLOBECOM*,,

2013.

[95] D Liu et. al., "Distributed delay-energy aware user association in 3-tier HetNets with hybrid energy sources,"*IEEE Globecom Workshops,* 2014.

[96] V. Chamola, B. Krishnamachari and B. Sikdar, "An Energy and Delay Aware Downlink Power Control Strategy for Solar Powered Base Stations", *IEEE Communications Letters*, vol. 20, no. 5, pp. 954-957, May 2016.

[97] V. Chamola, B. Krishnamachari and B. Sikdar, "Green Energy and Delay Aware Downlink Power Control and User Association for Solar Powered Base Stations," *IEEE Systems Journal* (Under second round of review).

[98] D. W. K. Ng and R. Schober, "Secure and Green SWIPT in Distributed Antenna Networks With Limited Backhaul Capacity," *IEEE Transactions on Wireless Communications,*, vol. 14, no. 9, pp. 5082-5097, Sept. 2015.

[99] D. W. K. Ng, Y. Wu, and R. Schober, "Power Efficient Resource Allocation for Full-Duplex Radio Distributed Antenna Networks," *IEEE Transactions on Wireless Communications,* vol. 15, no. 4, pp. 2896–2911, Apr. 2016.

[100] L. Kleinrock, *Queueing Systems, vol. II: Computer applications*, Wiley-Interscience, New York, 1976.

[101] J. Fehske, F. Richter, and G. P. Fettweis , "Energy Efficiency Improvements through Micro Sites in Cellular Mobile Radio Networks," *Proc. IEEE GLOBECOM,* Honolulu, HI, Dec. 4, 2009.

[102] T. Khatib , A. Mohamed and K. Sopian, "A review of solar energy modeling techniques," *Renewable and Sustainable Energy Reviews.*, vol. 16, iss. 5, pp. 2864-2869, 2012.

[103] G Reikard, "Predicting solar radiation at high resolutions: A comparison of time series forecasts," *Solar Energy* vol. 83, iss. 3, pp. 342-349, 2009.

[104] `http://www.nnergix.com/`, Last accessed: 30 June., 2015.

[105] `http://reuniwatt.com/en/`, Last accessed: 30 June., 2015.

[106] `http://steady-sun.com/solution/energy-trading/`, Last accessed: 30 June., 2015.

[107] M.Z. Shafiq, L. Ji, A.X. Liu and J. Wang, "Characterizing and modeling internet traffic dynamics of cellular devices," *Proc. ACM SIGMETRICS,* New York, NY, USA, 2011.

[108] X. Chen, Y. Jin, S. Qiang, W. Hu and K. Jiang, "Analyzing and modeling spatio-temporal dependence of cellular traffic at city scale," *Proc. IEEE ICC*, London, UK, 2015.

[109] U. Paul, A.P. Subramanian, M.M. Buddhikot and S.R. Das, "Understanding traffic dynamics in cellular data networks ," *Proc. INFOCOM*, Shanghai, China, 2011.

[110] D. Liu, Y. Chen, K.K. Chai, T. Zhang and K. Han, "Joint user association and green energy allocation in HetNets with hybrid energy sources," *Proc. IEEE WCNC*, LA, USA, 2015.

[111] T. Han T and N. Ansari, "On optimizing green energy utilization for cellular networks with hybrid energy supplies," *IEEE Transactions on Wireless Communications*, vol. 12, iss. 8, pp. 3872-3882, 2013.

[112] K. Son, H. Kim, Y. Yi, and B. Krishnamachari, "Base station operation and user association mechanisms for energy-delay tradeoffs in green cellular networks," *IEEE J. Sel. Areas Commun.*, vol. 29, no. 8, pp. 1525-1536, Sep. 2011.

[113] S. Boyd and L. Vandenberghe, *Convex Optimization*, Cambridge University Press, 2004.

[114] Recommendation ITU-R M.1225, Guidelines for evaluation of radio transmission technologies for IMT-2000, 1997.

[115] IEEE 802.16m-08/004r5: IEEE 802.16m Evaluation Methodology Document (EMD), 2009.

[116] V. Chamola, B. Sikdar and B. Krishnamachari, "Delay Aware Resource Management for Grid Energy Savings in Green Cellular Base stations with Hybrid Power Supplies,", Accepted for publication in *IEEE Transactions on Communications*.

[117] J. Gong, J. S. Thompson, S. Zhou and Z. Niu, "Base station sleeping and resource allocation in renewable energy powered cellular networks," *IEEE Transactions on Wireless Communications*, vol. 62, no. 11, pp. 3801-3813, 2014.

[118] G. Lee, W. Saad, M. Bennis, A. Mehbodniya and F. Adachi "Online ski rental for scheduling self-powered, energy harvesting small base stations," *Proc. IEEE ICC*, Kualalampur, Malaysia, May 2016.

[119] J. Leithon, T. J. Lim and S. Sun, "Battery-Aided Demand Response Strategy Under Continuous-Time Block Pricing. IEEE Trans. Signal Processing", vol. 64, iss. 2, pp. 395–405, 2016.

[120] J. Leithon, S. Sun and T. J. Lim, "An evolutionary algorithm for energy management in cellular base stations under time-of-use pricing", Proc. IEEE ICC, pp. 215–220, 2015.

[121] J. Leithon, T. J. Lim and S. Sun, "Energy exchange among base stations in a Cellular Network through the Smart Grid", Proc. IEEE ICC, pp. 4036–4041, 2014.

[122] J. Leithon, S. Sun and T. J. Lim, "Energy management strategies for base stations powered by the smart grid", Proc. IEEE GLOBECOM, pp. 2635–2640, 2013

[123] J. Leithon, T. J. Lim and S. Sun, "Online energy management strategies for base stations powered by the smart grid", Proc. IEEE SmartGridComm, pp. 199–204, 2013.

[124] X. Fang, S. Misra, G. Xue and D. Yang, "Smart grid—The new and improved power grid: A survey", *IEEE communications surveys & tutorials*, vol. 14(4), pp.944-980, 2012.

[125] A. Mahmood, N. Javaid, and S. Razzaq, "A review of wireless communications for smart grid", *Renewable and sustainable energy reviews*, vol. 41, pp.248-260, 2015.

[126] S. Zhang, N. Zhang, S. Zhou, J. Gong, Z. Niu and X. Shen , "Energy-aware traffic offloading for green heterogeneous networks," *IEEE Journal on Selected Areas in Communications,* vol. 34, iss. 5, pp. 1116-29, 2016.

[127] L.B. Le, D. Niyato, E. Hossain, D.I Kim and D.T Hoang,"QoS-aware and energy-efficient resource management in OFDMA femtocells," *IEEE Transactions on Wireless Communications,* vol. 12, no. 1, pp. 180-194, 2013.

[128] Y. Mao, J. Zhang, and K. B. Letaief, " A lyapunov optimization approach for green cellular networks with hybrid energy supplies," *IEEE Journal on Selected Areas in Communications*, vol. 33, no. 12, pp. 2463-2477, 2015.

[129] T. Han et. al., "A Traffic Load Balancing Framework for Software-Defined Radio Access Networks Powered by Hybrid Energy Sources," *IEEE/ACM Transactions on Networking*, vol. 24, no. 2, pp. 1038-1051, April 2016.

[130] D. Liu, Y. Chen, K. Chai, T. Zhang, and M. Elkashlan, "Two-dimensional optimization on user association and green energy allocation for hetnets with hybrid energy sources," *IEEE Transactions on Communications*, vol. 63, no. 11, pp. 4111–4124, Nov. 2015.

[131] D. Liu et al., "User Association in 5G Networks: A Survey and an Outlook," *IEEE Communications Surveys & Tutorials*, vol. 18, no. 2, pp. 1018-1044, 2016.

List of Publications

Journal papers

1. V. Chamola and B. Sikdar, "Solar Powered Base Stations: Current Scenario, Issues and proposed Solutions," *IEEE Communications Magazine,* vol. 54, no. 5, pp. 108-114, May 2016.
2. V. Chamola and B. Sikdar, " A Multi-State Markov Model for Dimensioning Solar Powered Cellular Base Stations," *IEEE Transactions on Sustainable Energy,* vol. 6, no. 4, pp. 1650-1652, 2015.
3. V. Chamola, B. Krishnamachari and B. Sikdar, "An Energy and Delay Aware Downlink Power Control Strategy for Solar Powered Base Stations", *IEEE Communications Letters*, vol. 20, no. 5, pp. 954-957, May 2016.
4. V. Chamola and B. Sikdar, "Power Outage Estimation and Resource Dimensioning for Solar Powered Cellular Base Stations," *IEEE Transactions on Communications*, Preprint online, pp. 1-12, July 2016 (DOI: 10.1109/TCOMM.2016.2587285).
5. V. Chamola, B. Sikdar and B. Krishnamachari, "Delay Aware Resource Management for Grid Energy Savings in Green Cellular Base stations with Hybrid Power Supplies,", Accepted for publication in *IEEE Transactions on Communications*.
6. V. Chamola, B. Krishnamachari and B. Sikdar, "Green Energy and Delay Aware Downlink Power Control and User Association for Solar Powered Base Stations," *IEEE Systems Journal* (Under second round of review).

Conference papers

1. V. Chamola, P. Narang and B. Sikdar, "Downlink Power Control for Latency Aware Grid Energy Savings in Green Cellular Networks," *Proc. 37th IEEE Sarnoff symposium*, NJ, USA, Sept. 2016.
2. V. Chamola, P. Narang and B. Sikdar "Battery lifetime estimation for Solar powered Base Stations," *IEEE Symposium on Emerging Topics in Smart and Sustainable Grids*, Singapore, Sept. 2016.
3. V. Chamola and B. Sikdar, "Outage Estimation for Solar Powered Cellular Base Stations," *Proc. IEEE ICC*, London, UK, June 2015.

4. V. Chamola and B. Sikdar, " Resource Provisioning and Dimensioning for Solar Powered Base stations", *Proc. IEEE GLOBECOM,* Austin, USA, Dec. 2014.

5. V. Chamola and B. Sikdar, "Dimensioning Stand-Alone Cellular Base Station using Series-of-Worst-Months Meteorological Data," *Proc. IEEE ICCS*, Macau, Hong Kong, Nov. 2014.

6. V. Chamola and B. Sikdar, "Synthetic Generation of Hourly Solar Irradiance Using a Multi-State Markov Model," *Proc. IEEE/IEIE ICEIC*, Singapore, Jan 2014.